Complex system modelling reveals oxalate homeostasis is driven by diverse oxalate-degrading bacteria

Sromona D. Mukherjee[1], Carlos A. Batagello[2], Ava Adler[3], Jose Agudelo[1], Anna Zampini[3], Mangesh Suryavanshi[1], Andrew Nguyen[4], Teri Orr[5], Denise Dearing[6], Manoj Monga[7], Aaron W. Miller[1,3#]

[1]Department of Cardiovascular and Metabolic Sciences, Cleveland Clinic, Cleveland, OH, USA

[2]Division of Urology, Hospital das Clínicas, University of Sao Paulo Medical School, Sao Paulo, Brazil.

[3]Department of Urology, Glickman Urological and Kidney Institute, Cleveland Clinic, Cleveland, OH, USA

[4]M Health Fairview Southdale Hospital, Edina, MN, USA

[5]Department of Biology, New Mexico State University, Las Cruces, NM, USA

[6]School of Biological Sciences, University of Utah, Salt Lake City, UT, USA

[7]Department of Urology, University of California San Diego, San Diego, CA, USA

#*Corresponding author.* Email: millera25@ccf.org

Phone: 1 216 444 6584
Fax: 1 216 444 9329

Running head: Oxalate metabolism within a complex system framework

Keywords: oxalate, gut microbiome, kidney stones, urinary stone disease, dietary toxins, antinutrients, complex systems, functional redundancy, homeostatic feedback, diet-mirobe-host

Abstract

Decades of research have made clear that host-associated microbiomes touch all facets of health. However, effective therapies that target the microbiome have been elusive given its inherent complexity. Here, we experimentally examined diet-microbe-host interactions through a complex systems framework, centered on dietary oxalate. Using multiple, independent molecular, animal, and *in vitro* experimental models, we found that microbiome composition influenced multiple oxalate-microbe-host interfaces. Importantly, administration of the oxalate-degrading specialist, *Oxalobacter formigenes,* was only effective against a poor oxalate-degrading microbiota background and gives critical new insights into why clinical intervention trials with this species exhibit variable outcomes. Data suggest that, while heterogeneity in the microbiome impacts multiple diet-host-microbe interfaces, metabolic redundancy among diverse microorganisms in specific diet-microbe axes is a critical variable that may impact the efficacy of bacteriotherapies, which can help guide patient and probiotic selection criteria in probiotic clinical trials.

Introduction

Research into the host-associated microbiome is at an inflection point. Decades of research have revealed that host-associated microbiomes are intimately linked to host health and touch all aspects of host physiology[1,2]. The first phase of microbiome research was focused on descriptive studies that characterized differences in the microbiome by host species, body site, and disease phenotypes[3-5]. Clinical case:control metagenome wide association studies that found differences in microbiome composition between healthy and disease cohorts gave rise to the ambiguous term “dysbiosis” and much of the literature is focused on “balancing” the gut microbiota[6]. In the second, and current, phase of research, studies have moved towards gaining more mechanistic insight into specific microbe-host interactions that influence host physiology and disease[6-9]. However, it is increasingly being recognized that, given the wide variability in microbiome composition, host genetics, and lifestyles, understanding mechanisms and causal relationships between gut bacteria and host physiological responses is not enough for the development of effective bacteriotherapies that target the gut microbiota[10,11]. In fact, many probiotic clinical trials, with known mechanistic links between the probiotics and host physiology, have exhibited wide variability in results[12-15]. It is currently unclear what sources of variability may drive the response to targeted bacteriotherapies. Some variables that have been proposed include heterogeneity in microbiome composition, alcohol consumption, and bowel movement quality[10].

Complex system theory is one means to potentially constrain hypotheses and bridge the gap between mechanistic studies and effective bacteriotherapies[16,17]. Studies of the host-associated microbiome often casually acknowledge that these systems are complex and, while, there has been progress made in developing mathematical approaches to complex modelling of host-microbiome relationships[16-19], few studies have bridged the gap between experimental biology and complex system theory.

Mammals and their gut microbiome, are often considered as a holobiont[20], defined as a discrete unit that exhibits collective action and evolves as a unit. Using evolutionary theory approaches, it is hypothesized that the form and function of the microbial part of the holobiont is driven primarily by host-microbe influences, but which require microbe-microbe interactions to help manage the enormous burden of microbiome constraint, which is termed an “ecosystem on a leash”[21]. Under this hypothesis, microbe-host interactions, in which host-associated microbes evolve to produce metabolic by-products for the sole benefit of the host, are necessarily rare. Essential features of complex systems include functional redundancy[21,22] and cooperation through chains of direct interactions[21-23], distinct functional nodes that process and transfer resources[22,23], fractality[22,23], and adaptability through specific homeostatic feedback mechanisms to maintain relatively consistent internal conditions given a dynamic external environment[21,24]. While considerable progress has been made in understanding the nature of complex systems, there is a lack of consensus on basic terminology and broadly applicable analytical or experimental models[25]. This limitation is due in part because complex systems necessarily transect many divergent entities in nature and is thus studied in diverse scientific disciplines[25]. Thus, while some essential features of complexity have been elucidated within specific real-world systems, such as the

conversion of polysaccharides to butyrate by multiple species in the gut[26], or feedback loops in blood pressure regulation[27], experimental evidence of multiple features of complexity within a single system is sparse, especially in microbe-host systems.

To overcome the limitations of applying complex systems theory to the microbe-host holobiont, new models and experimental frameworks are needed that balance complexity with tractability. Antinutrients, molecules produced in plants to deter herbivory, disrupt homeostasis by targeting the function of the microbiome, host, or both[28], and provide an effective focal point to study complexity. Oxalate is an antinutrient present in many plant-based foods, which typically provides the majority of oxalate in circulation[29], but is also produced as a terminal metabolite in the liver[30]. While some host genetic mutations increase endogenous production of oxalate[31], mammals do not produce enzymes capable of degrading oxalate[32]. However, multiple oxalate-degrading bacteria exist in the gut, which degrade oxalate through one of a handful of simple metabolic pathways involving one or two genes[33-35], which isolates this function to the gut microbiota. As such, oxalate degradation as a function, exhibits a moderate amount of complexity compared to other gut microbiota functions, such as the production of trimethylamine N-oxide (TMAO), that requires host input[36]. Beyond the moderate complexity, it is known that oxalate-degrading bacteria are susceptible to antibiotics and that antibiotic use decreases oxalate degradation[37-41]. Elevated levels of oxalate induce oxidative stress, activates the inflammasome, and disrupts epithelial barrier function through tight junction proteins[42-44]. This molecule has been linked to diseases including kidney stones and chronic kidney disease[45-47], breast cancer[48], and cardiometabolic disorders such as atherosclerosis[49], obesity[50], and diabetes[50]. *Oxalobacter formigenes,* which uses oxalate as a sole carbon and energy source[33], is a well-studied oxalate-degrading species of bacteria. The negative, at times lethal, effects of oxalate, along with the identification and mechanisms of oxalate-degrading bacteria in the gut, have been worked out for several decades[33,51-54], pre-dating the current microbiome era.

Despite this knowledge, clinical intervention trials involving *Oxalobacter formigenes,* which is perhaps the most effective oxalate-degrading species known, have successfully resulted in a significant reduction in urine oxalate levels in only 43% of studies[15,55]. Oxalate-degrading lactic acid bacteria have been successful in 37.5% of studies[15]. Both treatments led to a wide variability in patient responses. Given these data and the well worked out mechanisms of oxalate metabolism, it is clear that having an understanding of the mechanistic links between the gut microbiota and host physiology, alone, is demonstrably not sufficient to develop effective bacteriotherapies. Therefore, even though the history of oxalate-microbe-host interactions is much greater than most other microbe-host systems, oxalate degradation represents an accurate reflection of the challenges faced by microbiome research and is a prime candidate for complex system modelling to understand the critical variables that determine responsiveness to bacteriotherapies.

The objectives of the current study were to evaluate oxalate-microbe-host interactions, within the framework of complex systems. We used multi-omic approaches utilizing

multiple independent *in vivo* and *in vitro* models to understand the critical variables that influence the gut microbiota's maintenance of oxalate homeostasis and its impact on the host. We targeted several potential oxalate-microbe-host interfaces that include the gut microbiota itself, which is one of the first lines of defense against antinutrients[56,57], intestinal epithelium, which is an important barrier between microbe and host[21], the liver, which is important for the biotransformation of dietary or microbial metabolites[58], along with the kidneys and vasculature, where calcium oxalate can potentially form calcified deposits or induce inflammation[49,59-61]. Collectively, data indicate that multiple oxalate-microbe-host interfaces are influenced significantly by gut microbiota composition and that harboring diverse microorganisms capable of degrading oxalate can limit the impact of *O. formigenes* as a probiotic. Based on results from this study, we propose a phased approach for the development of bacteriotherapies whereby clinical case:control studies determine whether or not a clinical phenotype is associated with the microbiome and the microbial taxa/functions associated with specific phenotypes (Phase I).

Hypothesized taxa and/or microbial functions should be mechanistically resolved through *in vitro* and germ-free animal studies (Phase II). Finally, mechanistic insights should be applied to a complex systems theoretical framework to identify those variables that most impact the potential success of bacteriotherapies (Phase III). Such a phased approach would have broad implications for patient and probiotic selection in the development of targeted bacteriotherapies.

Results

Defining the oxalate-microbe-host as a complex system

To apply complex systems modeling to oxalate-microbe-host interactions, we first defined the system as a network of nodes, connections, and fractal layers. Nodes represent distinct sites where oxalate is processed, connections define the transfer of oxalate or its metabolites between nodes, and fractals represent autonomous subunits that perform analogous but distinct functions. For antinutrients like oxalate, we identified four primary nodes where transformation occurs or where oxalate directly affects the host. The first node is the stomach, where acidic conditions can chemically modify some molecules, such as glucosinolates[62]. A fraction of oxalate may be absorbed into circulation at this stage.

The second node is the intestine, where oxalate encounters high bacterial densities, particularly in the colon. Within the gut microbiome, two fractal layers exist: microbial species and the genes within each species. Microbial oxalate degradation follows one of three possible models: (a) one species/one function, (b) multiple species/one function, or (c) multiple species/multiple functions. Historically, *Oxalobacter formigenes* was considered the primary oxalate degrader[63], relying on a two-gene metabolic pathway (oxalyl-CoA decarboxylase and formyl-CoA transferase)[53,54]. However, more recent studies demonstrate that oxalate degradation is a broader function distributed across multiple bacterial species, utilizing diverse metabolic pathways that may require one or two genes[34,35,64,65]. Additionally, gut microbiota interactions influence oxalate

degradation[66-72] with by-products such as CO_2 and formate serving as substrates for downstream metabolic pathways, including acetogenesis, methanogenesis, and sulfate reduction[73-76]. Given the inconsistent results of *O. formigenes* trials and the recognition of broader oxalate-microbiota interactions, we hypothesize that oxalate homeostasis is maintained either by diverse oxalate-degrading bacteria or by cooperative networks in which a subset of bacteria degrades oxalate while others utilize its metabolic by-products.

A portion of intestinal oxalate is absorbed into circulation or excreted in the stool, while another fraction is secreted back into the gut via transporters such as SLC26A6[77,78]. Additionally, some oxalate is transported via the portal vein to the liver, forming the third node[79].

Unlike other metabolites that are detoxified by the liver, oxalate is a source rather than a sink in hepatic metabolism[32]. However, the liver plays a central role in metabolizing other gut-derived molecules, such as trimethylamine, which it converts into the more pathogenic TMAO[36]. Some complex antinutrients, such as creosote, require both gut microbial and hepatic metabolism for complete degradation[80]. The liver itself can be divided into fractal layers based on cell type and gene expression. The final node includes systemic circulation and target organs, where unmetabolized oxalate or other antinutrients may trigger immune responses before eventual urinary excretion.

This framework generates multiple testable hypotheses regarding the cooperative roles of gut microbiota, hepatic metabolism, and host physiology in oxalate homeostasis, which are explored in subsequent sections.

Constitutive and oxalate-dependent effects of the microbiome impact host hepatic gene expression

Both the gut microbiota and the liver are important organs for the neutralization of antinutrients[58,81], indicative of functional redundancy, cooperation, and fractality. While it is known that the liver does not degrade oxalate itself, it could still be impacted by oxalate, in gut microbiota dependent ways. To determine the effects of oxalate exposure and microbiome on host hepatic gene expression, we used a fecal transplant model to examine different host microbiomes with the same host genetics. The microbiota from two different host species were utilized for these experiments. Specifically, Swiss-Webster mice harbor a poor oxalate-degrading microbiota and are often used in studies of hyperoxaluria[38,69,72,82,83]. Conversely, the white-throated woodrat, *Neotoma albigula,* is a wild rodent that exclusively consumes *Opuntia* cactus, which is high in oxalate, and harbors a highly effective and responsive gut microbiota tuned to oxalate degradation[68,70,71,84,85]. For the transplant model, a five-day course of neomycin was used to suppress the native gut microbiota of Swiss-Webster mice (SWM)[38], followed by fecal transplants either from SWM (allograft; SW-SW) or *N. albigula* (NALB), which has a highly effective and transferable oxalate-degrading gut microbiota[68,69,72], (xenograft; SW-NALB). Subsequently, animals were fed either a 0% or 1.5% oxalate diet (Evigo, Fig. 1A, Table S1). Liver tissue was obtained after three weeks and processed for bulk RNAseq. The RNAseq data analyses revealed

236 constitutive microbiome and microbiome-dependent oxalate effects (Fig. 1B,C),
237 whereby SW-SW mice exhibited an oxalate-dependent alteration of 219 hepatic genes,
238 with a net increase in activity, while the SW-NALB mice exhibited an oxalate-dependent
239 alteration of 21 genes with a net decrease in activity (Fig. 1C, Table S2). In the SW-
240 NALB mice, the primary response was a decrease in sulfation activity with oxalate
241 exposure, which is involved in the deactivation, detoxication, and excretion of
242 xenobiotics (Fig 1C), and suggests oxalate may be beneficial for this host-microbe
243 system[86]. The primary response in the SW-SW mice was an increase in mitochondrial
244 activity, translation, protein regulation, and ribosome biogenesis, indicative of oxalate-
245 induced hepatic stress[49,87]. Since hosts only differed by gut microbiota composition,
246 these data demonstrate causative interactions between the gut microbiota and liver
247 activity through oxalate-dependent and independent pathways. Within the framework of
248 complex systems, results show microbe-host cooperation whereby oxalate effectively
249 processed within the SW-NALB gut microbiota[38,68,69,72] reduced overall liver activity,
250 indicative of a beneficial impact. Data also suggest that both the gut microbiota and the
251 immune system are involved in oxalate remediation (redundancy), such that if oxalate
252 cannot be neutralized in the gut microbiota or liver, then the molecule will be processed
253 through host immune response mechanisms (fractality), in this case indicated through
254 an overall increase in inflammatory cytokines with oxalate exposure combined with an
255 ineffective oxalate-degrading microbiota (Figs. S6a,b; S9a,b).
256
257 *Constitutive and oxalate-dependent effects of the microbiome impact microbial*
258 *metabolic activity in the gut*
259 Microbe-microbe interactions are important features of the microbe-host holobiont within
260 the conext of complex systems, both in terms of constraining the microbiome and in
261 processing dietary components[21,22,26,56]. To assess changes to microbial metabolic
262 output with oxalate exposure, we used the same animals as above. Following the diet
263 trial, colon stool was collected post-necr opsy and processed for untargeted
264 metabolomics, which is a measure of total metabolites present in stool from the diet,
265 microbial acitivity, and host host activity. Collectively, results are indicative of
266 constitutive microbiome and microbiome-dependent oxalate effects (Fig. 2A,B). The
267 SW-SW mice exhibited an alteration of 162 microbial metabolites upon oxalate
268 exposure, with a net decrease in activity compared to the no oxalate group, whereas the
269 SW-NALB mice exhibited an alteration of 83 microbial metabolites, with a net increase
270 in activity compared to the no oxalate group (Fig. 2B, Table S3). In SW-NALB mice, the
271 primary response was an increase in lipid metabolism and a shift (increase/decrease) in
272 fatty acid, secondary metabolite, and alkaloid profiles. In the SW-SW mice, the primary
273 response was an increase in fatty acid synthesis and phenylalanine metabolism, and a
274 decrease in synthesis of secondary metabolites, cholesterol, and alkaloids (Fig. 2B).
275 Therefore, while oxalate had a much greater impact on gut microbial metabolism in SW-
276 SW mice overall, the metabolic pathways impacted were similar. Net changes in
277 microbial metabolites produced are indicative of a negative impact of oxalate on
278 microbial activity in SW-SW and positive impact in SW-NALB mice. Integration of host
279 hepatic gene expression and gut metabolomic data shows that oxalate induces a small
280 decrease in hepatic activity overall for SW-NALB mice and a large increase in hepatic
281 activity for SW-SW mice (Fig. 2C, Table S4). From a complex systems perspective,

282 data reflect a causative effect of oxalate for the shift in microbial metabolic output.
283 Specifically, the SW-NALB mice exhibit hallmarks of homeostatic feedback with oxalate
284 exposure to maintain a consistent metabolic output, defined by the relatively small, net
285 negative, microbial metabolite-hepatic gene network compared to the large, net positive,
286 network of SW-SW mice. Additionally, data further support the cooperation,
287 redundancy, and fractality of the gut-liver axis. While SW-NALB exhibit a small increase
288 in microbial metabolic activity and decrease in liver activity, the SW-SW mice saw a
289 large decrease in microbial metabolic activity, coupled with a large increase in hepatic
290 activity, which is reflected in the multi-omic network profiles (Fig. 2C) and suggests that
291 the oxalate-induced change in microbial metabolism is responsible for the change in
292 hepatic activity.
293
294 *Oxalate stimulates the growth of microbial populations involved in oxalate metabolism,*
295 *formate metabolism, and their precursors*
296 To gain a deeper understanding of microbe-microbe interactions associated with
297 oxalate exposure and to identify specific microorganisms that positively respond to
298 oxalate exposure, NALB with their native microbiota were pair-fed increasing amounts
299 of oxalate, from 0.2% to 6% (Fig. 3A). Stool was sampled after 5 days on the 0.2% and
300 6% diets and processed for shotgun metagenomics. Analysis of metagenomic data
301 revealed that oxalate had a significant impact on metagenome composition (Fig. 3B),
302 with a significant increase of 1073 gene populations and decrease of 382 gene
303 populations (Fig. 3C; Table S5). Changes in gene abundance included four oxalate
304 metabolism gene populations, a shift in 48 gene populations involved in formate
305 metabolism (32 +/16 -), and a shift in genes related to glycine and
306 glyoxylate/dicarboxylate metabolism (6+/4-), which are precursors to oxalate (Fig. 3D).
307 A total of 128 differentially abundant genes were involved in sugar metabolism. Altered
308 gene populations primarily belonged to *O. formigenes* and *Alistipes senegalensis,* with
309 many genes belonging to the *Muribaculum* genus (Fig. 3E). *Muribaculum spp* harbor
310 oxalate-degrading genes, which suggests oxalate metabolic redundancy in the gut
311 microbiota[88]. The oxalate-dependent metagenomic divergence of the NALB gut
312 microbiota (Fig. 3), which has been replicated in multiple studies on the NALB gut
313 microbiota[68,71], combined with the lack of change in the NALB microbial metabolomic
314 profile with oxalate exposure (Fig. 2, SW-NALB mice), suggest that oxalate stimulates
315 taxonomically diverse, but metabolically redundant microorganisms, in support of
316 maintaining homeostasis. Given that data came from the same hosts sampled
317 longitudinally, these data also reflect a microbiota that is adaptive to oxalate exposure,
318 which is another important characteristic of complex systems, and suggests that
319 metabolic redundancy is critical for oxalate homeostasis.
320
321 *Oxalate and formate metabolism are highly redundant functions in the NALB gut*
322 To investigate the hypothesis that oxalate stimulates a taxonomically diverse,
323 metabolically redundant community, 248 full length genomes were extracted from
324 shotgun metagenomic data (Fig. S1). Genes for oxalate metabolism, formate
325 metabolism, or the formate metabolic pathways of acetogenesis, methanogenesis, and
326 sulfate reduction, were derived from the KEGG pathway database[89] and mapped to full
327 length genomes. This analysis provides a targeted assessment for the potential for

metabolic redundancy aimed at oxalate metabolism and pathways associated with the by-products of oxalate metabolism (potential cooperation). A total of 59.3% of genomes contained at least one gene associated with oxalate metabolism or handling (Fig. 4A), most represented by oxalyl-CoA decarboxylase, glycerate dehydrogenase, and formyl-CoA:oxalate CoA transferase (Fig. 4B). However, only 27.8% of genomes harbored a complete metabolic pathway for oxalate degradation (Fig. 4C). Taxa with oxalate genes were dominated by *Bacteroides, Muribaculaceae, Clostridium, Ruminococcus,* and *Lachnospiraceae* (Fig. 4D). Formate metabolism genes were found in 97.18% of genomes, which was dominated by serine hydroxymethyltransferase, and formate-tetrahydrofolate ligase (Fig. S2A-C). Acetogenic genes were also present in 97.18% of genomes, dominated by acetate kinase and formate-tetrahydrofolate ligase (Fig. S3A-C). Methanogenic genes were present in 100% of genomes, dominated by phosphoserine phosphatase, atp-dependent 6-phosphofructokinase, and phosphate acetyltransferase (Fig. S4A-C). Sulfate-reducing genes were present in 31.05% of genomes, dominated by bifunctional oligoribonuclease and PAP phosphatase, FMN reductase, and cysteine synthase (Fig. S5A-C). Data show highly redundant oxalate-associated metabolic pathways and thus provide evidence for very robust homeostatic feedback mechanisms to handle oxalate and metabolic by-products within the NALB gut microbiota. Additionally, the broad diversity of species that contain oxalate-related genes suggest that the distribution of metabolic genes is somewhat independent of the distribution of microbial species, which suggests that microbial genes exist in an autonomous fractal layer, to some degree. This hypothesis is supported by studies which show a high degree of horizontal gene transfer within the gut microbiota as a means of adaptation[90].

Oxalate metabolism is driven both by substrate availability and microbiota composition

Adaptability and homeostatic feedback within complex systems is driven by the convergence of system components and resource availability[24]. To examine the confluence of resource availability and oxalate metabolism, a custom medium based on previously published gut microbiota media[91] was modified by adding substrates associated with metabolic pathways enriched by oxalate (Fig. 3C, Table S6). The oxalate-degrading species *Enterococcus gallinarum,* previously isolated from NALB[70] and the whole NALB community were assessed. Chosen substrates impacted oxalate metabolism and the impact of oxalate on growth, particularly at the community level (Fig. 5A,B). A minimal media with the same substrates added as sole carbon and energy sources (Table S7) allowed for quantification of the proportion of the NALB microbiota that could use each substrate as sole carbon and energy sources. Culturomic data recapitulates molecular data to show a considerable amount of redundancy surrounding oxalate metabolism (Fig. 5C). Isolates generated from this assay were used for subsequent study (metabolic cohort; Fig. 5D). Additionally, a second cohort was defined and commercially purchased based both on known metabolic functions and the proportion of studies that saw an increase in their taxonomic population with oxalate consumption (Fig. 5D; taxonomic cohort). Where possible, isolates from human sources were obtained. Cohorts, defined in the STAR methods, were used to delineate hypotheses that either carbon and energy substrates are sufficient to explain known effects of the oxalate-degrading microbial network or that

374 additional aspects of taxa commonly stimulated by dietary oxalate are required to
375 explain past results (taxa defined through previous meta-analysis of studies)[15]. Oxalate
376 metabolism with the metabolic and taxonomic cohorts was assessed *in vitro* in minimal
377 media with oxalate as a sole carbon and energy source (Fig. 5E,F). There were
378 considerable differences in oxalate metabolism in both cohorts, dependent on the
379 microbes present. However, significant oxalate metabolism occurred even in the
380 absence of *O. formigenes,* indicative of metabolic redundancy. Collectively, data show
381 that both resource availability and community composition impacts oxalate metabolism,
382 which helps to define the adaptive nature of the NALB gut microbiota. Additionally,
383 results further bolster evidence for redundancy surrounding oxalate metabolism.
384
385 *Severity of oxalate-induced microbe-host effects is dependent on microbial oxalate*
386 *metabolism, independent of taxonomy*
387 To delineate hypotheses of metabolic redundancy or cooperation for mitigating the
388 negative effects of oxalate on the gut microbiota and host, two independent diet trials
389 were conducted with analogous microbial communities derived from the metabolic and
390 taxonomic cohorts. Following antibiotic suppression of the gut microbiota, SWM were
391 given microbial transplants from either the metabolic or taxonomic cohorts in a
392 longitudinal, crossover experimental design with either a 0% or 3% oxalate diet (Envigo;
393 Fig. 6A, S8A; Table S1). The 0% oxalate diet was designed to test the stability of
394 oxalate-degraders since *O. formigenes* is often lost when oxalate is removed from the
395 diet[15]. Transplanted microbial communities included the same as those for *in vitro*
396 studies (Fig. 5D-F). Animal metrics and microbial were tracked over the course of the
397 trial as was urinary/fecal oxalate, urinary formate, inflammatory cytokines, and
398 creatinine. Renal calcium oxalate (CaOx) deposition, cardiac fibrosis, and colitis was
399 assessed through histopathology. CaOx deposition and cardiac fibrosis was quantified
400 through a semi-automated process, based on stain color that differentiates calcium
401 deposits (Von Kossa) or collagen (Mason's Trichrome). Colitis severity was assessed
402 by two independent reviewers in hematoxylin and eosin stained tissues through a
403 standardized, multi-factorial assessment[92].

404 Using microorganisms from the taxonomic cohort, while the change in urinary and fecal
405 oxalate levels were greatest in mice given *O. formigenes,* the change in oxalate levels
406 were significantly greater than the no bacteria controls (Group 1) even in the absence of
407 *O. formigenes,* consistent with *in vitro* results (Fig. 6B,C). Interestingly, the change in
408 urinary formate levels was not different in any microbial group for the taxonomic cohort
409 (Fig. 6D). While IL1β was below detection levels, IL6 exhibited levels consistent with
410 oxalate induction, which decreased over the course of the trial (Fig. 6B, S6A).
411 Differences in IL18 were only seen as an increase over time in the No_ox (Group 5)
412 (Fig. S6B). The only changes in urinary creatinine seen was an increase and decrease
413 in the NALB and All (Group 4) (Fig. S6C), respectively, which indicates that while the
414 NALB bacteria may induce some inflammation, the minimal community present in the
415 All (Group 4) group may limit these effects and actually improve kidney health under
416 conditions of oxalate exposure. While some differences were seen in water or food
417 metrics, these can largely be explained by batch effects of the two trials conducted (Fig.
418 S6D-G). We did see a greater increase in body mass in animals receiving the No_ox
419 (Group 5) microorganisms than when *O. formigenes* was administered alone (Group 2)

420 , which can not be explained by batch effects. Renal CaOx deposition, cardiac fibrosis,
421 and colitis severity all closely tracked oxalate levels (Fig. 6E-J, S6H-I) and did not
422 depend on *O. formigenes* if the other probiotic microbes were present. Collectively,
423 data suggest that oxalate homeostasis and oxalate-induced pathologies are mitigated
424 by the presence of diverse oxalate-degrading bacteria and that adding *O. formigenes* on
425 an already effective oxalate-degrading microbiota will not improve oxalate homeostasis.

426 Based on high-throughput 16S rRNA sequencing, the microbiota composition of colon
427 contents from this diet trial was significantly different from excreted feces (Fig. S7A).
428 The microbiome composition in stool from mice was not different based on probiotic
429 administration (Fig. S7B), but within group differences for the All (Group 4) group was
430 significantly lower than other groups (Fig. S7C), indicative of a protective effect against
431 oxalate exposure. This conclusion is corroborated by the change in alpha diversity in
432 which the microbiota of animals given the All (Group 4) group exhibited the greatest
433 post-antibiotic recovery and is the only group that saw recovery beyond a marginally
434 significant increase in diversity, post-antibiotics (Fig. S7D). In general, there was not
435 much loss of the inoculated bacteria throughout the study, in any group (Fig. S7E).

436 Overall, metabolic cohort transplants were less effective than the taxonomic cohort in
437 terms of inducing oxalate metabolism, particularly in the group without bacteria (Group
438 1) isolated against oxalate (Figs. 6B,C, S8B,C). However, there was a much greater
439 change in format metabolism, dependent on the microbes present (Fig. S8D). Despite
440 the more moderate change in oxalate levels, there were similar oxalate-associated
441 effects on renal calcium oxalate deposition (Fig. S8F,G), which was not dependent on
442 formate levels (Fig. S8H). With the metabolic cohorts, the presence of known oxalate
443 degraders appeared to be more important for oxalate homeostasis than the taxonomic
444 cohort, since absence of known oxalate-degraders led to oxalate levels similar to the
445 No_bact (Group 1) controls (Figs. 6B,C; S8B,C). Collectively, data show that while the
446 taxa chosen for the taxonomic cohort enabled efficient oxalate even in the absence of
447 *O. formigenes*, the bacteria present in the metabolic cohort had a greater influence on
448 formate levels. In both diet trials, urinary oxalate, but not formate correlated with CaOx
449 deposition (Fig. S8G,H – metabolic, data not shown - taxonomic). The effects of oxalate
450 and transplant group differed between the two cohort studies with mice in the metabolic
451 cohort exhibiting higher levels of IL-6 of microbial transplant groups compared to the
452 negative controls. However, similar to the taxonomic cohort, there were no differences
453 in IL18. Urinary creatinine increased significantly over time for all groups receiving a
454 microbial transplant, in contrast with the taxonomic cohort (Figs. S6A-C,S9A-C). For the
455 metabolic cohort, there similar group-based differences observed in water based
456 metrics. However, animals in the taxonomic cohort exhibited greater positive changes
457 in food intake and body mass than the metabolic cohort (Fig. S9D-G).

458 In the metabolic cohort, we did not observe the same trends in the microbiota
459 composition, antibiotic recovery, or persistence as we did in the taxonomic trial
460 indicative of less effective microbial communities at protecting the community as a
461 whole (Fig. S10A-D), though probiotic bacteria were generally persistent (Fig. S10E).
462 Data were derived from high throughput sequencing of the 16S rRNA gene.
463

464 Overall, data from the taxonomic and metabolic cohorts indicate that oxalate
465 metabolism results from a defined community of microorganisms that includes
466 redundancy in oxalate metabolism as the primary driver. Importantly, the efficacy of *O.*
467 *formigenes* was apparent when administered alone, but the effect was diminished when
468 co-inoculated with other oxalate-degrading microbes.
469
470 **Discussion**
471 While research in the last two decades have made clear that the gut microbiota is
472 intimately tied to all facets of host health, translating those insights into actionable
473 biotherapies has been difficult due to the inherent complexity and heterogeneity present
474 in the microbe-host system. The study of complex systems holds enormous potential to
475 constrain hypotheses and offer insight into effective bacteriotherapy development[23].
476
477 However, the field is limited by inconsistent terminologies, concepts, and tractable
478 experimental frameworks[25]. The objective of the current study was to examine oxalate-
479 microbe-host interactions within a complex systems framework. Collectively, results of
480 the study offer quantifiable and generalizable metrics of diet-microbe-host systems that
481 can be used to guide more effective patient and probiotic selection criteria for clinical
482 trials involving bacteriotherapies that target the gut microbiota. Specifically, with
483 complex system modelling, we found through multiple *in vivo* and *in vitro* experimental
484 systems, that exogenous oxalate exhibits systemic effects on multiple organs, including
485 the gut microbiota, and oxalate homeostasis is specifically mitigated by diverse oxalate-
486 degrading bacteria rather than a single bacterial species or factors such as host
487 species, or microbe-microbe cooperation (Fig. 7).
488
489 Using our complex modelling approach, our findings establish that oxalate's effects on
490 both the host and the gut microbiota are primarily mediated by the metabolic
491 redundancy of oxalate metabolism in the gut microbiota, rather than a single species or
492 other factors. Specifically, experiments in Fig. 1 demonstrated that host responses to
493 oxalate were dependent on the composition of the gut microbiota. Expanding on this,
494 experiments in Fig. 2 revealed that oxalate's impact on microbial community structure
495 was similarly reliant on the whole microbiota, and direct multi-omic data integration
496 confirmed that these microbial changes subsequently influenced host responses to
497 oxalate. Once the gut microbiota composition was deemed to be critical, experiments in
498 Fig. 3 examined the specific oxalate impacts on the gut microbiota, using *N. albigula*
499 and its native microbiota as the model for high oxalate tolerance. This analysis identified
500 multiple genes associated with oxalate degradation, as well as acetogenic,
501 methanogenic, and sulfate-reducing pathways. To assess the functional redundancy of
502 these pathways, Fig. 4 and Supplemental Figs. 2-5 quantified the extent to which
503 multiple microbial species contribute to these pathways. The high degree of redundancy
504 observed suggested that oxalate degradation is maintained through diverse oxalate-
505 degrading bacteria rather than a single keystone species. To explore the environmental
506 factors influencing oxalate metabolism, we employed a culturomic approach to
507 characterize microbial responses under controlled conditions and to evaluate oxalate
508 degradation within our defined, hypothesized microbial communities (based on Fig. 3
509 data and past oxalate diet trials). Finally, Fig. 6 validated our metagenomic,

metabolomic, and culturomic findings through targeted microbial transplants in mice, specifically demonstrating that the diversity of oxalate-degrading microbes were transferable and influenced host oxalate homeostasis more than a single species. The overall complex modelling approach was designed to systematically identify the most critical factors in the oxalate-microbiota-host relationship. Each experiment was informed by prior results, allowing for a stepwise refinement of hypotheses and experimental design. This integrative framework underscores the importance of metabolic redundancy in modulating oxalate metabolism and its downstream effects on host physiology.

Microbial oxalate metabolism, which has been researched for several decades, pre-dating the current microbiome era, is an ideal focal point to understand pertinent variables that impact probiotic success. Here, we found that heterogeneity in microbiome composition, independent of host genetics, significantly impacted multiple diet-microbe-host interfaces that included hepatic activity (Figs. 1,2), gut microbiota metabolism (Figs. 2,3), renal mineralization (Fig. 6E,F; S8E,F), intestinal inflammation (Fig. 6H,I), and cardiac fibrosis (Fig. S6H,I). Importantly, we found that oxalate degradation was highly redundant among diverse species in the gut of *N. albigula,* which consumes a high oxalate diet in the wild (Fig. 4). Consistent with past studies, administering *O. formigenes* led to a significant reduction in both stool and urine oxalate (Fig. 6B,C). However, when co-administered with other oxalate-degrading microorganisms, there was no additive effect. Oxalate-based results were similar, but to a lower degree, in the metabolic cohort (Fig. S8B,C). In taxonomic cohort studies, we did not see significant differences in the change in urine formate, based on microbial transplant group (Fig. 6D), in contrast to metabolic cohort studies (Fig. S8D).

Collectively, data offer strong support for the hypothesis that metabolic redundancy among diverse taxa, is the primary driver of oxalate homeostasis, rather than metabolic cooperation in which the by-products of oxalate degradation are used in downstream pathways such as acetogenesis, methanogenesis, and sulfate reduction. However, data on the metabolic cooperation hypothesis were inconclusive and there are multiple known microbe and host sources of formate, which may confound results in these studies[74,93-95].

Modelling the microbe-host system through an evolutionary perspective, it has previously been suggested that while host control over the microbiome is the primary driver of the form and function of the gut microbiota, given the enormous biomass and diversity of the gut microbiota, microbe-microbe competition is also required to constrain the microbiota in mammalian microbe-host systems[21]. In the current (Figs. 2B, 5B) and previous studies[33,34,64,65], we and others have found that oxalate can differentially exhibit positive or negative effects on microbial growth and metabolism dependent on the species and environment present. These data provide two alternative ecological pressures to degrade oxalate. The first is to use oxalate as a carbon and energy source for growth, as is the case with *O. formigenes*[33]. The second is to degrade oxalate to remove it as a toxin, as is the case with some *Lactobacilli* and *Bifidobacteria*[64,65]. The data showing oxalate degradation as a metabolically redundant function among multiple

556 diverse microorganisms that maintains oxalate homeostasis (Figs. 4, 6, S8), suggest
557 that the amount of oxalate consumed or produced by the liver is too great for a single,
558 slow-growing oxalate-degrading specialist can handle alone, in contrast to prevailing
559 hypotheses[63], and in support of the ecosystem on a leash hypothesis. Importantly, the
560 near universal presence of formate metabolism genes suggest that formate may be an
561 even greater source of ecological pressure (Figs. S2-S5). In fact, multiple studies have
562 shown that formate is toxic both to many bacterial species and to mammalian hosts,
563 which supports this hypothesis[93-97]. Collectively, data from the current and previous
564 studies on the effect of oxalate exposure on the gut microbiota[68,71] support the
565 hypothesis that the gut microbiota serves as an adaptive organ[98-100] in which specific,
566 metabolically redundant microbes respond to and eliminate dietary components, for the
567 benefit of themselves, but which can residually protect or harm host health depending
568 on the dietary molecules and gut microbiota composition[6,98-100].
569
570 Oxalate degradation, as a focal point in diet-microbe-host interactions, is a special case
571 in which the effects of oxalate on host health and the mechanisms of microbial oxalate
572 degradation have largely been worked out for decades[33,51-54]. Furthermore, oxalate
573 degradation exhibits moderate complexity, both in that it is isolated to the gut microbiota
574 and is performed through a handful of simple metabolic pathways[31-35]. Despite this
575 knowledge, clinical trials designed to reduce systemic oxalate using either *O.*
576 *formigenes* or other oxalate-degrading bacteria have exhibited a wide variety of patient
577 and trial responses[15]. However, knowledge about other diet-microbe-host links are
578 largely in their infancy. Many of the other known features exhibit much greater
579 complexity than oxalate degradation. For instance, while the production of short chain
580 fatty acids are widely viewed as beneficial for both the gut microbiota and host health[101-
581 106], many short chain fatty acids are known and are produced by a wide variety of
582 species[107,108]. Other important diet-microbe-host links, such as the production of
583 secondary bile acids or TMAO[6,36,109-111], also involve host hepatic activity, increasing the
584 complexity further. Given the complexity of diet-microbe-host interactions and the fact
585 that understanding the mechanisms through which the gut microbiota modifies the diet
586 to influence host health is demonstrably insufficient for the development of effective
587 bacteriotherapies[12-15], we propose a three-phase, pre-clinical experimental workflow for
588 the development of targeted bacteriotherapies. In the first phase of research,
589 case:control metagenome-wide studies and research into other factors that modify the
590 microbiome, such as prior antibiotic exposure, can identify disease phenotypes that are
591 influenced by the microbiome, along with the microbial taxa and genes responsible for
592 this association. In the second phase of research, hypothesized taxa and/or metabolic
593 functions can be explored through *in vitro* and germ-free animal studies, using
594 appropriate models to determine the mechanistic links that drive disease phenotypes
595 through diet-microbe-host interactions. Finally, in phase three, these mechanistic links
596 can be applied to a complex system theoretical framework, as done in the current study,
597 to identify those variables most pertinent to successfully influence specific phenotypes
598 through targeted changes to the gut microbiota. Such a phased research structure will
599 provide for much more effective probiotic and patient selection criteria prior to clinical
600 trials.
601

There were some important limitations to the current study. First, while we did conduct one study with *N. albigula,* most animal studies here sought to eliminate host genetics from the equation, as a means of simplification. Host genetics are another layer of complexity that were not examined here and may have an impact on oxalate homeostasis beyond the gut microbiota. Second, in animal studies with the refined communities of microorganisms, the taxonomic and metabolic cohorts studies were conducted separately and some batch effects are apparent, such as with the change in creatinine values or urine output. Finally, it is apparent from our data and the literature that there are multiple host and microbial sources of formate. As such, data pertaining to formate utilization by our transplant communities are inconclusive.

In conclusion, using a complex systems theoretical framework, we examined the oxalate-microbe-host interactions of multiple oxalate-microbe-host interfaces and found multiple microbiome-dependent effects of oxalate. The negative effects of oxalate were mitigated by metabolically redundant oxalate-degrading bacteria, more so than by metabolic cooperation or a single oxalate-degrading species. Critically, we found that while *O. formigenes* can lower urine oxalate when placed on a background of a poor oxalate-degrading community, as current theory predicts, this effect is lost when co-administered with other oxalate-degrading bacteria. Collectively, data help to resolve why the gut microbiota of the white throated woodrat, *N. albigula,* effectively responds to and degrades even very high dietary oxalate levels[68,69,72] and offer a clear pathway for more effective patient and probiotic selection for future clinical trials to reduce urine oxalate. More importantly, the conceptual and experimental framework developed in this study, based on complex systems theory, paves the way for a phased approach to microbiome research in which clinical microbiome insights (Phase I) drive mechanistic insights between the gut microbiota and host physiology (Phase II), that can be applied to a complex system model to constrain hypotheses and identify the most pertinent variables that drive microbe-host interactions that influence host physiology and health (Phase III). Such an approach will allow for much more efficacious probiotic and patient selection criteria in clinical intervention trials.

Star Methods

Animal studies.

Tracking animal health

Throughout all diet trials, animals were monitored for evidence of trauma, dehydration, pain, or other forms of suffering. Additionally, water and food intake, urine output, and body mass was monitored daily (i.e., Figs. S6, S9). If animals lost >10% of their baseline body mass, they were removed from the diet trial and placed back onto standard mouse chow.

Effect of oxalate on the native gut microbiota of N. albigula

To determine the impact of dietary oxalate on *N. albigula* with their native microbiota, 14 adult *N. albigula* woodrats were collected from Castle Valley, UT (38.63′N, 109.41′W) in September 2014, using Sherman live traps. Animals were transported to the University of Utah and housed in individual cages (48 by 27 by 20 cm) with a 12-h/12-h light/dark

648 cycle, at 28°C and 20% humidity. Animals were initially maintained on a 0.2% oxalate,
649 high-fiber rabbit chow (Harlan Teklad formula 2031; Envigo) for 7 months prior to
650 experimentation. This diet reduces the overall detectable diversity of the microbiota of
651 these animals but maintains the members of the native microbiota overall [112]. All
652 methods were approved by the IACUC under protocol no. 12-12010.
653
654 Subsequently, *N. albigula* woodrats were placed in a diet trial in which the oxalate
655 concentration of the food was gradually increased over time along a gradient from 0.2%
656 (for days 1 to 5; herein referred to as 0%), 3% (days 6 to 10), and 6% (days 11 to 15;
657 Fig. 3A). The oxalate concentration of the diet was adjusted by adding the appropriate
658 amount of sodium oxalate (Fisher Scientific, Pittsburgh, PA) into the powdered rabbit
659 chow on a dry weight basis. The schedule for each concentration of dietary oxalate was
660 chosen to ensure that the gut microbiota had time to respond to the specific diet [66,71].
661 During diet trials, oxalate did not have a negative impact on *N. albigula* health and
662 neither fecal nor urinary oxalate levels increased significantly[68].
663
664 During the diet trial, animals were placed in metabolic cages to separate urine and
665 feces into sterile 50-ml conical tubes. A subsample of feces was collected from each
666 animal every 4 to 5 days on the 0% and 6% oxalate diets for shotgun metagenomic
667 sequencing. Samples were frozen at −80°C until DNA extraction.
668
669 *Stool collection for bacterial isolations and fecal transplant studies*
670 Feces for fecal transplants were collected from two sources. For the Swiss-Webster
671 feces, 20 individual animals (Taconic Farms, female, six weeks old) were placed on a
672 0% oxalate diet in cages with a custom-designed insert to separate urine and feces at
673 the Cleveland Clinic (IACUC #2016-1653) [38]. For the *N. albigula* feces, 14 individual
674 animals (mixed sex and age) were placed on a 3% oxalate diet in a metabolic chamber
675 at the University of Utah (IACUC #12-12010) to acclimate the microbiome to oxalate
676 metabolism[38]. After 3 days of acclimation on the respective diets, feces were collected
677 from animals within 2 h of defecation, submerged in sterile 15% glycerol and flushed
678 with CO_2 prior to freezing at −80 °C until use in animal studies approximately 12 months
679 after receipt (IACUC #2016-1653) or for bacterial isolations.
680
681 *Microbiota-dependent effects of oxalate on liver and gut microbiota*
682 All animal studies were approved through the Cleveland Clinic's IACUC (IACUC #'s
683 2016-1653, 2020-2312). To examine the host-independent effects of oxalate on gut
684 microbiota with either a low or high efficiency at degrading oxalate, two distinct host-
685 microbe model systems were developed. For both models, equal numbers of male and
686 female Swiss-Webster mice were used as the host. For the low oxalate-degrading gut
687 microbiota, Swiss-Webster mice were given fecal transplants using feces from other
688 Swiss-Webster mice (allografts), as discussed below. A 1.5% oxalate diet is sufficient to
689 induce hyperoxaluria in Swiss-Webster mice, defined as a 50% increase in urinary
690 oxalate excretion[69,72,113]. For the high oxalate-degrading gut microbiota, Swiss-Webster
691 mice were given fecal transplants from *N. albigula* (xenografts). We have previously
692 shown that fecal transplants from *N. albigula* are sufficient to induce significant and
693 persistent oxalate metabolism[69,72]. During and after fecal transplants, animals were

694 grouped four to a cage, with four cages assigned to each treatment group, for a total of
695 16 animals per experimental group. To minimize individual variability and eliminate any
696 cage effect in subsequent metrics, samples and data collected from all animals in a
697 cage were pooled together into an individual sample. To develop the two different
698 mouse models, the conversion of the gut microbiota from the native microbiota to the
699 grafted microbiota (allografts or xenografts) was completed in two stages. First, the
700 native microbiota was depleted with a five-day course of neomycin (0.5g/L water,
701 combined with 2g/L sucralose), while on a 0% oxalate diet. Mice were given *ad*
702 *libitum* access to water during this time and throughout the experiment. Neomycin is a
703 broad spectrum antibiotic that is poorly absorbed across the gut, and effectively reduces
704 gut microbiota density by up to 90%[114]. After antibiotic depletion, mice were given the
705 respective fecal transplants by first thawing feces, then aseptically mixing 32 g feces per
706 kg body weight directly into powdered mouse chow. Fecal transplants were performed
707 daily for 6 days (Fig. 1A), as previously described[38], during which animals were
708 switched to either a 0% or 1.5% oxalate diet. All animals were maintained on their
709 respective diets for two weeks following fecal transplants (Table S1). A total of four
710 treatment groups were defined based on allografts/xenografts and oxalate diet.
711
712 Following diet trials, animals were sacrificed through CO_2 asphyxiation and cervical
713 dislocation. Upon necropsies, liver tissue from each animal was dissected out and
714 placed into RNAlater on ice, prior to freezing at -80ºC, within two hours of necropsies.
715 Additionally, colon feces were collected and placed into screw-cap tubes with o-rings,
716 on ice, prior to freezing at -80ºC.
717
718 *Microbial cohort-dependent effects on mitigating the systemic effects of oxalate on host*
719 *and microbiome*
720 To determine the effect of specific microbial cohorts at mitigating the systemic host-
721 microbiome effects of oxalate, different combinations of two microbial cohorts were
722 established. First, based on the metabolic pathways enriched by oxalate in the *N.*
723 *albigula* gut microbiota (Fig. 3D,5C, Table S5), assessed through comparative shotgun
724 metagenomics (described below), we hypothesized that microorganisms that engage in
725 those metabolic pathways help to mitigate the systemic effects of oxalate. To test this
726 hypothesis, we isolated bacteria from *N. albigula* stool (described below) and grouped
727 microorganisms into four cohorts (Fig. 5D). These included oxalate-degrading bacteria
728 alone (Ox; Group 2), microorganisms that can utilize formate or oxalate (Ox_form;
729 Group 3), oxalate and formate users, in addition to the metabolism of selected sugars
730 (All; Group 4), or the complete cohort except for oxalate degraders (No_ox; Group 5).
731 Microorganisms isolated from *N. albigula* stool and used in microbial transplants were
732 termed the "metabolic cohort". In addition to the metabolic cohort, a "taxonomic cohort"
733 was defined by cross-referenced metabolic pathways enriched by oxalate with microbial
734 taxa previously reported to be stimulated by oxalate (Fig. 5D)[15]. Microorganisms from
735 this cohort were purchased commercially from the ATCC or DSMZ (Table S8). In
736 addition to these cohorts, we also examined a negative control in which animals were
737 inoculated with sterile media (No_bact (Group 1); Group 1), and a positive control in
738 which animals were inoculated with the whole gut microbiota of *N. albigula,* extracted
739 from stool by first vortexing in a 1:1 mixture of stool and sterile PBS, followed by

740 centrifuging at 8000RPM for 2 minutes. The supernatant was inoculated into gut
741 microbiota media with 20mM sodium oxalate (Table S6) overnight prior to microbial
742 transplant.
743
744 To prepare each isolate for transplants, an overnight culture of each species was grown
745 and mixed in equal proportions by volume for each cohort. The community was then
746 centrifuged and supernatant was decanted. After antibiotic depletion of the native gut
747 microbiota in Swiss-Webster mice, 38mg of pelleted bacteria of each preparation was
748 added directly to the food and administered over the course of six days (Figs. 6, S8), as
749 done previously[69,113]. Preparations corresponded to approximately 5 x
750 10^8 microorganisms for each isolate in the appropriate transplant groups. Quantification
751 of bacterial numbers was performed through absorbance of the microbial preparations
752 on a spectrophotometer at 600 nm, calibrated to direct microscopic counts.
753
754 As above, animals were grouped four to a cage, with samples from each cage pooled
755 together prior to collection and analyses. Similarly, animals were maintained on custom
756 inserts that mimic metabolic cage for the effective separation of urine and stool prior to
757 collection. During the microbial transplant animal studies, stool and urine was collected
758 daily and inserts disinfected. For oxalate and formate quantification, samples were
759 collected at the end of the antibiotic depletion, microbial transplants, a 0% oxalate
760 washout period, and after return to a 3% oxalate diet (Figs. 6B-D, S8B-D). Prior to
761 biochemical assays, urine was frozen (−20°C) and feces were dried at 45°C overnight.
762 Prior to freezing, aliquots of urine were equally divided into six fractions for each of the
763 biochemical assays performed (discussed below). Fractions for oxalate quantification
764 were collected into 4N HCl prior to freezing to prevent the non-enzymatic conversion of
765 ascorbic acid into oxalate [71]. For microbial inventories, a portion of feces and colon
766 feces (discussed below) were frozen at −80°C. All animals were maintained on a 3%
767 oxalate diet, except during the washout period (Table S1).
768
769 Following diet trials, animals were sacrificed through CO_2 asphyxiation and cervical
770 dislocation. Necropsies were performed to aseptically remove colon feces, colon,
771 kidneys, and heart tissue. Colon tissue was longitudinally bisected, swiss-rolled, and
772 placed into 4% paraformaldehyde overnight for fixation at 4ºC for histopathology [115].
773 Kidney and heart tissues were placed into 4% paraformaldehyde overnight for fixation at
774 4ºC prior to histopathology. Hearts were first perfused with paraformaldehyde solution
775 prior to immersion.
776
777 After fixation, colon, kidney, and heart tissue were placed in 70% ethanol at 4ºC prior to
778 paraffin embedding, serial sectioning, and staining. To quantify colitis, colon tissue was
779 stained with hematoxylin and eosin and imaged with light microscopy (Fig. 6H). Whole
780 colons were scored for colitis by two blinded, independent reviewers using a semi-
781 quantitative protocol that considers inflammatory infiltrates, goblet cell loss, crypt
782 density, crypt hyperplasia, muscle thickening, submucosal inflammation, crypt
783 abcesses, and ulcerations[92]. To quantify calcium oxalate deposition, kidney tissue was
784 stained with Von Kossa staining[116], which turns calcium deposits black and the
785 remaining tissue pink (Figs. 6E, S8E). Kidneys were imaged under light microscopy

786 and calcium oxalate deposition was quantified using an automated process in QuPath,
787 based on stain color. The area of the black calcium oxalate deposits was normalized to
788 total kidney area. To quantify cardiac fibrosis, heart tissue was stained with Masson's
789 trichrome stain, which stains collagen fibrosis blue and the remaining tissue red (Fig.
790 S6H). Hearts were imaged under light microscopy and fibrosis was quantified with an
791 automated process in QuPath, quantifying the blue and red stained areas[117]. Fibrosis
792 was normalized to total heart surface area.
793
794 **Biochemical assays.**
795 Urinary creatinine (Fisher Scientific), formate (VWR), IL-6 (R&D Systems), IL-18 (Fisher
796 Scientific), and IL-1β (R&D Systems) were quantified with ELISA-based assays,
797 following manufacturer's instructions. Positive controls that included a known amount of
798 substrate along with no substrate negative controls were included in all batches of
799 ELISA assays. Samples, standards and controls were all run in duplicate and values
800 averaged. Urinary and fecal oxalate were quantified with an ELISA-based assay
801 (Sigma-Aldrich), with a modified protocol, as follows. Upon initial testing of oxalate and
802 formate assays using solutions of sodium oxalate and sodium formate in water, it was
803 discovered that while formate assays only had affinity for formate, the oxalate assays
804 had equal affinity for both oxalate and formate (Figs. S11A). Specifically, when oxalate
805 alone was added to solution, the quantified concentration of oxalate matched the
806 amount added. However, when oxalate and formate was added at equal
807 concentrations, the quantified oxalate was approximately twice as high as what was
808 added (Fig. S11B). Furthermore, when adding 300uM of formate or oxalate to human
809 urine specimens, the amount of oxalate quantified was approximately 300uM higher
810 than urine without any modifications (Fig. S11C). To eliminate the formate
811 contamination on oxalate measurements, oxalate was extracted by first acidifying to pH
812 3 with 3M HNO_3. Acidified urine was centrifuged, and supernatant collected. The pH
813 was then brought up to 7 with NaOH. Subsequently, 5M $CaCl_2$ was added to solution to
814 precipitate calcium oxalate. The precipitates were extracted by centrifugation and
815 decanting. Finally, calcium oxalate solution was acidified in 1:4 parts of 4N HCl prior to
816 enzymatic assay, as previously described[71]. When oxalate was extracted from urine
817 specimens in this way, prior to quantification, we saw a significant decrease in
818 quantified oxalate (Fig. S11C), as expected given the assay affinity for formate. When
819 solutions containing formate alone went through the extraction process, no oxalate was
820 quantified. Given these results, urinary and fecal oxalate was extracted prior to ELISA-
821 based assays using the manufacturer's recommendations, post-extraction. For fecal
822 oxalate, samples were acidified with 6N H_2SO_4 to solubilize oxalate prior to following the
823 extraction protocol above. For creatinine, cytokines, and oxalate, values generated on
824 a 0% oxalate diet were substracted from all other values, matched by cage, with the
825 assumption that this would isolate oxalate-induced molecule generation. For urinary
826 formate, this substraction was not done since formate can come from multiple sources
827 other than oxalate degradation and values on a 0% oxalate diet were not clearly lower
828 than on a 3% oxalate diet. For all values, data are presented as the change from
829 baseline. Data were statistically compared with two-way analyses and post-hoc,
830 Holm's-corrected, paired t-tests.
831

832 **Culturomic assays.**
833 All assays were conducted under strict anaerobic conditions (90% N_2, 5% H_2, 5% CO_2)
834 in an anaerobic chamber (Bactron 300).
835
836 The stool from *N. albigula* were used to determine the impact of environmental factors
837 on oxalate metabolism *in vitro* and to isolate bacteria for the metabolic cohort.
838 *Enterococcus gallinarum,* an oxalate-degrading species previously isolated from *N.*
839 *albigula,* was also used in culturomic assays to determine the impact of environmental
840 factors on oxalate metabolism[70]. To test environmental factors on oxalate metabolism,
841 gut microbiota media, previously designed to support a broad array of gut bacteria[91],
842 was used as a base media. From there, compounds were added to the media based on
843 metabolic pathways enriched by dietary oxalate in the *N. albigula* gut microbiota (Fig.
844 3D, Table S6). Concentrations of added chemicals were based on previously published
845 media recipes where necessary. For assays using the NALB stool, the microbiota was
846 extracted by first vortexing thawed stool, then centrifuging at 8000rpm for two minutes.
847 For *in vitro* assays involving pure cultures or synthetic cohorts, bacteria were first grown
848 in media, with or without oxalate, that was first validated to allow for the growth of each
849 isolate in pure culture (Table S6). Subsequently, extracted microbiota or pure cultures
850 were normalized to 10^8 microorganisms, as above. Pure cultures were mixed in equal
851 proportions as needed and inoculated into the target media to evaluate oxalate
852 metabolism under different chemical or microbial profiles. Media was incubated for 48-
853 120hrs at 37ºC. All microbiological procedures were done under anaerobic conditions
854 in a Bactron300 anaerobic chamber or sealed containers, as needed. To assess
855 oxalate metabolism in different culture conditions, oxalate was quantified by extracting
856 oxalate and quantification through titration with $KMnO_4$, as we have done previously[70].
857 To assess the impact of oxalate on the growth of *E. gallinarum* or the NALB community,
858 bacteria were grown in their respective media, with or without oxalate, and colony-
859 forming units were quantified from serially diluted media after the incubation period.
860
861 To isolate bacteria for the metabolic cohort and to validate the metabolic redundancy of
862 oxalate metabolism and other pathways stimulated by oxalate, a minimal media with the
863 same substrates from above were added as sole carbon and energy sources (Table
864 S7). In this medium, oxalate was added at 50mM to specifically select for bacteria that
865 can use oxalate as a carbon and energy source. Subsequently, the NALB microbiota
866 from the stool was first diluted to ~1 bacterium/100ul and then inoculated into 5 or 10
867 96-well plates, depending on the rarity of positive hits, and quantifying growth through
868 spectrophotometry. Wells in which the absorbance values at 600nm for greater than
869 one standard deviation above the average for all well were considered positive for
870 growth. Wells with positive growth had bacteria isolated by streaking on rich media,
871 transferred to broth cultures, and had stocks made in 15% glycerol that were frozen at -
872 80ºC until needed. Bacteria were chosen for downstream *in vitro* and *in vivo* studies
873 (metabolic cohort) by screening a minimum of ten isolates for each target substrate (Fig.
874 5D). Those isolates grown in oxalate or formate containing media were subsequently
875 enriched in the minimal media and oxalate or formate degradation was validated
876 through broth cultures and ELISA-based assays. Isolates that utilized the greatest
877 amount of oxalate and formate were chosen for the metabolic cohort. For the other

878 substrates, isolates were chosen based on those that exhibited the greatest amount of
879 growth using the target substrates as a sole carbon and energy source, based on
880 absorbance values at 600nm. Subsequently, chosen isolates for the metabolic cohort
881 along with isolates for the taxonomic cohort underwent PCR with the 27F and 1492R
882 primers to amplify the 16S rRNA gene. Amplicons were purified and sequenced with
883 Sanger sequencing to determine or validate taxonomy and purity. Taxonomy of isolates
884 and the substrates each could utilize are presented in Fig. 5D.
885
886 **Metabolomics.**
887 For untargeted metabolomic assays, fecal samples were re-suspended in Optima
888 LC/MS grade water (50mg stool to 150ul water. The samples were then placed briefly in
889 a water bath at 37°C and placed on dry ice. An aliquot of each sample was taken out for
890 protein concentration measurement. Then, 150 µL of chilled acetonitrile containing
891 internal standards (Betaine-d9, Carnitine-d9, Orinithine-d6, Valine-13C3, Tyrosine-13C,
892 15N, Estrone-13C3, and Cholesterol-13C3) was added to the remaining samples
893 followed by centrifugation at 14,000g for 10 minutes to precipitate out the protein pellet.
894 The supernatants were recovered and transferred to fresh tubes. The samples were
895 dried briefly and re-suspended in 2% acetonitrile and 0.1% formic acid for subsequent
896 LCMS analysis. One-microliter aliquots taken from each sample were pooled and this
897 QC standard was analyzed every 10 injections. The untargeted metabolomics was
898 performed by injecting 0.5uL of each sample onto a 10 cm C18 column (Thermo Fisher
899 CA) coupled to a Vanquish UHPLC running at 0.35mL/min using water and 0.1% formic
900 acid as solvent A and acetonitrile and 0.1% formic acid as solvent B. The 15-min
901 gradient used is given below. The Orbitrap Q Exactive HF was operated in positive and
902 negative electrospray ionization modes in different LC-MS runs over a mass range of
903 50-750 Da using full MS at 120,000 resolution. The data dependent acquisitions were
904 obtained on the pooled QC sample. The DDA acquisition (DDA) include MS full scans at
905 a resolution of 120,000 and HCD MS/MS scans taken on the top 10 most abundant ions
906 at a resolution of 30,000 with dynamic exclusion of 4.0 seconds and the apex trigger set
907 at 2.0 to 4.0 seconds. The resolution of the MS2 scans were taken at a stepped NCE
908 energy of 20.0, 30.0 and 45.0.
909
910 XCMS was used to deconvolute the data using 5 ppm consecutive scan error, 7 to 75
911 seconds as minimum and maximum peak width, S/N threshold of 10, and span of 0.2 in
912 positive and negative electrospray ionization modes for retention time correction. The
913 resulting peak table was normalized to total protein concentration and further analyzed
914 via MetaboLyzer [118]. Briefly, the ion presence threshold was set at 0.7 in each study
915 group. Data were then log-transformed and analyzed for statistical significance via non-
916 parametric Mann-Whitney U test. Ions present in just a subset of samples were to be
917 analyzed as categorical variables for presence status via Fisher's exact test. All p-
918 values were set to be corrected via the Benjamini-Hochberg step-up procedure for false
919 discovery rate (FDR < 0.05). The data could then be utilized for PCA, putative
920 identification assignment, and pathway enrichment analysis via KEGG[89], HMDB[119],
921 LIPIDMAPS[120], and BioCyc[121] databases. In addition to differential abundance analysis
922 provided by MetaboLyzer, whole metabolome comparisons were made as a Binomial
923 dissimilarity matrix, which is optimal for metabolomic datasets[122], with statistical analysis

924 provided by PERMANOVA with 999 permutations and a principal component
925 visualization in Vegan[123].
926
927 **Transcriptomics.**
928 For transcriptomic analysis, RNA was extracted from liver tissue with a TRIzol RNA
929 purification kit (Invitrogen), following manufacturer's recommendations. Extracted RNA
930 was converted to cDNA using a cDNA synthesis kit (Fisher Scientific) and stored at -
931 20ºC. The cDNA quality was checked on a bioanalyzer and libraries were prepared with
932 the TruSeq stranded mRNA library prep kit. Sequencing occurred on an Illumina HiSeq
933 2500 at the Genomics Core (Cleveland Clinic) for paired 100bp sequencing.
934
935 The raw sequencing files, with 33.5 million +/- 950,000 reads per sample, were pre-
936 processed using an established protocol[124]. Specifically, FastQC and SortMeRNA was
937 used to remove low quality reads, remove rRNA reads, and merge paired reads[125,126].
938 Subsequently, trimmomatic was used to remove adapter sequences[127] and the
939 remaining high quality reads were mapped to the mm10 mouse reference genome for
940 annotation, using HISAT[128,129]. The annotated gene counts were normalized to
941 fragments per kilobase of transcript per million mapped reads. Comparative whole
942 transcriptome analyses were conducted as a Bray-Curtis dissimilarity index and
943 principal components visualization with statistical analysis provided by PERMANOVA
944 with 999 permutations, in the Vegan package of R statistical software[123,130]. Differential
945 abundance analysis was conducted in Cuffdiff2, with significance defined at a false
946 discovery rate <0.05 [131]. Sequences mapping to mouse genes were annotated to
947 metabolic pathway with the gene ontology database[132].
948
949 To integrate transcriptomic and metabolomic data, the normalized metabolite
950 concentrations and normalized transcript counts of metabolites and genes that were
951 significantly different between the SWM-SWM and SWM-NALB groups were correlated,
952 within each group, using SPARCC correlations in R[133]. Significant positive and negative
953 correlations were calculated at an R greater or less than 0.4 or -0.4, respectively and an
954 FDR <0.05. Significant correlations were visualized in Cytoscape version 3.3.0[134].
955
956 **Shotgun metagenomics.**
957 For shotgun metagenomic analysis, DNA from *N. albigula* stool was extracted with the
958 QIAmp DNA stool minikit (Qiagen). The extracted DNA was submitted to Argonne
959 National Laboratory (Chicago, IL) for 150bp paired-end shotgun metagenomic
960 sequencing on an Illumina HiSeq 2500. The low quality reads were trimmed from raw
961 sequencing data and paired ends were merged using default parameters in
962 BBMerge[135]. Reads were first mapped to the *Neotoma* genome [136] with BWA mem with
963 default settings[137], and removed. Paired, non-rodent sequences were assembled in
964 MetaSpades with default parameters[138].
965
966 Full-length microbial genes were extracted and annotated from the assembled contigs
967 using PROKKA software[139]. Gene annotation was achieved by mapping to the UniProt
968 and Hamap protein databases[140,141]. To dereplicate genes, ensure common
969 nomenclature across samples, and build a reference gene catalog for the quantification

970 of gene counts, full-length genes were clustered at 90% homology in CD-hit[142]. After the
971 creation of a non-redundant gene catalogue, high quality reads for each sample were
972 mapped to the annotated gene catalog to generate gene-level count tables with BWA
973 mem.
974
975 Gene count tables were normalized and differential abundance analysis was conducted
976 with a negative binomial Wald test in DESeq2[143]. Significantly different genes were
977 considered at an FDR <0.05. The normalized count tables were also used to generate a
978 weighted Bray–Curtis dissimilarity matrix in the Vegan R package, with statistical
979 comparisons with a PERMANOVA at 999 permutations[123]. To annotate differentially
980 abundant genes to taxonomy, genes were mapped to full length genomes extracted
981 directly from the shotgun metagenomic data, as described below.
982
983 de novo *genome construction and calculation of metabolic redundancy*
984 For the *de novo* construction of genomes, the metaspades assembled contigs were
985 binned to genomes with Autometa software[144], as previously described[145]. The
986 Autometa algorithm takes assembled contigs as input, bins the data to genomes using
987 contig coverage values, GC content, and the Barnes-Hut t-Distributed Stochastic
988 Neighbor Embedding (BH t-SNE) distribution of the contigs. Taxonomy is assigned
989 based on the consensus classification of all contigs in a genomic bin. Completeness
990 and purity calculations are based on the presence of known, unique universal single
991 copy genes in Autometa. After genomic binning, the contigs were oriented and
992 scaffolded in CSAR[146], which compares the genomic bins to reference genomes of
993 close relatives. Gaps within the genomes were filled with Abyss-Sealer[147] using the
994 original raw sequencing reads as input. The completeness and purity of genomes were
995 recalculated and taxonomic assignment was validated through phylogenetic analysis of
996 the *de novo* constructed genomes in comparison with all complete NCBI genomes (Fig
997 S1), achieved through Phylophlan, using the "—accurate" parameter which considers
998 more phylogenetic positions at the cost of computational speed[148]. Phylophlan allows
999 for the phylogenetic analysis of bacteria and archaea using complete genomes rather
1000 than gene amplicons, which provides greater resolution on phylogenetic analysis.
1001 Collectively, we extracted 248 high quality, full length genomes, defined as being >80%
1002 complete and >90% pure, based on current standards[149].
1003
1004 To quantify the proportion of the *N. albigula* microbiota that contained genes related to
1005 oxalate metabolism, formate metabolism, acetogenesis, methanogenesis, or sulfate
1006 reduction, all genes that contribute to those metabolic pathways were extracted from the
1007 KEGG database[150]. Subsequently, PROKKA[139] was run on the 248 full length genomes
1008 to extract and annotate full length genes. The PROKKA extracted genes were then
1009 cross-referenced with the gene databases from KEGG to determine the proportion of
1010 genomes that contained at least one gene in the target pathways and determine which
1011 taxa had those genes.
1012
1013 **16S rRNA metagenomics.**
1014 Fecal DNA from the stool and colon feces from the mouse studies, underwent DNA
1015 extraction through a semi-automated protocol on a KingFisher Duo Prime System

(Thermo Scientific) following the manufacturer's protocol for stool. The protocol includes mechanical lysis with bead-beating, piston driven lysis, and proteinase K chemical lysis. The extracted DNA, which attaches to magnetic beads in a proprietary salt solution, is removed from solution and eluted in buffer. Duplicate samples of a commercial DNA positive of known composition (Zymboiomcs, USA) were included as positive controls, as well as the DNA reagents that went through the entire workflow, sterile water, and a PCR negative as negative controls.

The fecal DNA was submitted to the Microbial Sequencing and Analytics Core at Cleveland Clinic for high throughput sequencing of the 16S rRNA gene on an Illumina MiSeq. The DNA was first PCR amplified with the 515F and 806R primers that target the V4 hypervariable region of the 16S gene. The DNA concentrations were quantified before and after PCR amplification on a Qubit and normalized prior to library prep with the Illumina Nextera XT library prep kit. The sequence run was conducted to generate 150bp, paired-end sequences.

The raw sequencing data were processed in the R statistical package (4.2.0)[130]. Quality control, removal of bimeras, and assignment of amplicon sequence variants (ASV) were completed in dada2[151]. For ASV taxonomic assignment, a combined, non-redundant database of the Silva 138 SSURef and NCBI 16S rRNA databases were used[152]. Taxa assigned to mitochondria or chloroplasts were removed from subsequent analysis. The resulting ASV's were aligned in MSA[153] and arranged into a maximum likelihood phylogeny in phangorn[154]. The resulting phylogenetic tree and ASV table were merged with sample data for loading into PhyloSeq[155]. The sequencing depth threshold required to adequately capture microbial diversity was calculated with a rarefaction analysis in Vegan[123]. Non-control samples below the depth threshold were removed from further analysis.

The raw count table of 16S rRNA sequences was normalized with the DESeq2 algorithm and α-diversity was calculated as phylogenetic diversity in Phyloseq, along with beta-diversity as a weighted UniFrac distance[156]. Alpha diversity was analyzed with a paired t-test with a Holm's correction where applicable, while beta-diversity analyses were conducted with a PERMANOVA after 999 permutations.

Data availability Sequence reads from the animal study are available at the Sequence Read Archive under Accession numbers for gut microbiota genomes: PRJNA833303, Shotgun metagenomics: PRJNA839366, Liver transcriptomics: PRJNA1018952
Gut microbiota data: 16SPRJNA1018559

Acknowledgements: We would like to thank animal care facility, Metabolomics core, Microbial sequencing and analytics core, and Imaging core at Cleveland Clinic. We are thankful for the NIH funding to AWM R01 DK121689-01A1 and funding from the Cleveland Clinic Foundation to AWM.

Author contributions: SM, DD, MM and AWM conceived and designed the study. SM, CAB, AA, AN, and AWM designed and performed most *in vitro* and animal-based biological experiments. JA, MS, AZ, TO performed addtional animal and *in vitro* experiments and contributed to data analysis. SM and AWM wrote the manuscript with input from all authors. AWM supervised the study. All authors reviewed the manuscript.

Declaration of interests: The authors declare no conflict of interest

Figure titles and legends

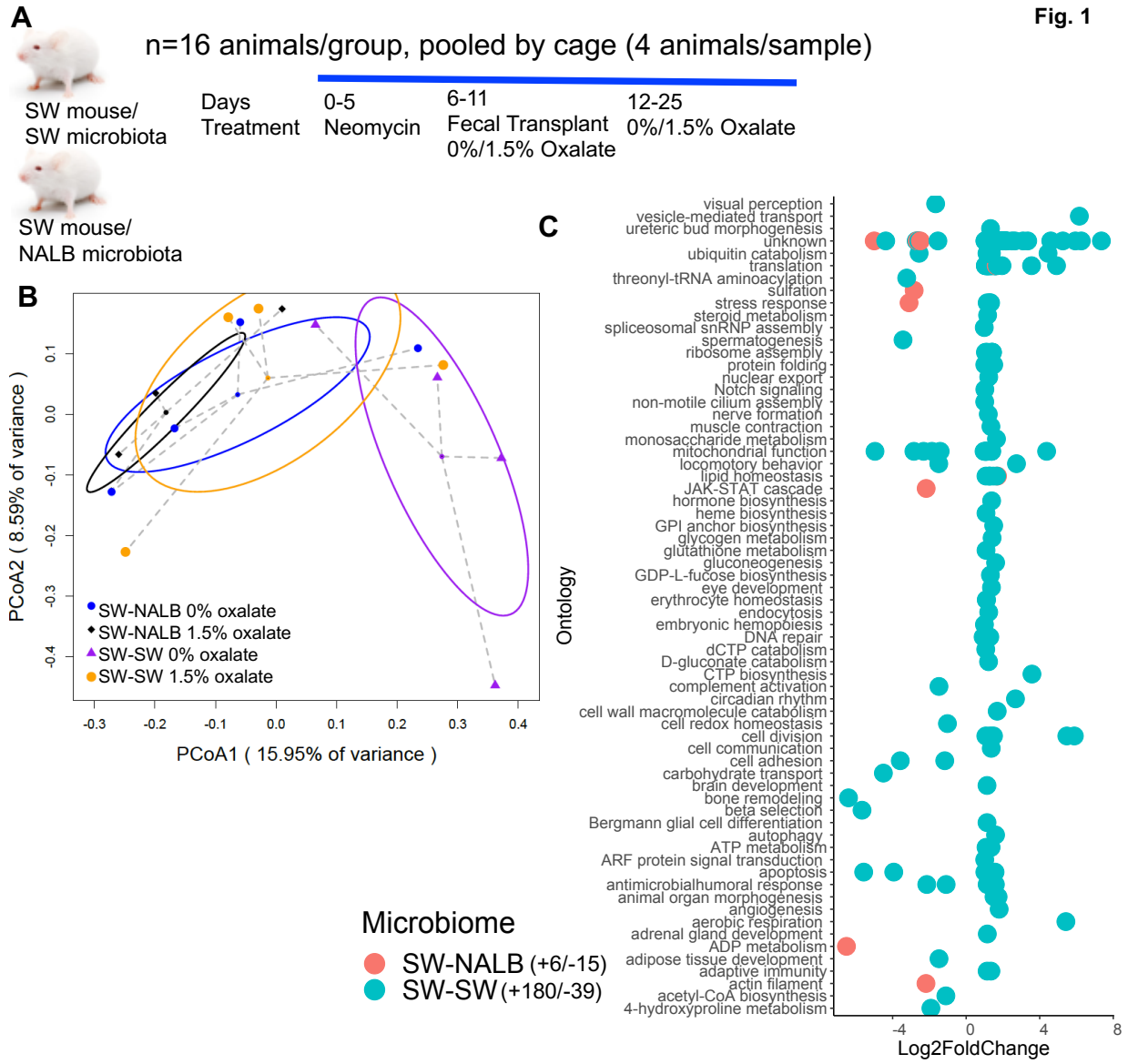

Fig. 1. Oxalate exposure impacted host hepatic activity in a microbiota dependent fashion. A) Swiss Webster mice were given neomycin, followed by an allograft (SWM) or xenograft (NALB) fecal transplant, then maintained on a 0% or 1.5% oxalate diet prior to necropsy for fecal metabolomics (Fig. 2) and hepatic transcriptomics. B) PCoA of normalized, whole-transcriptome data. p=0.02 for microbiome composition, p=0.07 for dietary oxalate content, p=0.3 in 2-way analysis; 2-way PERMANOVA. C) Total number of hepatic genes significantly stimulated or inhibited by dietary oxalate. Significant genes are plotted by Log2FoldChange. Positive values reflect genes increased with oxalate exposure and negative values are genes decreased with exposure. FDR < 0.05, Wald test. Hepatic genes are annotated to pathway (Kegg, Uniprot, PubChem,

1085 Metacyc) and the total number of genes that exhibit a positive or negative shift with
1086 oxalate exposure are listed in the legend. Complete gene list is in Table S2.
1087

1088

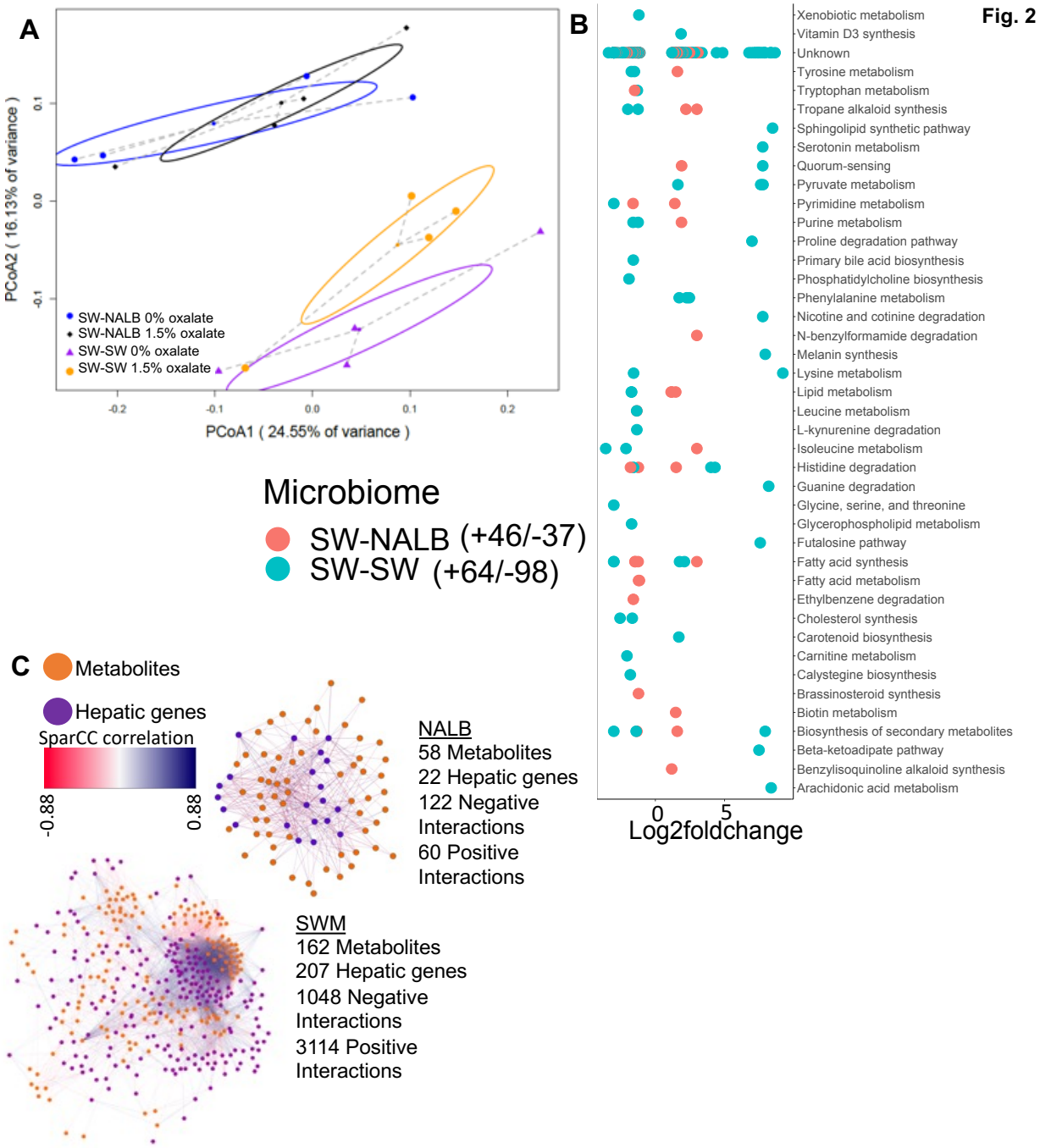

1089
1090
1091
1092 Fig. 2. Oxalate exposure impacted microbial metabolic activity in a microbiota
1093 dependent fashion. A) PCoA of protein normalized, log-transformed metabolomic data.
1094 p=0.001 for microbiome composition, p=0.1 for dietary oxalate content, p=0.3 in 2-way
1095 analysis; 2-way PERMANOVA. B) Total number of fecal metabolites significantly
1096 stimulated or inhibited by dietary oxalate. Significant metabolites are plotted by
1097 Log2FoldChange. Positive values reflect metabolites increased with oxalate exposure

1098 and negative values are metabolites decreased with exposure. FDR < 0.05, Mann-
1099 Whitney U or Fisher's exact test. Metabolites are annotated to pathway (Kegg, Uniprot,
1100 PubChem, Metacyc) the total number of metabolites that exhibit a positive or negative
1101 shift with oxalate exposure are listed in the legend. Complete list is in Table S3. C)
1102 Change in the host-microbe interaction network upon exposure to oxalate, quantified as
1103 hepatic gene-microbe metabolite correlations R > +/- 0.3 and FDR < 0.05 with SparCC,
1104 visualized in Cytoscape. All host-microbe interactions are listed in Table S4.
1105

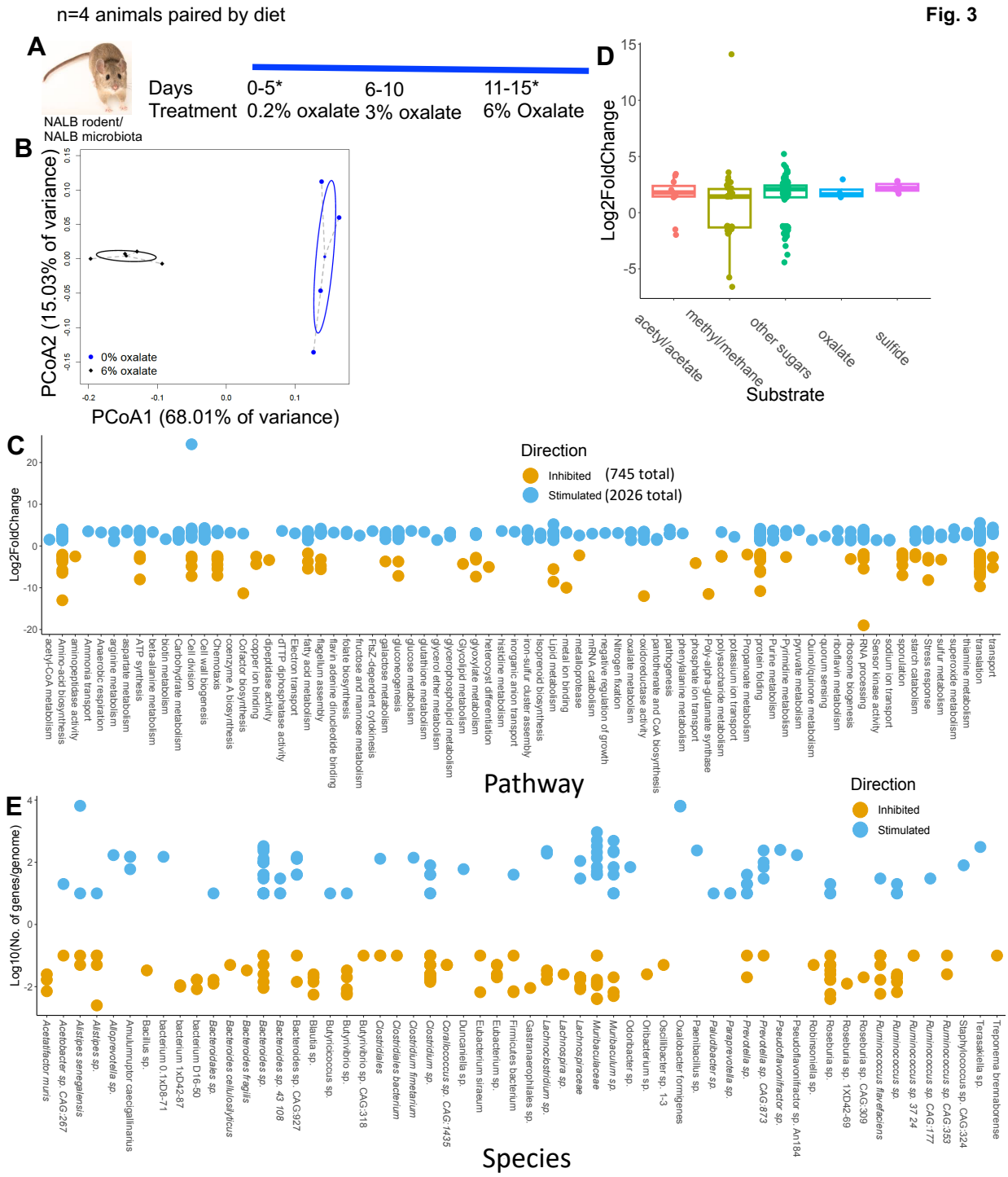

Fig. 3. Oxalate exposure stimulates taxonomically diverse microorganisms, with a few strains that dominate the response. A) *Neotoma albigula* with native microbiota were given increasing amounts of dietary oxalate up to 6% w/w. *indicates sampling

1112 timepoints. B) PCoA of normalized metagenomic data. p=0.02; PERMANOVA. C) Total
1113 number of microbial genes significantly stimulated or inhibited by dietary oxalate,
1114 annotated to pathway (Kegg, UniProt, PubChem, Metacyc) and listed by
1115 Log2FoldChange. The total number of genes stimulated or inhibited by oxalate are
1116 listed in the legend. Genes with unknown annotation are not listed. The complete list of
1117 annotated genes is listed in Table S5. D) Number of significantly differentiated genes
1118 involved in oxalate degradation, sulfate reduction, acetogenic, methanogenic, or sugar
1119 metabolic pathways or utilization of by-products of those pathways stimulated (positive)
1120 or inhibited (negative) by dietary oxalate. Genes are listed by their Log2FoldChange
1121 between no and high oxalate diets. FDR < 0.05, Wald test. E) The number of
1122 genes/genome significantly altered by oxalate, mapped to microbial genomes extracted
1123 from *N. albigula.* Number of genes/genomes are log10-transformed to show the
1124 distribution more clearly. A total of 92% of genomes had at least one significantly
1125 altered gene population mapped to them.
1126
1127
1128
1129
1130
1131

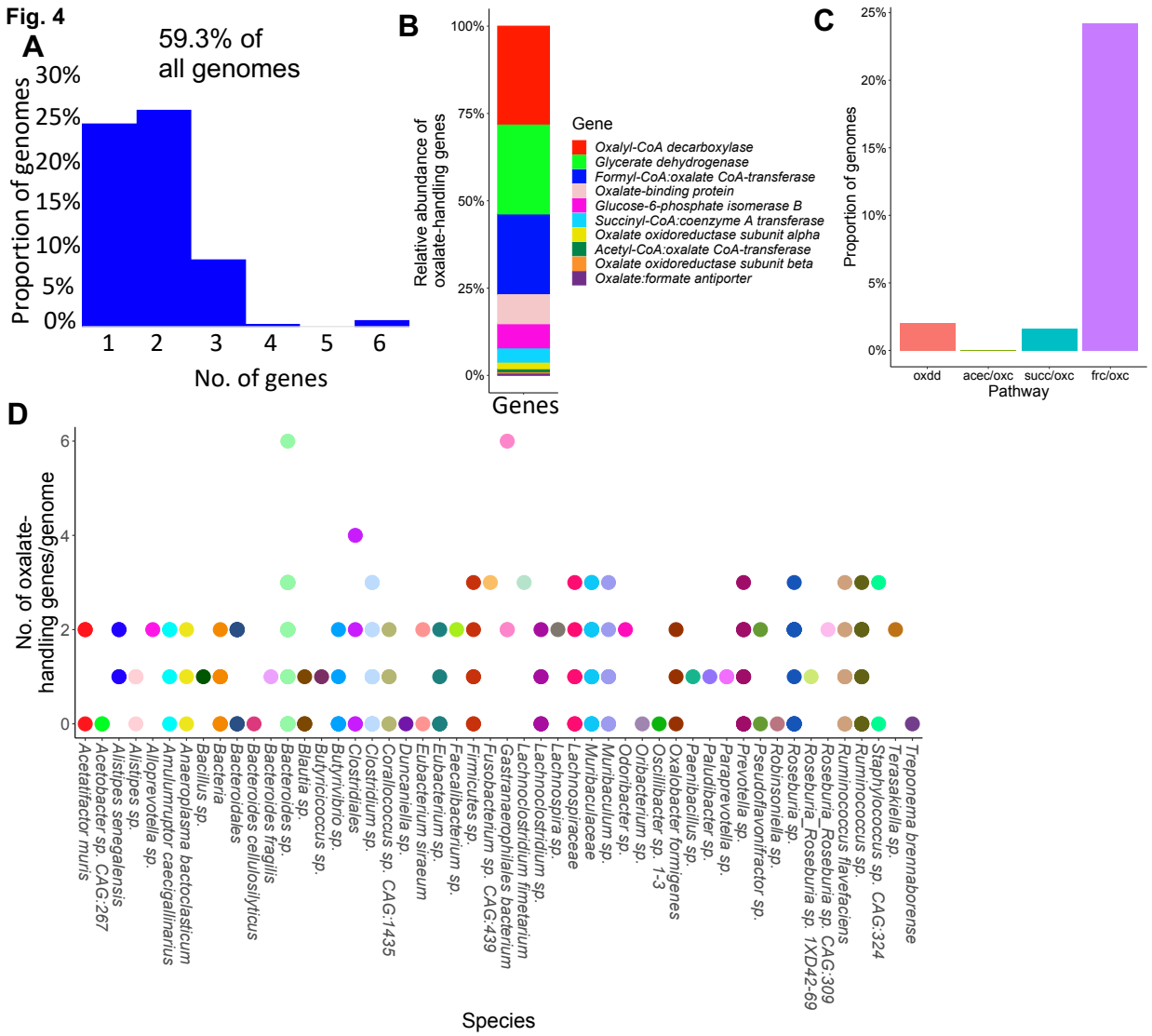

Fig. 4. Genes related to the metabolism or handling of oxalate are present in >50% of 248 full length NALB microbial genomes from the gut. A) Proportion of the genomes extracted from *N. albigula* that had at least one oxalate-related gene. B) Relative distribution of oxalate-handling genes by gene function. C) Proportion of genomes that have a complete pathway for oxalate degradation, specifically. oxdd=oxalate oxidoreductase; acec=acetyl-CoA:oxalate CoA-transferase; oxc=Oxalyl-CoA decarboxylase; succ=succinyl-CoA:coenzyme A transferase; frc=Formyl-CoA transferase; D) Number of oxalate-handling genes by genome.

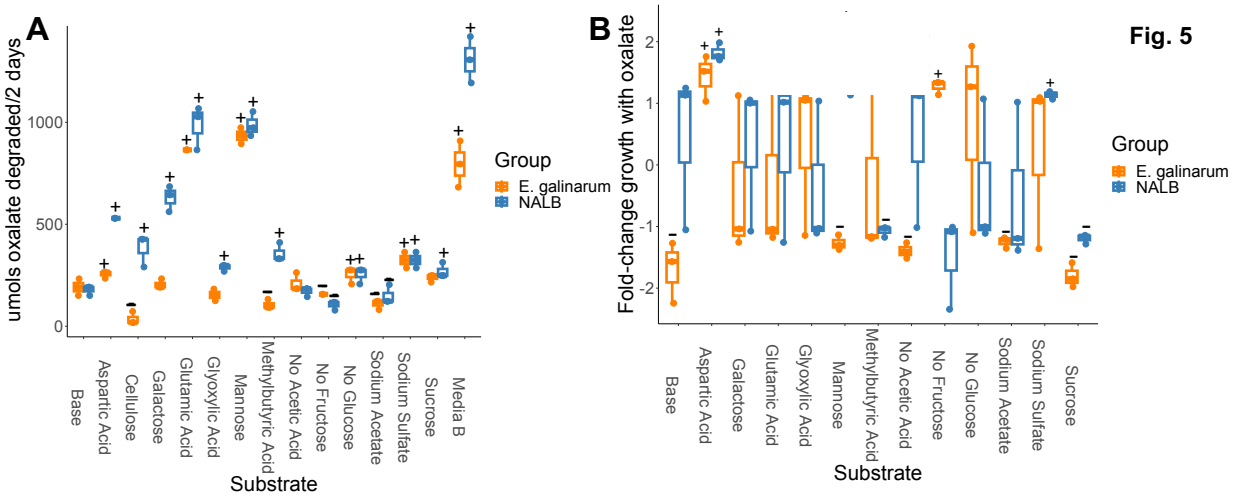

Fig. 5

C

Substrate	No. of Isolates	% of Community
Oxalate	70	14.58%
Cellulose	68	14.17%
Sucrose	65	13.54%
D-Glucose	45	9.38%
Aspartic acid	38	7.92%
Galactose	19	3.96%
Formate	16	1.67%
Mannose	12	1.25%
Fructose	10	1.04%
Acetate	7	0.73%
Methylvaric/ butyric acid	4	0.42%
Glutamic acid	1	0.10%

D

Group	Substrate usage	Metabolic cohort	Taxonomic cohort	% of studies
All, No_ox	Fructose	Ruminococcus sp.	Lactobacillus helveticus	71%
All, No_ox	Galactose	Bacteroides acidofaciens	Lactobacillus helveticus	71%
All, No_ox	Sucrose	Bacteroides acidofaciens	Bacteroides thetaiotaomicron	86%
All, No_ox, Ox_form	Formate	Enterobacter sp.	Desulfovibrio piger, Methanobrevibacter smithii, Ruminococcus gnavus	71%, 71%, 86%
All, Ox, Ox_form	Oxalate	Bacteroides vulgatus	Oxalobacter formgienes	86%
All, No_ox	Glucose	Bacteroides vulgatus	Coprococcus comes	100%
All, No_ox	Mannose	Bacteroides acidofaciens	Lactobacillus plantarum	71%
All, No_ox	Methyl	Bacteroides dorei	Bacteroides thetaiotaomicron	86%
All, No_ox	Acetate	Bacteroides dorei	Bacteroides thetaiotaomicron	86%
All, No_ox	Aspartic	Bacteroides dorei	Bacteroides thetaiotaomicron	86%

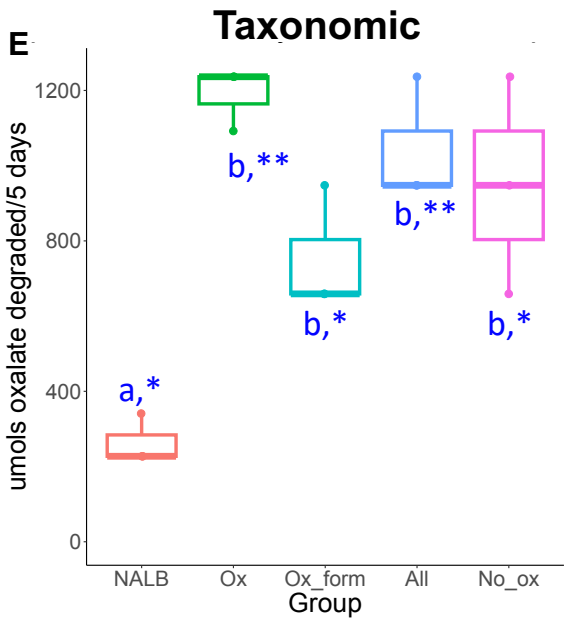

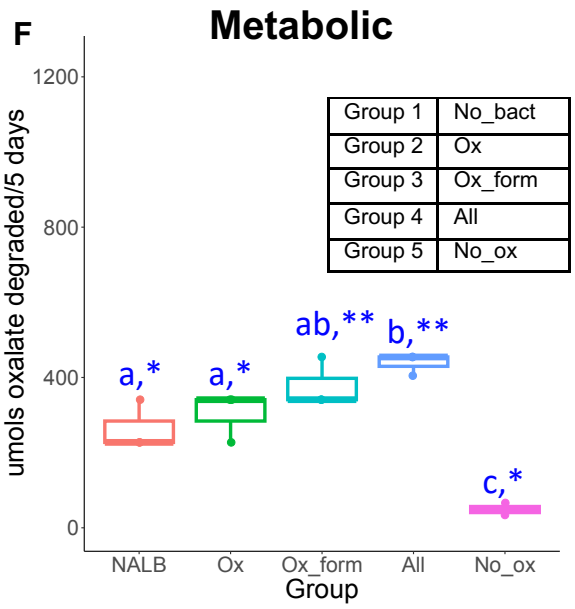

1148 Fig. 5. Microbial community composition and available substrates impact oxalate
1149 metabolism and the impact of oxalate on growth. A) Substrates associated with
1150 metabolic pathways enriched by exposure to dietary oxalate *in vivo* differentially impact
1151 oxalate metabolism. $p<0.001$ in one-way and two-way ANOVA against bacterial group
1152 and substrate; +/- reflects $p<0.05$, Holm's-corrected, pairwise t-test compared to base
1153 media for an increase (+) or decrease (-) in oxalate degradation. B) Substrates
1154 differentially impact the influence of oxalate on microbial growth; $p<0.001$ in two-way
1155 ANOVA against substrate and bacterial group, and one-way analysis against substrate;
1156 +/- reflects $p<0.05$, Holm's-corrected, one-sample t-test compared 0 (no impact of
1157 oxalate) for an increase (+) or decrease (-) in growth due to oxalate exposure. The
1158 impact of oxalate on growth was not calculated for cellulose or Media B. C) Culture-
1159 based means to quantify proportion of the NALB community that can use substrates
1160 identified through shotgun metagenomics as sole carbon and energy sources. D)
1161 Defined microbial communities to assess oxalate metabolism *in vitro* and *in vivo*. Listed
1162 are the microbial consortia, which substrate the microbes utilize that corresponds to the
1163 shotgun metagenomic data, taxonomic classification of microorganisms used in the two
1164 cohorts, and the proportion of studies in which microorganisms in the taxonomic cohort
1165 were stimulated by oxalate exposure. E,F) Oxalate metabolism in minimal media with
1166 20mM oxalate from the microbial communities listed in 5D, in comparison to the NALB
1167 community. $p<0.001$, ANOVA comparing microbial groups. *$p<0.05$, **$p<0.01$;
1168 ***$p<0.001$; Holm's corrected, one sample t-tests against 0 (no oxalate metabolism).
1169 Blue letters reflect statistical groups between microbial groups for oxalate metabolism.
1170
1171

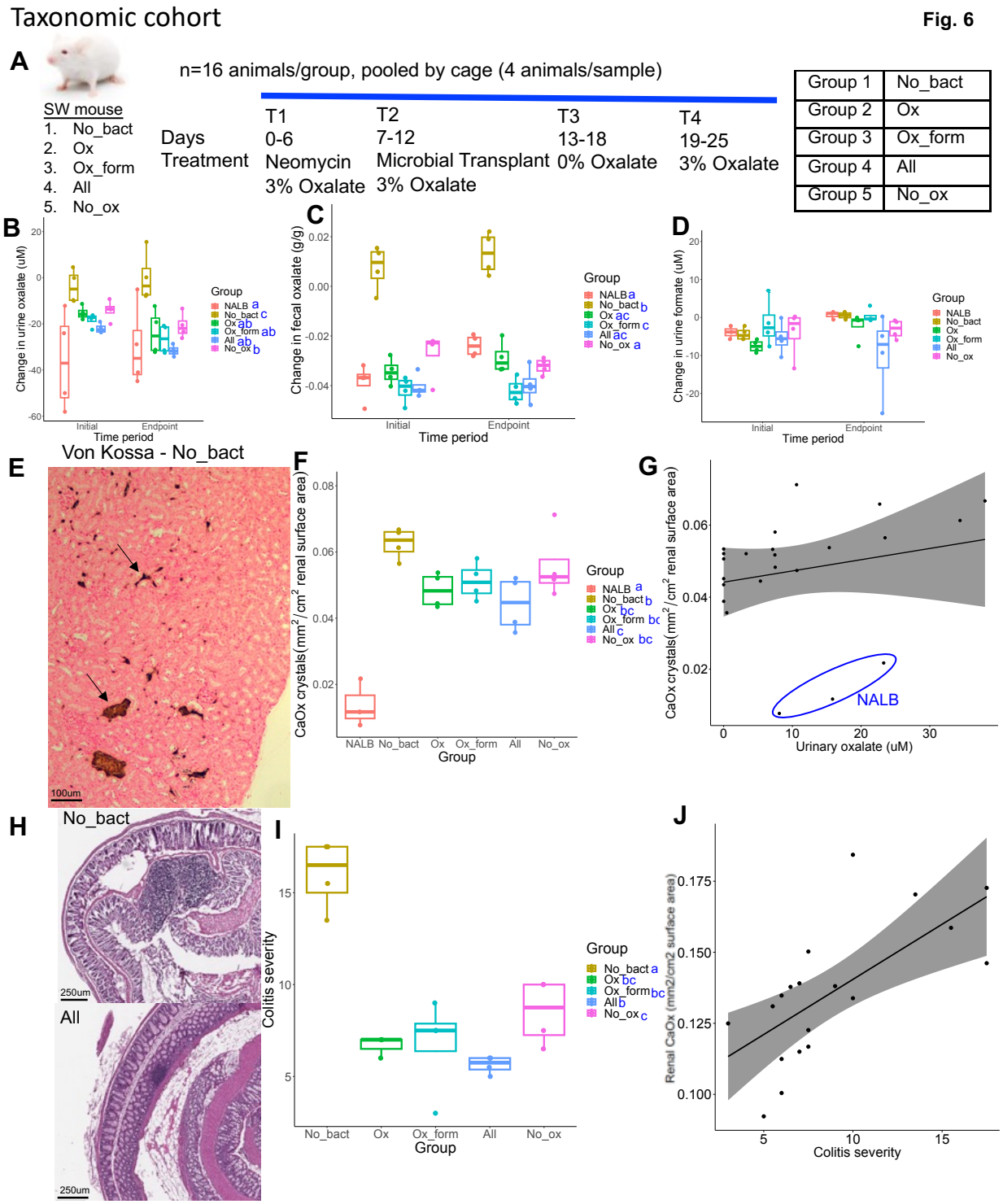

Fig. 6. Microbial community composition (taxonomic cohort) impacted the effect of exogenous oxalate on host health. A) Swiss Webster mice were given neomycin, followed by inoculation of microbial consortia that included either no bacteria or the taxonomic cohort listed in Figure 5C. B,C) The effect of microbial transplants on urinary (B) or fecal (C) oxalate levels over the course of the diet trial, compared to baseline.

ANOVA $p<0.001$ for microbial group, but was not significant by timeperiod or 2-way analyses for both B & C. D) The effect of microbial transplants on urinary formate levels over the course of the diet trial, compared to baseline. ANOVA was not significant in one-way and two-way analyses. E) Renal calcium oxalate deposition. Arrows show stained calcium deposits, which were quantified through an automated algorithm in QuPath. F) Quantification of renal calcium oxalate deposition by group. $p<0.001$, ANOVA. Blue letters reflect statistical groups between microbial groups for renal calcification by Holm's corrected paired t-tests. G) Pearson correlation between urinary oxalate and renal calcium oxalate deposition. $R=0.22$, $p=0.32$ with NALB samples included (blue circle); $R=0.7$, $p=0.001$ excluding the NALB group. H) Representative colon tissues from the No_bact (Group 1) and All (Group 4) groups, exhibiting high and low colitis severity scores, respectively. Tissues were stained with hematoxylin and eosin and scored based on standardized, multifactorial metrics. I) Quantification of colitis severity by group. $p<0.001$, ANOVA. Blue letters reflect statistical groups between microbial groups for renal calcification by Holm's corrected paired t-tests. J) Pearson correlation between colitis severity and renal calcium oxalate deposition. $R=0.7$, $p=0.002$. Colitis severity was not quantified for the NALB group.

Fig. 7

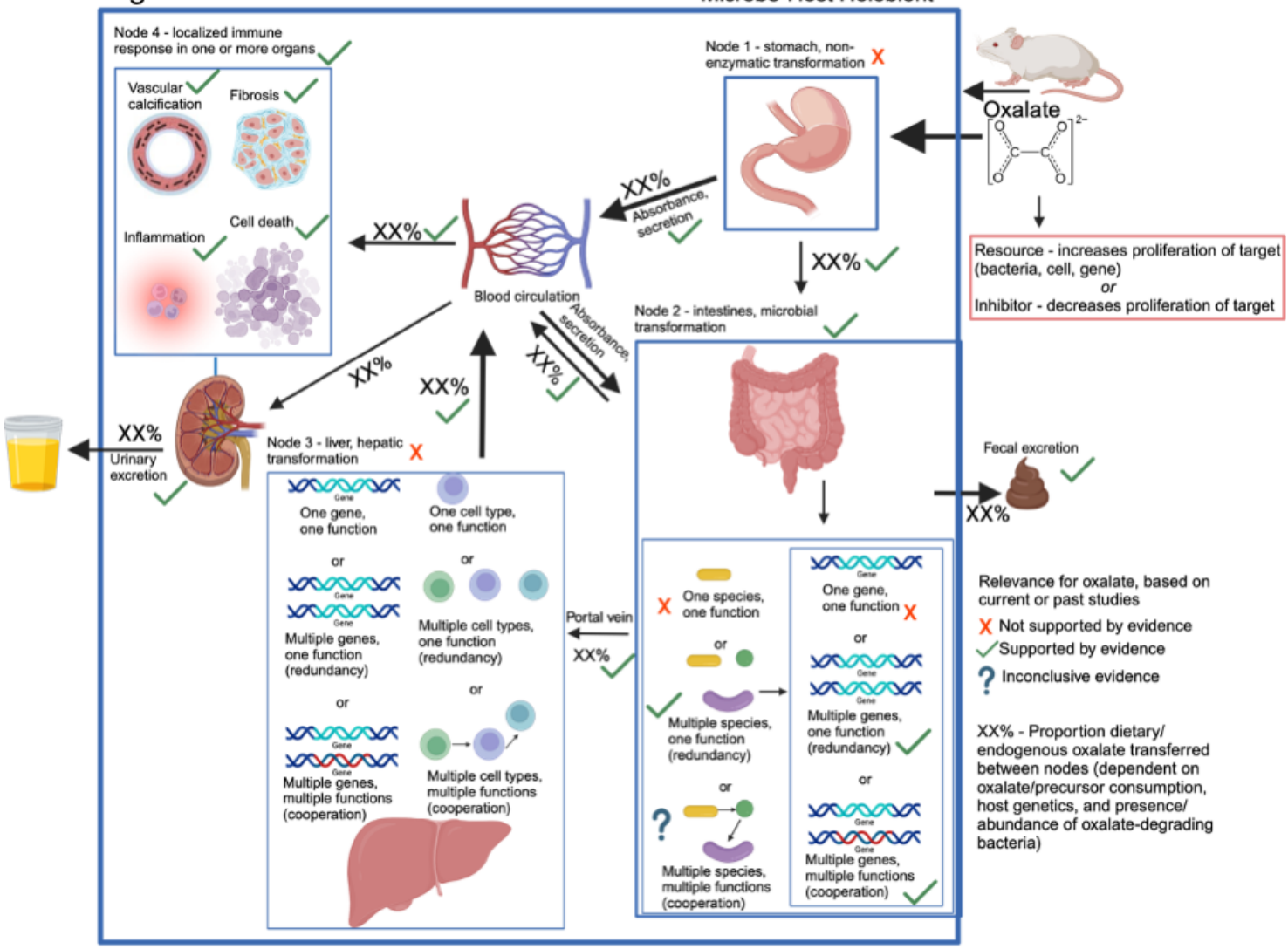

Fig. 7 Model of oxalate-host-microbiome interactions, based on experiments here. Model starts in the top left and proceeds along arrows through fecal or urinary excretion. Included in the model are the processing nodes, the potential hypotheses on cooperative vs. redundant functions, and which hypotheses our data favor or refute. Red x's are hypotheses refuted by our data, green arrows are those confirmed by our data, and question marks reflect hypotheses where evidence is inconclusive.

References

1. Gomaa, E.Z. (2020). Human gut microbiota/microbiome in health and diseases: a review. Antonie Van Leeuwenhoek *113*, 2019-2040.
2. Cox, T.O., Lundgren, P., Nath, K., and Thaiss, C.A. (2022). Metabolic control by the microbiome. Genome Medicine *14*, 80.
3. Turnbaugh, P.J., Ley, R.E., Hamady, M., Fraser-Liggett, C.M., Knight, R., and Gordon, J.I. (2007). The human microbiome project. Nature *449*, 804-810.
4. Lloyd-Price, J., Mahurkar, A., Rahnavard, G., Crabtree, J., Orvis, J., Hall, A.B., Brady, A., Creasy, H.H., McCracken, C., and Giglio, M.G. (2017). Strains, functions and dynamics in the expanded Human Microbiome Project. Nature *550*, 61-66.
5. Wang, J., and Jia, H. (2016). Metagenome-wide association studies: fine-mining the microbiome. Nature Reviews Microbiology *14*, 508-522.
6. Tang, W.W., and Hazen, S.L. (2024). Unraveling the Complex Relationship Between Gut Microbiome and Cardiovascular Diseases. Circulation *149*, 1543-1545.
7. de Vos, W.M., and de Vos, E.A. (2012). Role of the intestinal microbiome in health and disease: from correlation to causation. Nutrition reviews *70*, S45-S56.
8. De Vos, W.M., Tilg, H., Van Hul, M., and Cani, P.D. (2022). Gut microbiome and health: mechanistic insights. Gut *71*, 1020-1032.
9. Zimmermann, M., Patil, K.R., Typas, A., and Maier, L. (2021). Towards a mechanistic understanding of reciprocal drug–microbiome interactions. Molecular systems biology *17*, e10116.
10. Vujkovic-Cvijin, I., Sklar, J., Jiang, L., Natarajan, L., Knight, R., and Belkaid, Y. (2020). Host variables confound gut microbiota studies of human disease. Nature *587*, 448-454.
11. Walter, J., Armet, A.M., Finlay, B.B., and Shanahan, F. (2020). Establishing or exaggerating causality for the gut microbiome: lessons from human microbiota-associated rodents. Cell *180*, 221-232.
12. Barkhidarian, B., Roldos, L., Iskandar, M.M., Saedisomeolia, A., and Kubow, S. (2021). Probiotic supplementation and micronutrient status in healthy subjects: A systematic review of clinical trials. Nutrients *13*, 3001.
13. Rogers, N.J., and Mousa, S.A. (2012). The shortcomings of clinical trials assessing the efficacy of probiotics in irritable bowel syndrome. The Journal of Alternative and Complementary Medicine *18*, 112-119.
14. Ceccherini, C., Daniotti, S., Bearzi, C., and Re, I. (2022). Evaluating the efficacy of probiotics in IBS treatment using a systematic review of clinical trials and multi-criteria decision analysis. Nutrients *14*, 2689.
15. Batagello, C.A., Monga, M., and Miller, A.W. (2018). Calcium oxalate urolithiasis: a case of missing microbes? Journal of endourology *32*, 995-1005.
16. Foster, J.A., Krone, S.M., and Forney, L.J. (2008). Application of ecological network theory to the human microbiome. Interdisciplinary perspectives on infectious diseases *2008*, 839501.
17. Layeghifard, M., Hwang, D.M., and Guttman, D.S. (2017). Disentangling interactions in the microbiome: a network perspective. Trends in microbiology *25*, 217-228.

18. Ridenhour, B.J., Brooker, S.L., Williams, J.E., Van Leuven, J.T., Miller, A.W., Dearing, M.D., and Remien, C.H. (2017). Modeling time-series data from microbial communities. The ISME journal *11*, 2526.
19. Kumar, M., Ji, B., Zengler, K., and Nielsen, J. (2019). Modelling approaches for studying the microbiome. Nature microbiology *4*, 1253-1267.
20. Richardson, L.A. (2017). Evolving as a holobiont. PLoS biology *15*, e2002168.
21. Foster, K.R., Schluter, J., Coyte, K.Z., and Rakoff-Nahoum, S. (2017). The evolution of the host microbiome as an ecosystem on a leash. Nature *548*, 43-51.
22. Palla, G., Derényi, I., Farkas, I., and Vicsek, T. (2005). Uncovering the overlapping community structure of complex networks in nature and society. nature *435*, 814-818.
23. Lambiotte, R., Rosvall, M., and Scholtes, I. (2019). From networks to optimal higher-order models of complex systems. Nature physics *15*, 313-320.
24. Cohen, A.A., Ferrucci, L., Fülöp, T., Gravel, D., Hao, N., Kriete, A., Levine, M.E., Lipsitz, L.A., Olde Rikkert, M.G., and Rutenberg, A. (2022). A complex systems approach to aging biology. Nature Aging *2*, 580-591.
25. Torres, L., Blevins, A.S., Bassett, D., and Eliassi-Rad, T. (2021). The why, how, and when of representations for complex systems. SIAM Review *63*, 435-485.
26. Roediger, W. (1980). Role of anaerobic bacteria in the metabolic welfare of the colonic mucosa in man. Gut *21*, 793-798.
27. Javorka, M., Czippelova, B., Turianikova, Z., Lazarova, Z., Tonhajzerova, I., and Faes, L. (2017). Causal analysis of short-term cardiovascular variability: state-dependent contribution of feedback and feedforward mechanisms. Medical & biological engineering & computing *55*, 179-190.
28. Kolodziejczyk, A.A., Zheng, D., and Elinav, E. (2019). Diet–microbiota interactions and personalized nutrition. Nature Reviews Microbiology *17*, 742-753.
29. Crivelli, J.J., Mitchell, T., Knight, J., Wood, K.D., Assimos, D.G., Holmes, R.P., and Fargue, S. (2021). Contribution of Dietary Oxalate and Oxalate Precursors to Urinary Oxalate Excretion. Nutrients *13*, 62.
30. Holmes, R.P., Goodman, H.O., and Assimos, D.G. (2001). Contribution of dietary oxalate to urinary oxalate excretion. Kidney international *59*, 270-276.
31. Cochat, P., and Rumsby, G. (2013). Primary hyperoxaluria. New England Journal of Medicine *369*, 649-658.
32. Hodgkinson, A. (1977). Oxalic acid in biology and medicine. London—New York.
33. Allison, M.J., Dawson, K.A., Mayberry, W.R., and Foss, J.G. (1985). Oxalobacter formigenes gen. nov., sp. nov.: oxalate-degrading anaerobes that inhabit the gastrointestinal tract. Archives of Microbiology *141*, 1-7.
34. Miller, A.W., and Dearing, D. (2013). The metabolic and ecological interactions of oxalate-degrading bacteria in the mammalian gut. Pathogens *2*, 636-652.
35. Liu, M., Devlin, J.C., Hu, J., Volkova, A., Battaglia, T.W., Ho, M., Asplin, J.R., Byrd, A., Loke, P.n., and Li, H. (2021). Microbial genetic and transcriptional contributions to oxalate degradation by the gut microbiota in health and disease. Elife *10*, e63642.
36. Tang, W.W., Wang, Z., Kennedy, D.J., Wu, Y., Buffa, J.A., Agatisa-Boyle, B., Li, X.S., Levison, B.S., and Hazen, S.L. (2015). Gut microbiota-dependent trimethylamine N-oxide (TMAO) pathway contributes to both development of renal insufficiency and mortality risk in chronic kidney disease. Circulation research *116*, 448-455.

1291 37. Nazzal, L., Francois, F., Henderson, N., Liu, M., Li, H., Koh, H., Wang, C., Gao, Z.,
1292 Perez, G.P., and Asplin, J.R. (2021). Effect of antibiotic treatment on Oxalobacter
1293 formigenes colonization of the gut microbiome and urinary oxalate excretion. Scientific
1294 Reports *11*, 16428.
1295 38. Miller, A.W., Orr, T., Dearing, D., and Monga, M. (2019). Loss of function dysbiosis
1296 associated with antibiotics and high fat, high sugar diet. The ISME journal *13*, 1379-
1297 1390.
1298 39. Kharlamb, V., Schelker, J., Francois, F., Jiang, J., Holmes, R.P., and Goldfarb, D.S.
1299 (2011). Oral antibiotic treatment of Helicobacter pylori leads to persistently reduced
1300 intestinal colonization rates with Oxalobacter formigenes. Journal of Endourology *25*,
1301 1781-1785.
1302 40. Lange, J.N., Wood, K.D., Wong, H., Otto, R., Mufarrij, P.W., Knight, J., Akpinar, H.,
1303 Holmes, R.P., and Assimos, D.G. (2012). Sensitivity of human strains of Oxalobacter
1304 formigenes to commonly prescribed antibiotics. Urology *79*, 1286-1289.
1305 41. Mittal, R., Kumar, R., Bid, H., and Mittal, B. (2005). Effect of antibiotics on Oxalobacter
1306 formigenes colonization of human gastrointestinal tract. Journal of endourology *19*, 102-
1307 106.
1308 42. Mulay, S.R., Kulkarni, O.P., Rupanagudi, K.V., Migliorini, A., Darisipudi, M.N.,
1309 Vilaysane, A., Muruve, D., Shi, Y., Munro, F., and Liapis, H. (2012). Calcium oxalate
1310 crystals induce renal inflammation by NLRP3-mediated IL-1β secretion. The Journal of
1311 clinical investigation *123*.
1312 43. Peerapen, P., and Thongboonkerd, V. (2011). Effects of calcium oxalate monohydrate
1313 crystals on expression and function of tight junction of renal tubular epithelial cells.
1314 Laboratory Investigation *91*, 97.
1315 44. Peerapen, P., and Thongboonkerd, V. (2021). Calcium oxalate monohydrate crystal
1316 disrupts tight junction via F-actin reorganization. Chem Biol Interact *345*, 109557.
1317 10.1016/j.cbi.2021.109557.
1318 45. Holmes, R.P., Knight, J., and Assimos, D.G. (2016). Lowering urinary oxalate excretion
1319 to decrease calcium oxalate stone disease. Urolithiasis *44*, 27-32. 10.1007/s00240-015-
1320 0839-4.
1321 46. Nazzal, L., Puri, S., and Goldfarb, D.S. (2015). Enteric hyperoxaluria: an important cause
1322 of end-stage kidney disease. Nephrology Dialysis Transplantation *31*, 375-382.
1323 47. Waikar, S.S., Srivastava, A., Palsson, R., Shafi, T., Hsu, C.-y., Sharma, K., Lash, J.P.,
1324 Chen, J., He, J., and Lieske, J. (2019). Association of urinary oxalate excretion with the
1325 risk of chronic kidney disease progression. JAMA internal medicine *179*, 542-551.
1326 48. Castellaro, A.M., Tonda, A., Cejas, H.H., Ferreyra, H., Caputto, B.L., Pucci, O.A., and
1327 Gil, G.A. (2015). Oxalate induces breast cancer. BMC Cancer *15*, 761. 10.1186/s12885-
1328 015-1747-2.
1329 49. Liu, Y., Zhao, Y., Shukha, Y., Lu, H., Wang, L., Liu, Z., Liu, C., Zhao, Y., Wang, H.,
1330 Zhao, G., et al. (2021). Dysregulated oxalate metabolism is a driver and therapeutic target
1331 in atherosclerosis. Cell Rep *36*, 109420. 10.1016/j.celrep.2021.109420.
1332 50. Efe, O., Verma, A., and Waikar, S.S. (2019). Urinary oxalate as a potential mediator of
1333 kidney disease in diabetes mellitus and obesity. Curr Opin Nephrol Hypertens *28*, 316-
1334 320. 10.1097/MNH.0000000000000515.
1335 51. James, L.F., and Butcher, J.E. (1972). Halogeton poisoning of sheep: effect of high level
1336 oxalate intake. Journal of animal science *35*, 1233-1238.

1337 52. Anantharam, V., Allison, M.J., and Maloney, P.C. (1989). Oxalate:formate exchange.
1338 The basis for energy coupling in Oxalobacter. J Biol Chem *264*, 7244-7250.
1339 53. Baetz, A.L., and Allison, M.J. (1989). Purification and characterization of oxalyl-
1340 coenzyme A decarboxylase from Oxalobacter formigenes. Journal of bacteriology *171*,
1341 2605-2608.
1342 54. Baetz, A.L., and Allison, M.J. (1990). Purification and characterization of formyl-
1343 coenzyme A transferase from Oxalobacter formigenes. Journal of bacteriology *172*,
1344 3537-3540.
1345 55. Ariceta, G., Collard, L., Abroug, S., Moochhala, S.H., Gould, E., Boussetta, A., Ben
1346 Hmida, M., De, S., Hunley, T.E., and Jarraya, F. (2023). ePHex: a phase 3, double-blind,
1347 placebo-controlled, randomized study to evaluate long-term efficacy and safety of
1348 Oxalobacter formigenes in patients with primary hyperoxaluria. Pediatric Nephrology *38*,
1349 403-415.
1350 56. Dearing, M.D., and Weinstein, S.B. (2022). Metabolic enabling and detoxification by
1351 mammalian gut microbes. Annual Review of Microbiology *76*, 579-596.
1352 57. Kohl, K.D., Weiss, Robert B., Cox, James, Dale, Colin, Dearing, M. Denise (2014). Gut
1353 microbes of mammalian herbivores facillitate intake of plant toxins. Ecology letters *17*,
1354 1238-1246.
1355 58. Grant, D. (1991). Detoxification pathways in the liver. Journal of inherited metabolic
1356 disease *14*, 421-430.
1357 59. Robertson, W., and Peacock, M. (1980). The cause of idiopathic calcium stone disease:
1358 hypercalciuria or hyperoxaluria? Nephron *26*, 105-110.
1359 60. Nishizawa, Y., Miyata, S., Tosaka, M., Hirasawa, E., Hosoda, Y., Horimoto, A., Omae,
1360 K., Ito, K., Nagano, N., and Hoshino, J. (2023). Serum oxalate concentration is associated
1361 with coronary artery calcification and cardiovascular events in Japanese dialysis patients.
1362 Scientific Reports *13*, 18558.
1363 61. Fishbein, G.A., Micheletti, R.G., Currier, J.S., Singer, E., and Fishbein, M.C. (2008).
1364 Atherosclerotic oxalosis in coronary arteries. Cardiovascular Pathology *17*, 117-123.
1365 62. Frandsen, H.B., Sørensen, J.C., Jensen, S.K., Markedal, K.E., Joehnke, M.S., Maribo, H.,
1366 Sørensen, S., and Sørensen, H. (2019). Non-enzymatic transformations of dietary 2-
1367 hydroxyalkenyl and aromatic glucosinolates in the stomach of monogastrics. Food
1368 chemistry *291*, 77-86.
1369 63. Daniel, S.L., Moradi, L., Paiste, H., Wood, K.D., Assimos, D.G., Holmes, R.P., Nazzal,
1370 L., Hatch, M., and Knight, J. (2021). Forty years of Oxalobacter formigenes, a gutsy
1371 oxalate-degrading specialist. Applied and Environmental Microbiology *87*, e00544-
1372 00521.
1373 64. Turroni, S., Bendazzoli, C., Dipalo, S.C., Candela, M., Vitali, B., Gotti, R., and Brigidi,
1374 P. (2010). Oxalate-degrading activity in Bifidobacterium animalis subsp. lactis: impact of
1375 acidic conditions on the transcriptional levels of the oxalyl coenzyme A (CoA)
1376 decarboxylase and formyl-CoA transferase genes. Applied and environmental
1377 microbiology *76*, 5609-5620.
1378 65. Turroni, S., Vitali, B., Bendazzoli, C., Candela, M., Gotti, R., Federici, F., Pirovano, F.,
1379 and Brigidi, P. (2007). Oxalate consumption by lactobacilli: evaluation of oxalyl-CoA
1380 decarboxylase and formyl-CoA transferase activity in Lactobacillus acidophilus. Journal
1381 of applied microbiology *103*, 1600-1609.

66. Belenguer, A., Bati, M.B., Hervás, G., Toral, P.G., Yáñez-Ruiz, D.R., and Frutos, P. (2013). Impact of oxalic acid on rumen function and bacterial community in sheep. animal *7*, 940-947.
67. Miller, A.W., Choy, D., Penniston, K.L., and Lange, D. (2019). Inhibition of urinary stone disease by a multi-species bacterial network ensures healthy oxalate homeostasis. Kidney international.
68. Miller, A.W., Dale, C., and Dearing, M.D. (2017). Microbiota Diversification and Crash Induced by Dietary Oxalate in the Mammalian Herbivore Neotoma albigula. mSphere *2*. 10.1128/mSphere.00428-17.
69. Miller, A.W., Dale, C., and Dearing, M.D. (2017). The Induction of Oxalate Metabolism In Vivo Is More Effective with Functional Microbial Communities than with Functional Microbial Species. MSystems *2*, e00088-00017.
70. Miller, A.W., Kohl, K.D., and Dearing, M.D. (2014). The gastrointestinal tract of the white-throated woodrat (Neotoma albigula) harbors distinct consortia of oxalate-degrading bacteria. Applied and environmental microbiology *80*, 1595-1601.
71. Miller, A.W., Oakeson, K.F., Dale, C., and Dearing, M.D. (2016). Effect of Dietary Oxalate on the Gut Microbiota of the Mammalian Herbivore Neotoma albigula. Applied and environmental microbiology *82*, 2669-2675.
72. Miller, A.W., Oakeson, K.F., Dale, C., and Dearing, M.D. (2016). Microbial community transplant results in increased and long-term oxalate degradation. Microbial ecology *72*, 470-478.
73. Drake, H.L. (2012). Acetogenesis (Springer Science & Business Media).
74. Asanuma, N., Iwamoto, M., and Hino, T. (1999). The production of formate, a substrate for methanogenesis, from compounds related with the glyoxylate cycle by mixed ruminal microbes. Nihon Chikusan Gakkaiho *70*, 67-73.
75. Ferry, J.G. (2012). Methanogenesis: ecology, physiology, biochemistry & genetics (Springer Science & Business Media).
76. Oremland, R.S., and Polcin, S. (1982). Methanogenesis and sulfate reduction: competitive and noncompetitive substrates in estuarine sediments. Applied and Environmental Microbiology *44*, 1270-1276.
77. Freel, R.W., Hatch, M., Green, M., and Soleimani, M. (2006). Ileal oxalate absorption and urinary oxalate excretion are enhanced in Slc26a6 null mice. American Journal of Physiology-Gastrointestinal and Liver Physiology *290*, G719-G728.
78. Hatch, M., and Freel, R.W. (2008). The roles and mechanisms of intestinal oxalate transport in oxalate homeostasis. In 2. (Elsevier), pp. 143-151.
79. Dancygier, H., and Dancygier, H. (2010). Hepatic biotransformation. Clinical Hepatology: Principles and Practice of Hepatobiliary Diseases, 127-130.
80. Kohl, K.D., and Dearing, M.D. (2011). Induced and constitutive responses of digestive enzymes to plant toxins in an herbivorous mammal. Journal of Experimental Biology *214*, 4133-4140.
81. Kohl, K.D., and Dearing, M.D. (2016). The woodrat gut microbiota as an experimental system for understanding microbial metabolism of dietary toxins. Frontiers in microbiology *7*, 1165.
82. Hatch, M., Cornelius, J., Allison, M., Sidhu, H., Peck, A., and Freel, R. (2006). Oxalobacter sp. reduces urinary oxalate excretion by promoting enteric oxalate secretion. Kidney international *69*, 691-698.

1428 83. Hatch, M., and Freel, R.W. (2013). A human strain of Oxalobacter (HC-1) promotes
1429 enteric oxalate secretion in the small intestine of mice and reduces urinary oxalate
1430 excretion. Urolithiasis *41*, 379-384.
1431 84. Justice, K.E. (1985). Oxalate digestibility in Neotoma albigula and Neotoma mexicana.
1432 Oecologia *67*, 231-234.
1433 85. Kohl, K.D., Miller, A.W., Marvin, J.E., Mackie, R., and Dearing, M.D. (2014).
1434 Herbivorous rodents (Neotoma spp.) harbour abundant and active foregut microbiota.
1435 Environmental microbiology *16*, 2869-2878.
1436 86. Koppel, N., Maini Rekdal, V., and Balskus, E.P. (2017). Chemical transformation of
1437 xenobiotics by the human gut microbiota. Science *356*. 10.1126/science.aag2770.
1438 87. Strzelecki, T., and Menon, M. (1986). The uptake of oxalate by rat liver and kidney
1439 mitochondria. J Biol Chem *261*, 12197-12201.
1440 88. Ormerod, K.L., Wood, D.L.A., Lachner, N., Gellatly, S.L., Daly, J.N., Parsons, J.D.,
1441 Dal'Molin, C.G.O., Palfreyman, R.W., Nielsen, L.K., Cooper, M.A., et al. (2016).
1442 Genomic characterization of the uncultured Bacteroidales family S24-7 inhabiting the
1443 guts of homeothermic animals. Microbiome *4*, 1-17. 10.1186/s40168-016-0181-2.
1444 89. Okuda, S., Yamada, T., Hamajima, M., Itoh, M., Katayama, T., Bork, P., Goto, S., and
1445 Kanehisa, M. (2008). KEGG Atlas mapping for global analysis of metabolic pathways.
1446 Nucleic acids research *36*, W423-W426.
1447 90. Groussin, M., Poyet, M., Sistiaga, A., Kearney, S.M., Moniz, K., Noel, M., Hooker, J.,
1448 Gibbons, S.M., Segurel, L., and Froment, A. (2021). Elevated rates of horizontal gene
1449 transfer in the industrialized human microbiome. Cell *184*, 2053-2067. e2018.
1450 91. Goodman, A.L., Kallstrom, G., Faith, J.J., Reyes, A., Moore, A., Dantas, G., and Gordon,
1451 J.I. (2011). Extensive personal human gut microbiota culture collections characterized
1452 and manipulated in gnotobiotic mice. Proceedings of the National Academy of Sciences
1453 *108*, 6252-6257.
1454 92. Koelink, P.J., Wildenberg, M.E., Stitt, L.W., Feagan, B.G., Koldijk, M., van 't Wout,
1455 A.B., Atreya, R., Vieth, M., Brandse, J.F., and Duijst, S. (2018). Development of reliable,
1456 valid and responsive scoring systems for endoscopy and histology in animal models for
1457 inflammatory bowel disease. Journal of Crohn's and Colitis *12*, 794-803.
1458 93. Hughes, E.R., Winter, M.G., Duerkop, B.A., Spiga, L., de Carvalho, T.F., Zhu, W.,
1459 Gillis, C.C., Büttner, L., Smoot, M.P., and Behrendt, C.L. (2017). Microbial respiration
1460 and formate oxidation as metabolic signatures of inflammation-associated dysbiosis. Cell
1461 host & microbe *21*, 208-219.
1462 94. Pietzke, M., Meiser, J., and Vazquez, A. (2020). Formate metabolism in health and
1463 disease. Molecular metabolism *33*, 23-37.
1464 95. Ternes, D., Tsenkova, M., Pozdeev, V.I., Meyers, M., Koncina, E., Atatri, S., Schmitz,
1465 M., Karta, J., Schmoetten, M., and Heinken, A. (2022). The gut microbial metabolite
1466 formate exacerbates colorectal cancer progression. Nature metabolism *4*, 458-475.
1467 96. Kirkpatrick, C., Maurer, L.M., Oyelakin, N.E., Yoncheva, Y.N., Maurer, R., and
1468 Slonczewski, J.L. (2001). Acetate and formate stress: opposite responses in the proteome
1469 of Escherichia coli. Journal of bacteriology *183*, 6466-6477.
1470 97. Voskuhl, L., Brusilova, D., Brauer, V., and Meckenstock, R. (2022). Inhibition of sulfate-
1471 reducing bacteria with formate. FEMS Microbiology Ecology *98*, fiac003.
1472 98. Scott, K.P., Gratz, S.W., Sheridan, P.O., Flint, H.J., and Duncan, S.H. (2013). The
1473 influence of diet on the gut microbiota. Pharmacological research *69*, 52-60.

99. Doré, J., and Blottière, H. (2015). The influence of diet on the gut microbiota and its consequences for health. Current opinion in biotechnology *32*, 195-199.
100. Britton, R.A., and Young, V.B. (2014). Role of the intestinal microbiota in resistance to colonization by Clostridium difficile. Gastroenterology *146*, 1547-1553.
101. Deleu, S., Machiels, K., Raes, J., Verbeke, K., and Vermeire, S. (2021). Short chain fatty acids and its producing organisms: An overlooked therapy for IBD? EBioMedicine *66*.
102. Kelly, C.J., Zheng, L., Campbell, E.L., Saeedi, B., Scholz, C.C., Bayless, A.J., Wilson, K.E., Glover, L.E., Kominsky, D.J., and Magnuson, A. (2015). Crosstalk between microbiota-derived short-chain fatty acids and intestinal epithelial HIF augments tissue barrier function. Cell host & microbe *17*, 662-671.
103. Portincasa, P., Bonfrate, L., Vacca, M., De Angelis, M., Farella, I., Lanza, E., Khalil, M., Wang, D.Q.-H., Sperandio, M., and Di Ciaula, A. (2022). Gut microbiota and short chain fatty acids: implications in glucose homeostasis. International journal of molecular sciences *23*, 1105.
104. Shimizu, H., Masujima, Y., Ushiroda, C., Mizushima, R., Taira, S., Ohue-Kitano, R., and Kimura, I. (2019). Dietary short-chain fatty acid intake improves the hepatic metabolic condition via FFAR3. Scientific reports *9*, 1-10.
105. Tian, Y., Xu, Q., Sun, L., Ye, Y., and Ji, G. (2018). Short-chain fatty acids administration is protective in colitis-associated colorectal cancer development. The Journal of Nutritional Biochemistry *57*, 103-109.
106. Vieira, A.T., Galvão, I., Macia, L.M., Vinolo, M.A.R., Garcia, C.C., Tavares, L.P., Amaral, F.A., Sousa, L.P., Martins, F.S., and Mackay, C.R. (2017). Dietary fiber and the short-chain fatty acid acetate promote resolution of neutrophilic inflammation in a model of gout in mice. Journal of leukocyte biology *101*, 275-284.
107. Fusco, W., Lorenzo, M.B., Cintoni, M., Porcari, S., Rinninella, E., Kaitsas, F., Lener, E., Mele, M.C., Gasbarrini, A., and Collado, M.C. (2023). Short-chain fatty-acid-producing bacteria: key components of the human gut microbiota. Nutrients *15*, 2211.
108. Mann, E.R., Lam, Y.K., and Uhlig, H.H. (2024). Short-chain fatty acids: linking diet, the microbiome and immunity. Nature Reviews Immunology, 1-19.
109. Chiang, J.Y. (2009). Bile acids: regulation of synthesis: thematic review series: bile acids. Journal of lipid research *50*, 1955-1966.
110. Collins, S.L., Stine, J.G., Bisanz, J.E., Okafor, C.D., and Patterson, A.D. (2023). Bile acids and the gut microbiota: Metabolic interactions and impacts on disease. Nature Reviews Microbiology *21*, 236-247.
111. Gérard, P. (2013). Metabolism of cholesterol and bile acids by the gut microbiota. Pathogens *3*, 14-24.
112. Kohl, K.D., and Dearing, M.D. (2014). Wild-caught rodents retain a majority of their natural gut microbiota upon entrance into captivity. Environmental microbiology reports *6*, 191-195.
113. Hatch, M., Gjymishka, A., Salido, E.C., Allison, M.J., and Freel, R.W. (2011). Enteric oxalate elimination is induced and oxalate is normalized in a mouse model of primary hyperoxaluria following intestinal colonization with Oxalobacter. American Journal of Physiology-Gastrointestinal and Liver Physiology *300*, G461-G469.
114. Vijay-Kumar, M., Aitken, J.D., Carvalho, F.A., Cullender, T.C., Mwangi, S., Srinivasan, S., Sitaraman, S.V., Knight, R., Ley, R.E., and Gewirtz, A.T. (2010). Metabolic

1519 syndrome and altered gut microbiota in mice lacking Toll-like receptor 5. Science *328*,
1520 228-231.
1521 115. Le Naour, J., Montégut, L., Joseph, A., Garbin, K., Vacchelli, E., Kroemer, G., Pol, J.G.,
1522 and Maiuri, M.C. (2022). Improved Swiss-rolling method for histological analyses of
1523 colon tissue. MethodsX *9*, 101630.
1524 116. Rungby, J., Kassem, M., Eriksen, E.F., and Danscher, G. (1993). The von Kossa reaction
1525 for calcium deposits: silver lactate staining increases sensitivity and reduces background.
1526 The Histochemical Journal *25*, 446-451.
1527 117. Bankhead, P., Loughrey, M.B., Fernández, J.A., Dombrowski, Y., McArt, D.G., Dunne,
1528 P.D., McQuaid, S., Gray, R.T., Murray, L.J., and Coleman, H.G. (2017). QuPath: Open
1529 source software for digital pathology image analysis. Scientific reports *7*, 1-7.
1530 118. Mak, T.D., Laiakis, E.C., Goudarzi, M., and Fornace Jr, A.J. (2013). Metabolyzer: A
1531 novel statistical workflow for analyzing postprocessed lc–ms metabolomics data.
1532 Analytical chemistry *86*, 506-513.
1533 119. Wishart, D.S., Feunang, Y.D., Marcu, A., Guo, A.C., Liang, K., Vázquez-Fresno, R.,
1534 Sajed, T., Johnson, D., Li, C., and Karu, N. (2017). HMDB 4.0: the human metabolome
1535 database for 2018. Nucleic acids research *46*, D608-D617.
1536 120. O'Donnell, V.B., Dennis, E.A., Wakelam, M.J., and Subramaniam, S. (2019). LIPID
1537 MAPS: Serving the next generation of lipid researchers with tools, resources, data, and
1538 training. Science signaling *12*, eaaw2964.
1539 121. Karp, P.D., Billington, R., Caspi, R., Fulcher, C.A., Latendresse, M., Kothari, A.,
1540 Keseler, I.M., Krummenacker, M., Midford, P.E., and Ong, Q. (2019). The BioCyc
1541 collection of microbial genomes and metabolic pathways. Briefings in bioinformatics *20*,
1542 1085-1093.
1543 122. Qi, Z., and Voit, E.O. (2016). Strategies for comparing metabolic profiles: Implications
1544 for the inference of biochemical mechanisms from metabolomics data. IEEE/ACM
1545 transactions on computational biology and bioinformatics *14*, 1434-1445.
1546 123. Oksanen, J., Blanchet, F.G., Kindt, R., Legendre, P., O'hara, R., Simpson, G.L.,
1547 Solymos, P., Stevens, M.H.H., and Wagner, H. (2010). Vegan: community ecology
1548 package. R package version 1.17-4. http://cran. r-project. org>. Acesso em *23*, 2010.
1549 124. Delhomme, N., Mähler, N., Schiffthaler, B., Sundell, D., Mannapperuma, C., Hvidsten,
1550 T.R., and Street, N.R. (2014). Guidelines for RNA-Seq data analysis. Epigenesys Protoc
1551 *67*, 1-24.
1552 125. Kopylova, E., Noé, L., and Touzet, H. (2012). SortMeRNA: fast and accurate filtering of
1553 ribosomal RNAs in metatranscriptomic data. Bioinformatics *28*, 3211-3217.
1554 126. Andrews, S., Krueger, F., Segonds-Pichon, A., Biggins, L., Krueger, C., and Wingett, S.
1555 (2010). FastQC. A quality control tool for high throughput sequence data *370*.
1556 127. Bolger, A.M., Lohse, M., and Usadel, B. (2014). Trimmomatic: a flexible trimmer for
1557 Illumina sequence data. Bioinformatics *30*, 2114-2120.
1558 128. Karolchik, D., Barber, G.P., Casper, J., Clawson, H., Cline, M.S., Diekhans, M., Dreszer,
1559 T.R., Fujita, P.A., Guruvadoo, L., and Haeussler, M. (2014). The UCSC genome browser
1560 database: 2014 update. Nucleic acids research *42*, D764-D770.
1561 129. Pertea, M., Kim, D., Pertea, G.M., Leek, J.T., and Salzberg, S.L. (2016). Transcript-level
1562 expression analysis of RNA-seq experiments with HISAT, StringTie and Ballgown.
1563 Nature protocols *11*, 1650-1667.
1564 130. Team, R.C. (2013). R: A language and environment for statistical computing.

1565 131. Trapnell, C., Hendrickson, D.G., Sauvageau, M., Goff, L., Rinn, J.L., and Pachter, L.
1566 (2013). Differential analysis of gene regulation at transcript resolution with RNA-seq.
1567 Nature biotechnology *31*, 46-53.
1568 132. Bult, C.J., Blake, J.A., Smith, C.L., Kadin, J.A., and Richardson, J.E. (2019). Mouse
1569 genome database (MGD) 2019. Nucleic acids research *47*, D801-D806.
1570 133. Watts, S.C., Ritchie, S.C., Inouye, M., and Holt, K.E. (2019). FastSpar: rapid and
1571 scalable correlation estimation for compositional data. Bioinformatics *35*, 1064-1066.
1572 134. Shannon, P., Markiel, A., Ozier, O., Baliga, N.S., Wang, J.T., Ramage, D., Amin, N.,
1573 Schwikowski, B., and Ideker, T. (2003). Cytoscape: a software environment for
1574 integrated models of biomolecular interaction networks. Genome research *13*, 2498-2504.
1575 135. Bushnell, B., Rood, J., and Singer, E. (2017). BBMerge–accurate paired shotgun read
1576 merging via overlap. PLoS One *12*, e0185056.
1577 136. Campbell, M., Oakeson, K.F., Yandell, M., Halpert, J.R., and Dearing, D. (2016). The
1578 draft genome sequence and annotation of the desert woodrat Neotoma lepida. Genomics
1579 Data *9*, 58-59.
1580 137. Li, H. (2013). Aligning sequence reads, clone sequences and assembly contigs with
1581 BWA-MEM. arXiv preprint arXiv:1303.3997.
1582 138. Nurk, S., Meleshko, D., Korobeynikov, A., and Pevzner, P.A. (2017). metaSPAdes: a
1583 new versatile metagenomic assembler. Genome research *27*, 824-834.
1584 139. Seemann, T. (2014). Prokka: rapid prokaryotic genome annotation. Bioinformatics *30*,
1585 2068-2069.
1586 140. Consortium, U. (2015). UniProt: a hub for protein information. Nucleic acids research *43*,
1587 D204-D212.
1588 141. Pedruzzi, I., Rivoire, C., Auchincloss, A.H., Coudert, E., Keller, G., De Castro, E.,
1589 Baratin, D., Cuche, B.A., Bougueleret, L., and Poux, S. (2015). HAMAP in 2015:
1590 updates to the protein family classification and annotation system. Nucleic acids research
1591 *43*, D1064-D1070.
1592 142. Fu, L., Niu, B., Zhu, Z., Wu, S., and Li, W. (2012). CD-HIT: accelerated for clustering
1593 the next-generation sequencing data. Bioinformatics *28*, 3150-3152.
1594 143. Love, M.I., Huber, W., and Anders, S. (2014). Moderated estimation of fold change and
1595 dispersion for RNA-seq data with DESeq2. Genome biology *15*, 1.
1596 144. Miller, I.J., Rees, E.R., Ross, J., Miller, I., Baxa, J., Lopera, J., Kerby, R.L., Rey, F.E.,
1597 and Kwan, J.C. (2019). Autometa: automated extraction of microbial genomes from
1598 individual shotgun metagenomes. Nucleic acids research *47*, e57-e57.
1599 145. Kachroo, N., Monga, M., and Miller, A.W. (2022). Comparative functional analysis of
1600 the urinary tract microbiome for individuals with or without calcium oxalate calculi.
1601 Urolithiasis *50*, 303-317. 10.1007/s00240-022-01314-5.
1602 146. Chen, K.-T., Liu, C.-L., Huang, S.-H., Shen, H.-T., Shieh, Y.-K., Chiu, H.-T., and Lu,
1603 C.L. (2018). CSAR: a contig scaffolding tool using algebraic rearrangements.
1604 Bioinformatics *34*, 109-111.
1605 147. Simpson, J.T., Wong, K., Jackman, S.D., Schein, J.E., Jones, S.J., and Birol, I. (2009).
1606 ABySS: a parallel assembler for short read sequence data. Genome research *19*, 1117-
1607 1123.
1608 148. Asnicar, F., Thomas, A.M., Beghini, F., Mengoni, C., Manara, S., Manghi, P., Zhu, Q.,
1609 Bolzan, M., Cumbo, F., and May, U. (2020). Precise phylogenetic analysis of microbial

1610 isolates and genomes from metagenomes using PhyloPhlAn 3.0. Nature communications
1611 *11*, 1-10.
1612 149. Bowers, R.M., Kyrpides, N.C., Stepanauskas, R., Harmon-Smith, M., Doud, D., Reddy,
1613 T., Schulz, F., Jarett, J., Rivers, A.R., and Eloe-Fadrosh, E.A. (2017). Minimum
1614 information about a single amplified genome (MISAG) and a metagenome-assembled
1615 genome (MIMAG) of bacteria and archaea. Nature biotechnology *35*, 725-731.
1616 150. Kanehisa, M., Sato, Y., Furumichi, M., Morishima, K., and Tanabe, M. (2018). New
1617 approach for understanding genome variations in KEGG. Nucleic acids research *47*,
1618 D590-D595.
1619 151. Callahan, B.J., McMurdie, P.J., Rosen, M.J., Han, A.W., Johnson, A.J.A., and Holmes,
1620 S.P. (2016). DADA2: high-resolution sample inference from Illumina amplicon data.
1621 Nature methods *13*, 581.
1622 152. Balvočiūtė, M., and Huson, D.H. (2017). SILVA, RDP, Greengenes, NCBI and OTT—
1623 how do these taxonomies compare? BMC genomics *18*, 114.
1624 153. Bodenhofer, U., Bonatesta, E., Horejš-Kainrath, C., and Hochreiter, S. (2015). msa: an R
1625 package for multiple sequence alignment. Bioinformatics *31*, 3997-3999.
1626 154. Schliep, K.P. (2011). phangorn: phylogenetic analysis in R. Bioinformatics *27*, 592-593.
1627 155. McMurdie, P.J., and Holmes, S. (2013). phyloseq: an R package for reproducible
1628 interactive analysis and graphics of microbiome census data. PloS one *8*, e61217.
1629 156. Lozupone, C., Hamady, M., and Knight, R. (2006). UniFrac–an online tool for comparing
1630 microbial community diversity in a phylogenetic context. BMC bioinformatics *7*, 1.
1631

1632 **Supplemental information titles and legends**
1633
1634 Supplementary Figures and table legends
1635 Figs. S1 to S10
1636 Tables S1 and S9
1637
1638
1639 **Supplementary figure legends:**
1640
1641 Fig. S1. Phylogeny of genomes extracted from the *N. albigula* metagenome, in
1642 comparison to >3000 full length microbial genomes. Stars indicate taxonomic
1643 placement of extracted genomes. All other points indicate reference genomes.
1644
1645 Fig. S2. Representation of formate metabolism genes in the NALB metagenome derived
1646 from 248 full length genomes. A) Proportion of the genomes extracted from *N. albigula*
1647 that had at least one formate metabolism gene. B) Representation of formate
1648 metabolism genes among the metagenome, broken down by gene function and
1649 proportion of total formate metabolism genes. C) Representation of formate metabolism
1650 genes broken down by taxon.
1651
1652 Fig. S3. Representation of acetogenic genes in the NALB metagenome derived from
1653 248 full length genomes. A) Proportion of the genomes extracted from *N. albigula* that
1654 had at least one acetogenic gene. B) Representation of acetogenic genes among the
1655 metagenome, broken down by gene function and proportion of total acetogenic genes.
1656 C) Representation of acetogenic genes broken down by taxon.
1657
1658 Fig. S4. Representation of methanogenic genes in the NALB metagenome derived from
1659 248 full length genomes. A) Proportion of the genomes extracted from *N. albigula* that
1660 had at least one methanogenic gene. B) Representation of methanogenic genes
1661 among the metagenome, broken down by gene function and proportion of total
1662 methanogenic genes. C) Representation of methanogenic genes broken down by
1663 taxon.
1664
1665 Fig. S5. Representation of sulfate-reducing genes in the NALB metagenome derived
1666 from 248 full length genomes. A) Proportion of the genomes extracted from *N. albigula*
1667 that had at least one sulfate-reducing gene. B) Representation of sulfate-reducing
1668 genes among the metagenome, broken down by gene function and proportion of total
1669 sulfate-reducing genes. C) Representation of sulfate-reducing genes broken down by
1670 taxon.
1671
1672 Fig. S6. Microbial transplant composition impact on urinary inflammation, renal health,
1673 and overall mouse health for the taxonomic cohort. A-G) The effect of microbial
1674 transplants on urinary IL-6 (A), IL-18 (B), and creatinine (C) levels, along with water
1675 intake (D), urine output (E), food intake (F) and body mass (G). H) Masson's Trichrome
1676 staining of heart tissue reveals fibrosis. Shown are representative images from the
1677 No_bact (Group 1) and All (Group 4) groups. I) Quantification of cardiac fibrosis from

different microbial transplant groups. Statistical significance - 2-way ANOVA (shown on charts) and post-hoc, Holm's corrected, paired t-tests. Blue letters reflect statistical groups between microbial transplants and *p<0.05, **p<0.01; ***p<0.001 for longitudinal comparisons within each microbial transplant group.

Fig. S7. Effect of microbial transplants on microbial community composition for the taxonomic cohort. A,B) Beta-diversity analysis based on a weighted UniFrac dissimilarity matrix of colon feces collected at the end of the study period vs. stool (A; . p=0.006, PERMANOVA) or in the endpoint stool samples by group (B; no significant differences). Similar results for (B) were obtained with colon feces. Statistical differences shown by blue letters in legend. C) Within group beta-diversity distance of colon feces. p=0.006, one-way ANOVA. Blue letters represent statistical groups, based on post-hoc, Holm's corrected, paired t-tests. Similar results were found with endpoint stool samples. D) Change in phylogenetic diversity of stool for each microbial transplant group. Stats, shown on graph, are based on Pearson correlations. E) Normalized counts of transplanted microorganisms in the stool across timepoints and in the colon feces at the end of the diet trial.

Fig. S8. Microbial community composition (metabolic cohort) impacted the effect of exogenous oxalate on kidney health. A) Experimental design. Swiss Webster mice were given neomycin, followed by inoculation of one of five microbial consortia that included either no bacteria, the NALB community, or the metabolic cohort listed in Figure 5C. Animals were maintained on a 3% oxalate diet throughout the trial except for a 0% oxalate washout period after the microbial transplant period. B,C) The effect of microbial transplants on urinary (B) or fecal (C) oxalate levels over the course of the diet trial, compared to baseline. ANOVA p<0.001 for microbial group (B&C), and p<0.01 for both timeperiod and in 2-way analysis for (B only). D) The effect of microbial transplants on urinary formate levels over the course of the diet trial. ANOVA p<0.001 for microbial group and timeperiod. E) Renal calcium oxalate deposition based on Von Kossa staining of renal tissue sections. Arrows show calcium deposits stained black, which were quantified through an automated algorithm in QuPath. F) Quantification of renal calcium oxalate deposition by group. p=0.014; ANOVA. G,H) Pearson correlation between urinary oxalate (R=0.7, p<0.001) (G) or formate (R=0.026, p=0.9) (H) and renal calcium oxalate deposition. Where applicable, statistical significance was assessed through an ANOVA and post-hoc, Holm's corrected, paired t-tests. Statistical groups shown by blue letters.

Fig. S9. Microbial transplant composition impact on urinary inflammation, renal health, and overall mouse health for the metabolic cohort. A-G) The effect of microbial transplants on urinary IL-6 (A), IL-18 (B), and creatinine (C) levels, along with water intake (D), urine output (E), food intake (F) and body mass (G). Statistical significance - 2-way ANOVA (shown on charts) and post-hoc, Holm's corrected, paired t-tests. Blue letters reflect statistical groups between microbial transplants and *p<0.05, **p<0.01; ***p<0.001 for longitudinal comparisons within each microbial transplant group.

1723 Fig. S10. Effect of microbial transplants on microbial community composition for the
1724 metabolic cohort. A,B) Beta-diversity analysis based on a weighted UniFrac
1725 dissimilarity matrix of colon feces collected at the end of the study period vs. stool (A; .
1726 p=0.006, PERMANOVA) or in the endpoint stool samples by group (B; no significant
1727 differences). Similar results for (B) were obtained with colon feces. Statistical
1728 differences shown by blue letters in legend. C) Within group beta-diversity distance of
1729 colon feces. p=0.006, one-way ANOVA. Blue letters represent statistical groups, based
1730 on post-hoc, Holm's corrected, paired t-tests. Similar results were found with endpoint
1731 stool samples. D) Change in phylogenetic diversity of stool for each microbial transplant
1732 group. Stats, shown on graph, are based on Pearson correlations. E) Normalized
1733 counts of transplanted microorganisms in the stool across timepoints and in the colon
1734 feces at the end of the diet trial.
1735
1736 Fig. S11. Effect of oxalate and formate on oxalate quantification using an enzymatic,
1737 ELISA-based assay. A) Correlation between oxalate or oxalate + formate, added to
1738 water, on oxalate concentration quantified through the enzymatic kit. B) Ratio of the
1739 calculated oxalate vs. the added concentration of oxalate and formate. C) The effect of
1740 adding oxalate or formate to urine, or of extracting oxalate from urine. R values and p-
1741 values (A) or p-values from one-way ANOVA (B,C) shown on chart. Blue letters
1742 represent statistical groups, based on pairwise t-tests.
1743
1744
1745

1746 **Supplementary legends**
1747
1748 Table S1. Diets used in animal studies.
1749
1750 Table S2. The number of host hepatic genes in each metabolic pathway that exhibited
1751 a significant increase (positive numbers) or decrease (negative numbers) in expression
1752 upon consumption of a 1.5% oxalate diet.
1753
1754 Table S3. The number of microbial metabolites in each metabolic pathway that
1755 exhibited a significant increase (positive numbers) or decrease (negative numbers) in
1756 expression upon consumption of a 1.5% oxalate diet by the host.
1757
1758 Table S4. The significant positive and negative correlations between microbial
1759 metabolites and host hepatic gene expression for those metabolites/genes significantly
1760 altered by 1.5% oxalate consumption. Data are listed with the host microbiome,
1761 metabollite and gene ID, long with correlation values and false discovery rate corrected
1762 p-values.
1763
1764 Table S5. The number of microbial genes in each metabolic pathway that exhibited a
1765 significant increase (positive numbers) or decrease (negative numbers) in abundance
1766 upon consumption of a 6% oxalate diet by the host.
1767
1768 Table S6. Media recipe used to test the impact of substrates on oxalate metabolism.
1769
1770 Table S7. Media recipe used to test the proportion of the NALB community that can
1771 utilize substrates as sole carbon and energy sources.
1772
1773 Table S8. Microorganisms used in the taxonomic cohort.
1774
1775 Table S9. Information for 248 complete genomes extracted from the shotgun
1776 metagenomic data from the *N. albigula* gut microbiota.

1777 **Supplementary Figures**

Fig. S1

A: Bacteroidetes
B: Firmicutes
C: Proteobacteria
D: Synergistetes
E: Tenericutes
F: Actinobacteria
G: Actinobacteria
H: Thermotogae
I: Thermotogae
J: Spirochaetes
K: Spirochaetes
L: Chrysiogenetes
M: Chrysiogenetes
N: Thermi
O: Thermi
P: Thermodesulfobacteria
Q: Thermodesulfobacteria
R: Deferribacteres
S: Deferribacteres
T: Cyanobacteria
U: Caldithrix
V: Caldithrix
W: Chloroflexi
X: Chloroflexi
Y: Fusobacteria
Z: Fusobacteria
a: Aquificae
b: Aquificae
c: Verrucomicrobia
d: Planctomycetes
e: Acidobacteria
f: Acidobacteria
g: Chlamydiae
h: Chlamydiae
i: Deinococcus-Thermus
j: Chlorobi
k: Lentisphaerae
l: Lentisphaerae
m: WWE1
n: Elusimicrobia
o: Elusimicrobia
p: TM7
q: Dictyoglomi
r: Nitrospirae
s: Gemmatimonadetes
t: Gemmatimonadetes
u: Fibrobacteres
v: Fibrobacteres
w: Euryarchaeota
x: Crenarchaeota
y: Nanoarchaeota

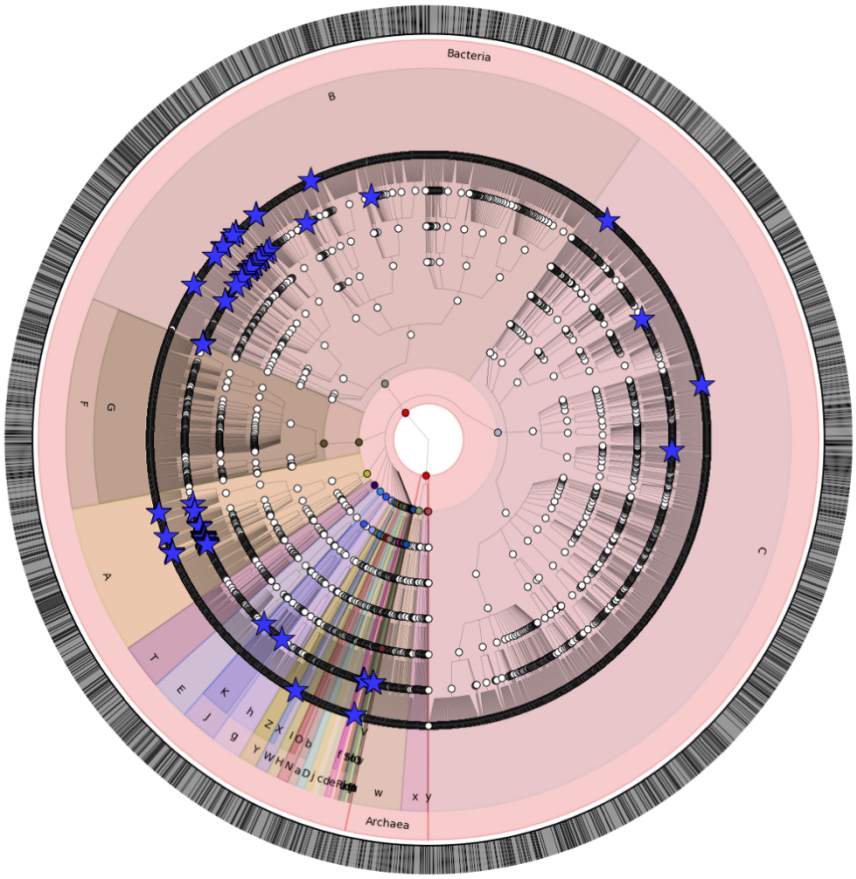

1778
1779 .

Fig. S2

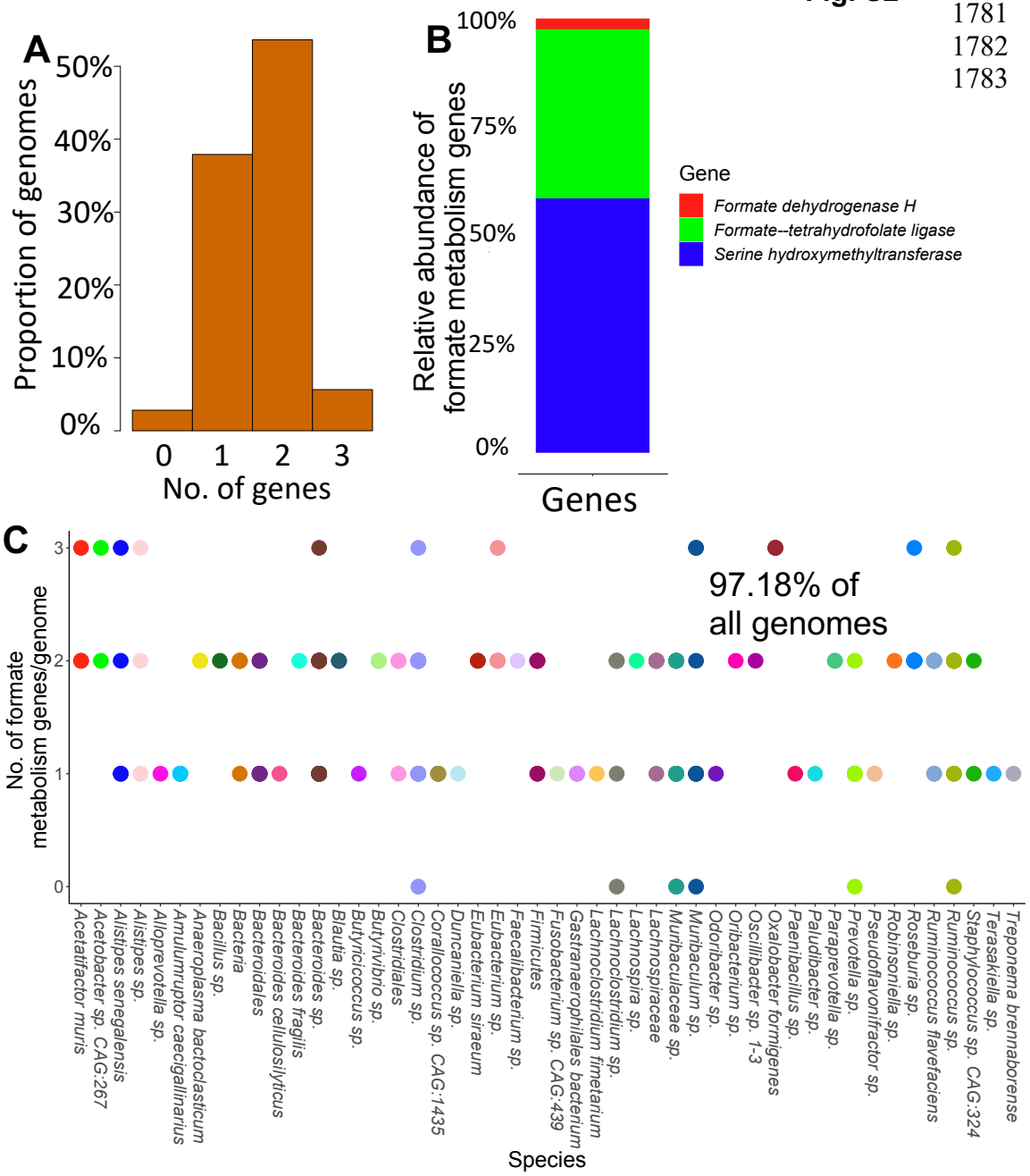
A
Proportion of genomes
50%
40%
30%
20%
10%
0%
0
1
2
3
No. of genes
B
Relative abundance of formate metabolism genes
100%
75%
50%
25%
0%
Genes
Gene
Formate dehydrogenase H
Formate--tetrahydrofolate ligase
Serine hydroxymethyltransferase
C
No. of formate metabolism genes/genome
97.18% of all genomes
Acetatifactor muris
Acetobacter sp. CAG:267
Alistipes senegalensis
Alistipes sp.
Alloprevotella sp.
Amulumruptor caecigallinarius
Anaeroplasma bactoclasticum
Bacillus sp.
Bacteria
Bacteroidales
Bacteroides cellulosilyticus
Bacteroides fragilis
Bacteroides sp.
Blautia sp.
Butyricicoccus sp.
Butyrivibrio sp.
Clostridiales
Clostridium sp.
Coprococcus sp. CAG:1435
Duncaniella sp.
Eubacterium siraeum
Eubacterium sp.
Faecalibacterium sp.
Firmicutes
Fusobacterium sp. CAG:439
Gastranaerophilales bacterium
Lachnoclostridium fimetarium
Lachnoclostridium sp.
Lachnospira sp.
Lachnospiraceae
Muribaculum sp.
Muribaculaceae sp.
Odoribacter sp.
Oribacterium sp.
Oscillibacter sp. 1-3
Oxalobacter formigenes
Paenibacillus sp.
Paludibacter sp.
Paraprevotella sp.
Prevotella sp.
Pseudoflavonifractor sp.
Robinsoniella sp.
Roseburia sp.
Ruminococcus flavefaciens
Ruminococcus sp.
Staphylococcus sp. CAG:324
Terasakiella sp.
Treponema brennaborense
Species

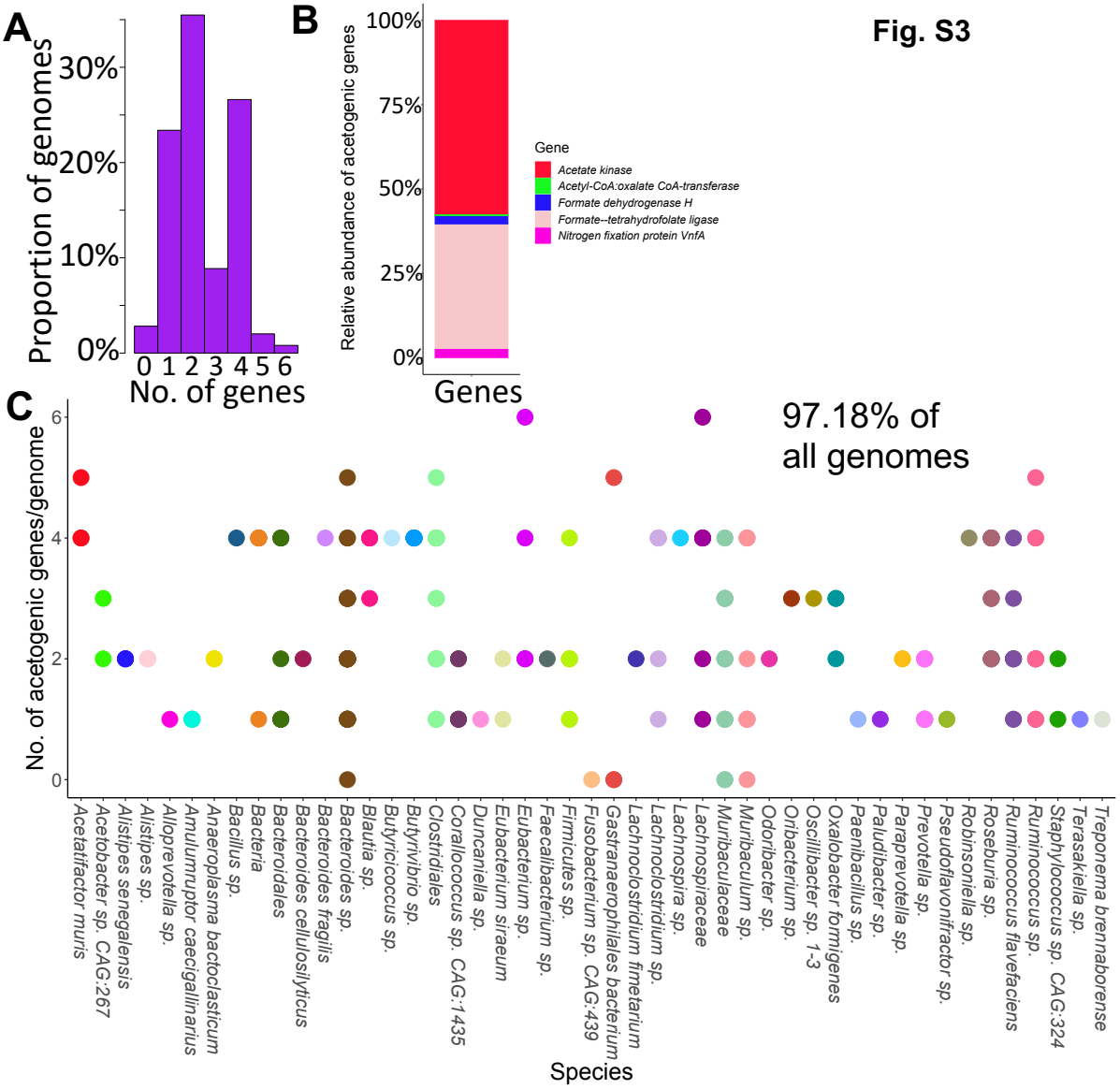
A
Proportion of genomes
30%
20%
10%
0%
0 1 2 3 4 5 6
No. of genes
B
Relative abundance of acetogenic genes
100%
75%
50%
25%
0%
Genes
Gene
Acetate kinase
Acetyl-CoA:oxalate CoA-transferase
Formate dehydrogenase H
Formate--tetrahydrofolate ligase
Nitrogen fixation protein VnfA
C
No. of acetogenic genes/genome
97.18% of
all genomes
Acetatifactor muris
Acetobacter sp. CAG:267
Alistipes senegalensis
Alistipes sp.
Alloprevotella sp.
Amulumruptor caecigallinarius
Anaeroplasma bactoclasticum
Bacillus sp.
Bacteria
Bacteroidales
Bacteroides cellulosilyticus
Bacteroides fragilis
Bacteroides sp.
Blautia sp.
Butyricicoccus sp.
Butyrivibrio sp.
Clostridiales
Coprococcus sp. CAG:1435
Duncaniella sp.
Eubacterium siraeum
Eubacterium sp.
Faecalibacterium sp.
Firmicutes sp.
Fusobacterium sp. CAG:439
Gastranaerophilales bacterium
Lachnoclostridium fimetarium
Lachnoclostridium sp.
Lachnospira sp.
Lachnospiraceae
Muribaculum sp.
Muribaculaceae
Odoribacter sp.
Oribacterium sp.
Oscillibacter sp. 1-3
Oxalobacter formigenes
Paludibacter sp.
Paenibacillus sp.
Paraprevotella sp.
Prevotella sp.
Pseudoflavonifractor sp.
Robinsoniella sp.
Roseburia sp.
Ruminococcus flavefaciens
Ruminococcus sp.
Staphylococcus sp. CAG:324
Terasakiella sp.
Treponema brennaborense
Species

Fig. S3

1784

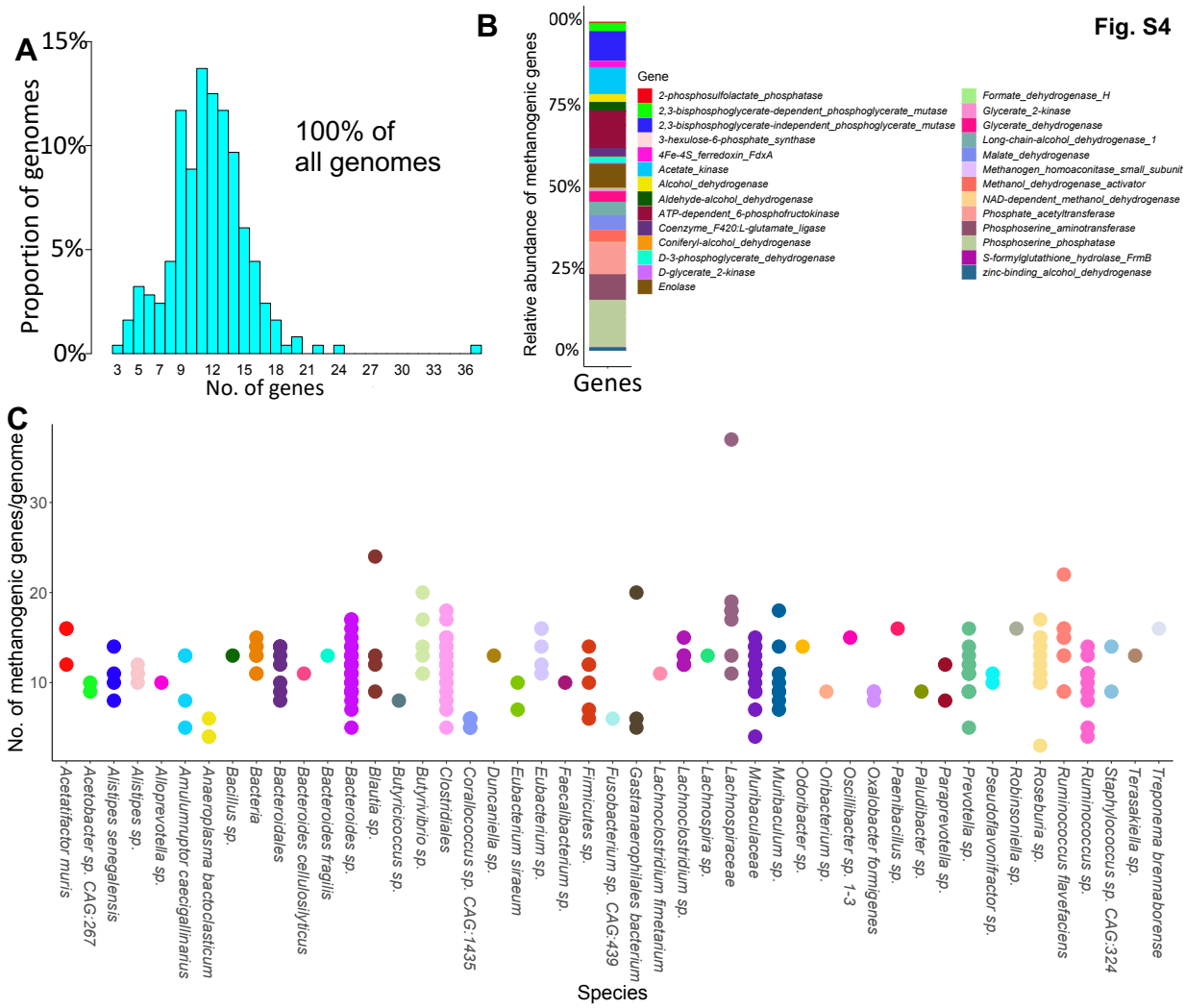
Fig. S4
A
Proportion of genomes
15%
10%
5%
0%
100% of
all genomes
3 5 7 9 12 15 18 21 24 27 30 33 36
No. of genes
B
Relative abundance of methanogenic genes
00%
75%
50%
25%
0%
Genes
Gene
2-phosphosulfolactate_phosphatase
2,3-bisphosphoglycerate-dependent_phosphoglycerate_mutase
2,3-bisphosphoglycerate-independent_phosphoglycerate_mutase
3-hexulose-6-phosphate_synthase
4Fe-4S_ferredoxin_FdxA
Acetate_kinase
Alcohol_dehydrogenase
Aldehyde-alcohol_dehydrogenase
ATP-dependent_6-phosphofructokinase
Coenzyme_F420:L-glutamate_ligase
Coniferyl-alcohol_dehydrogenase
D-3-phosphoglycerate_dehydrogenase
D-glycerate_2-kinase
Enolase
Formate_dehydrogenase_H
Glycerate_2-kinase
Glycerate_dehydrogenase
Long-chain-alcohol_dehydrogenase_1
Malate_dehydrogenase
Methanogen_homoaconitase_small_subunit
Methanol_dehydrogenase_activator
NAD-dependent_methanol_dehydrogenase
Phosphate_acetyltransferase
Phosphoserine_aminotransferase
Phosphoserine_phosphatase
S-formylglutathione_hydrolase_FrmB
zinc-binding_alcohol_dehydrogenase
C
No. of methanogenic genes/genome
30
20
10
Acetatifactor muris
Acetobacter sp. CAG:267
Alistipes senegalensis
Alistipes sp.
Alloprevotella sp.
Amulumruptor caecigallinarius
Anaeroplasma bactoclasticum
Bacillus sp.
Bacteria
Bacteroidales
Bacteroides cellulosilyticus
Bacteroides fragilis
Bacteroides sp.
Blautia sp.
Butyrivibrio sp.
Butyricicoccus sp.
Clostridiales
Coprococcus sp. CAG:1435
Duncaniella sp.
Eubacterium siraeum
Eubacterium sp.
Faecalibacterium sp.
Firmicutes sp.
Fusobacterium sp. CAG:439
Gastranaerophilales bacterium
Lachnoclostridium fimetarium
Lachnoclostridium sp.
Lachnospira sp.
Lachnospiraceae
Muribaculum sp.
Muribaculaceae
Odoribacter sp.
Oribacterium sp.
Oscillibacter sp. 1-3
Oxalobacter formigenes
Paenibacillus sp.
Paludibacter sp.
Parapreotella sp.
Prevotella sp.
Pseudoflavonifractor sp.
Robinsoniella sp.
Roseburia sp.
Ruminococcus flavefaciens
Ruminococcus sp.
Staphylococcus sp. CAG:324
Terasakiella sp.
Treponema brennaborense
Species

1785

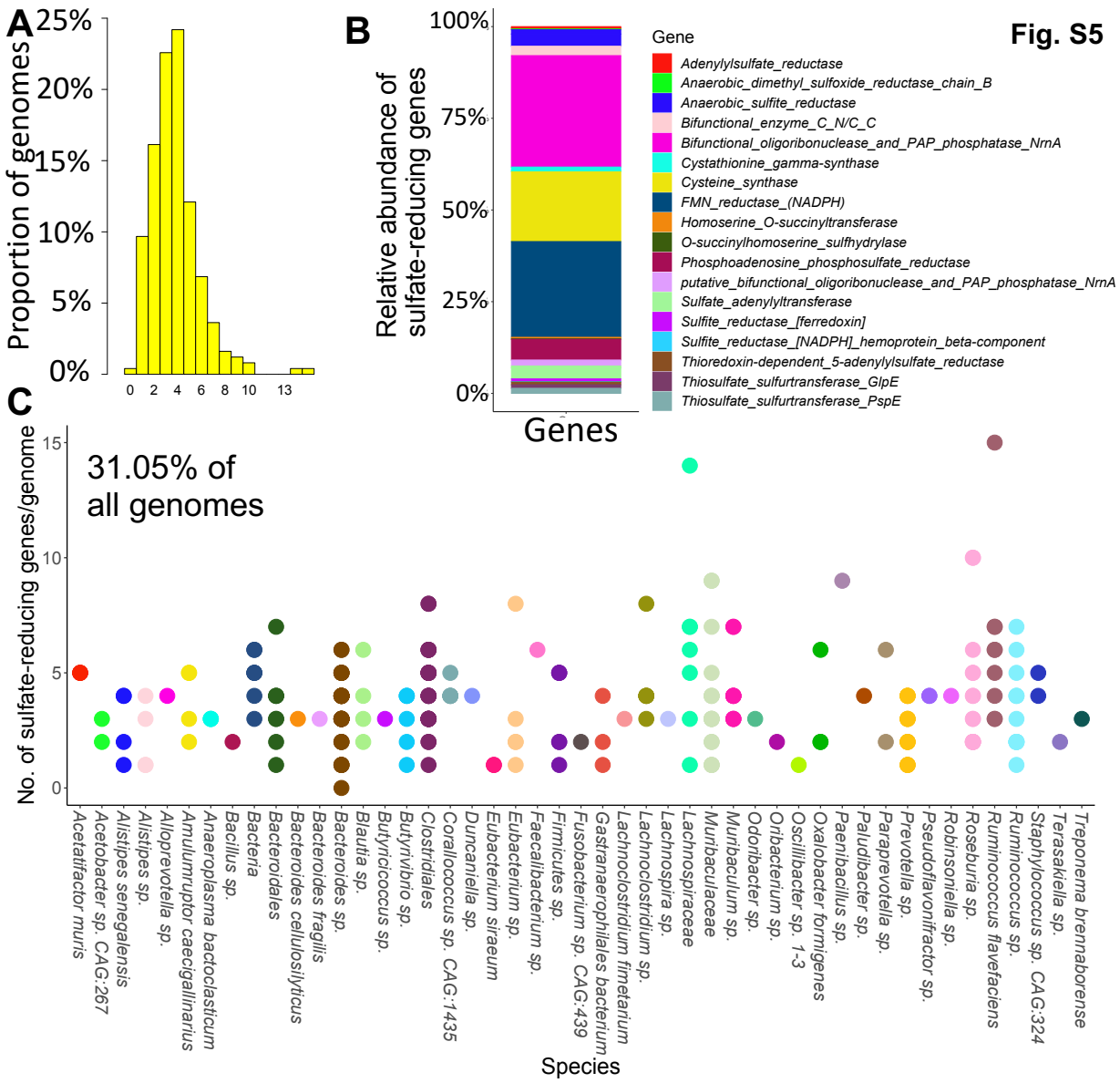
Fig. S5
A
Proportion of genomes
25%
20%
15%
10%
5%
0%
0 2 4 6 8 10 13
B
Relative abundance of sulfate-reducing genes
100%
75%
50%
25%
0%
Genes
Gene
Adenylylsulfate_reductase
Anaerobic_dimethyl_sulfoxide_reductase_chain_B
Anaerobic_sulfite_reductase
Bifunctional_enzyme_C_N/C_C
Bifunctional_oligoribonuclease_and_PAP_phosphatase_NrnA
Cystathionine_gamma-synthase
Cysteine_synthase
FMN_reductase_(NADPH)
Homoserine_O-succinyltransferase
O-succinylhomoserine_sulfhydrylase
Phosphoadenosine_phosphosulfate_reductase
putative_bifunctional_oligoribonuclease_and_PAP_phosphatase_NrnA
Sulfate_adenylyltransferase
Sulfite_reductase_[ferredoxin]
Sulfite_reductase_[NADPH]_hemoprotein_beta-component
Thioredoxin-dependent_5-adenylylsulfate_reductase
Thiosulfate_sulfurtransferase_GlpE
Thiosulfate_sulfurtransferase_PspE
C
No. of sulfate-reducing genes/genome
15
10
5
0
31.05% of all genomes
Acetatifactor muris
Acetobacter sp. CAG:267
Alistipes senegalensis
Alistipes sp.
Alloprevotella sp.
Amulumruptor caecigallinarius
Anaeroplasma bactoclasticum
Bacillus sp.
Bacteria
Bacteroidales
Bacteroides cellulosilyticus
Bacteroides fragilis
Bacteroides sp.
Blautia sp.
Butyricicoccus sp.
Butyrivibrio sp.
Clostridiales
Coprococcus sp. CAG:1435
Duncaniella sp.
Eubacterium siraeum
Eubacterium sp.
Faecalibacterium sp.
Firmicutes sp.
Fusobacterium sp. CAG:439
Gastranaerophilales bacterium
Lachnoclostridium fimetarium
Lachnoclostridium sp.
Lachnospira sp.
Lachnospiraceae
Muribaculaceae
Muribaculum sp.
Odoribacter sp.
Oribacterium sp.
Oscillibacter sp. 1-3
Oxalobacter formigenes
Paenibacillus sp.
Paludibacter sp.
Paraprevotella sp.
Prevotella sp.
Pseudoflavonifractor sp.
Robinsoniella sp.
Roseburia sp.
Ruminococcus flavefaciens
Ruminococcus sp.
Staphylococcus sp. CAG:324
Terasakiella sp.
Treponema brennaborense
Species

1786

Taxonomic cohort

Fig. S6

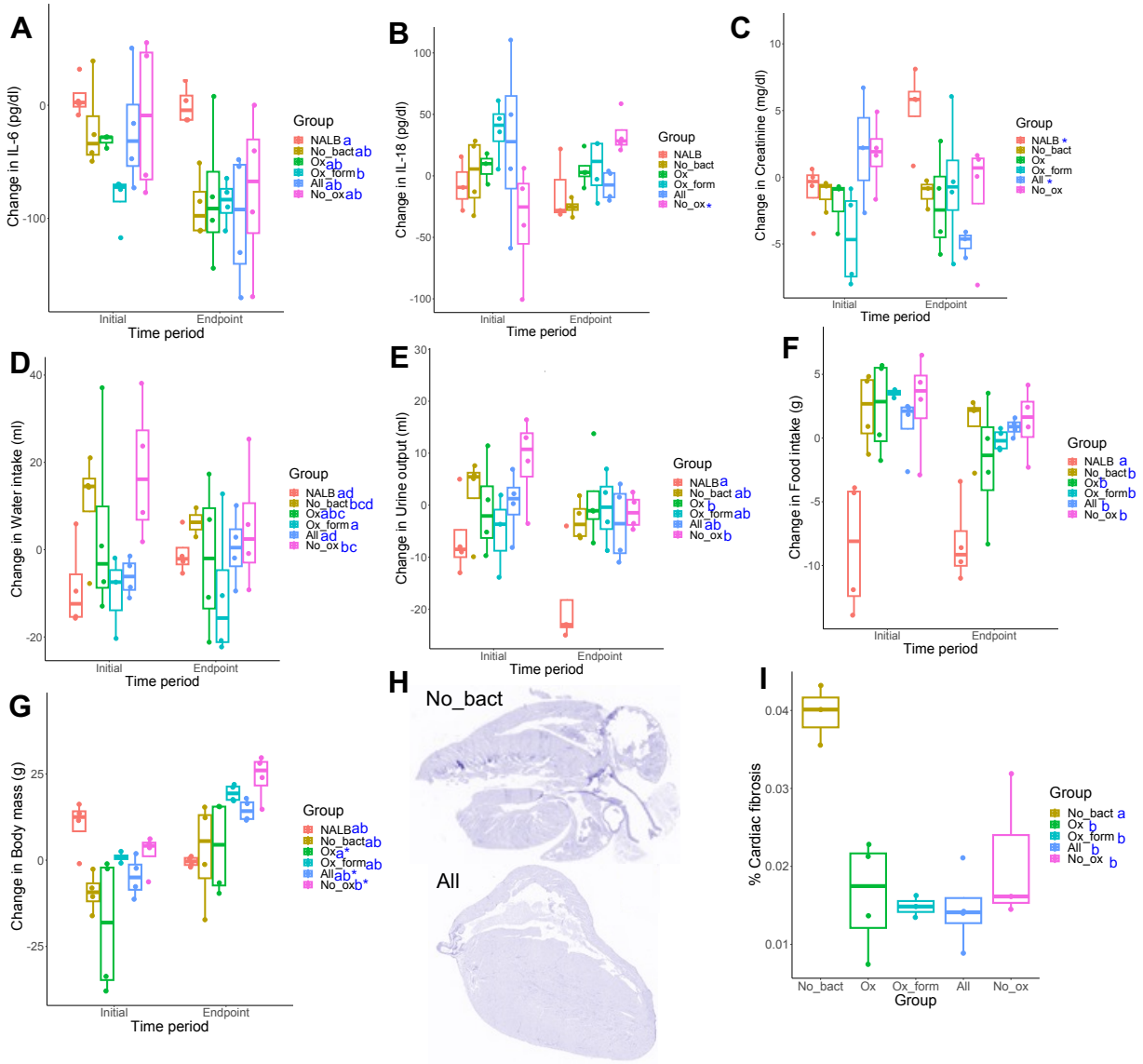

Group 1	No_bact
Group 2	Ox
Group 3	Ox_form
Group 4	All
Group 5	No_ox

Taxonomic cohort

Fig. S7

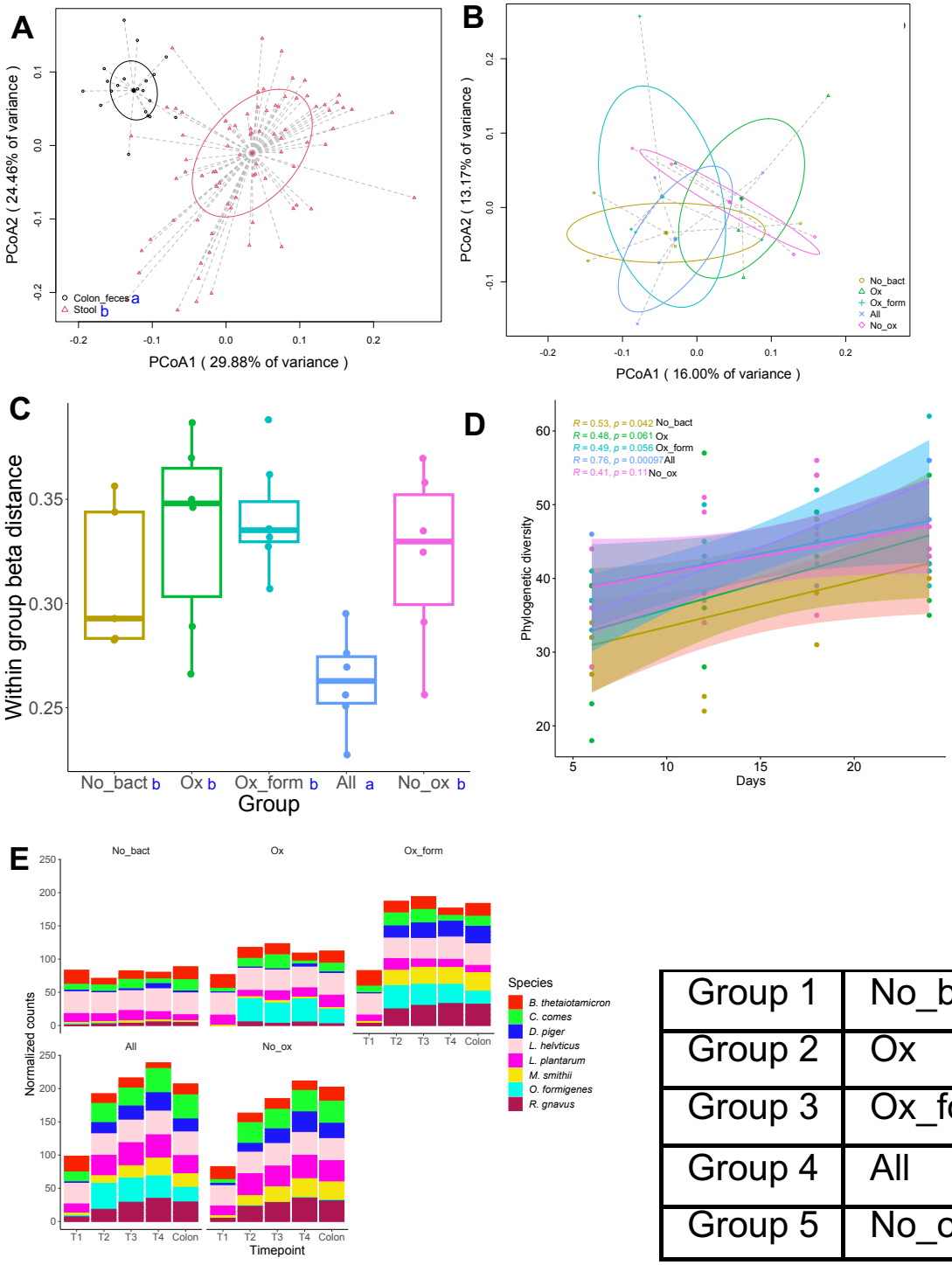

Group 1	No_bact
Group 2	Ox
Group 3	Ox_form
Group 4	All
Group 5	No_ox

1790

1791

Metabolic cohort

Fig. S8

A

n=16 animals/group, pooled by cage (4 animals/sample)

SW mouse
1. NALB
2. Ox
3. Ox_form
4. All
5. No_ox

	T1	T2	T3	T4
Days	0-6	7-12	13-18	19-25
Treatment	Neomycin 3% Oxalate	Microbial Transplant 3% Oxalate	0% Oxalate	3% Oxalate

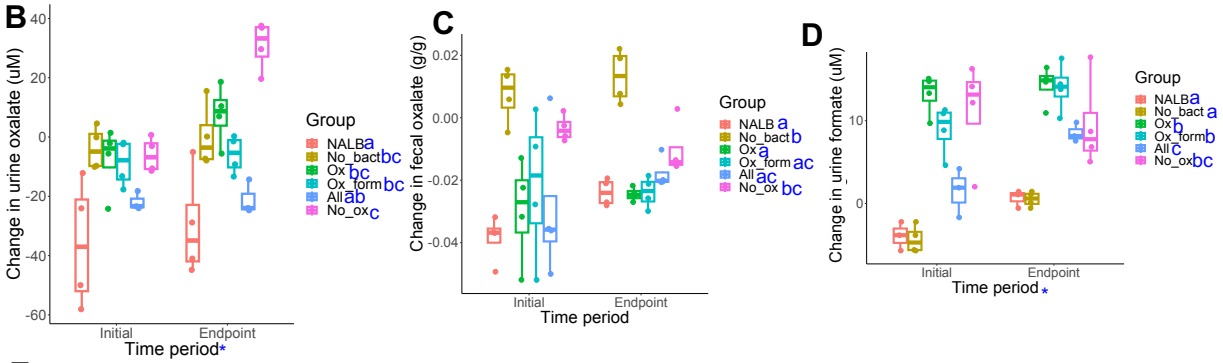

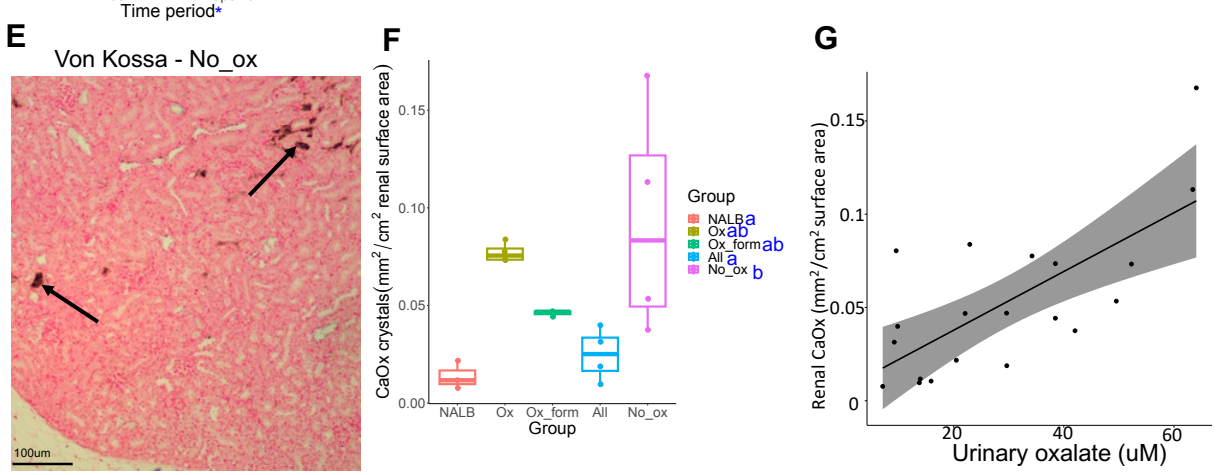

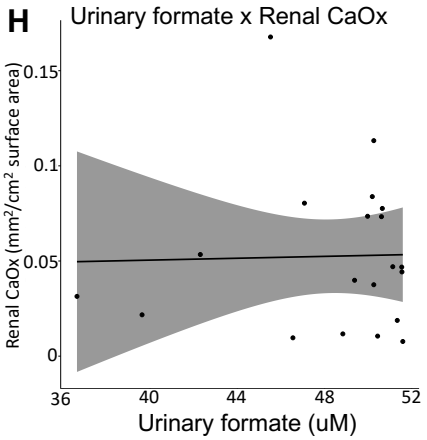

Group 1	No_bact
Group 2	Ox
Group 3	Ox_form
Group 4	All
Group 5	No_ox

1792

Metabolic cohort

Fig. S9

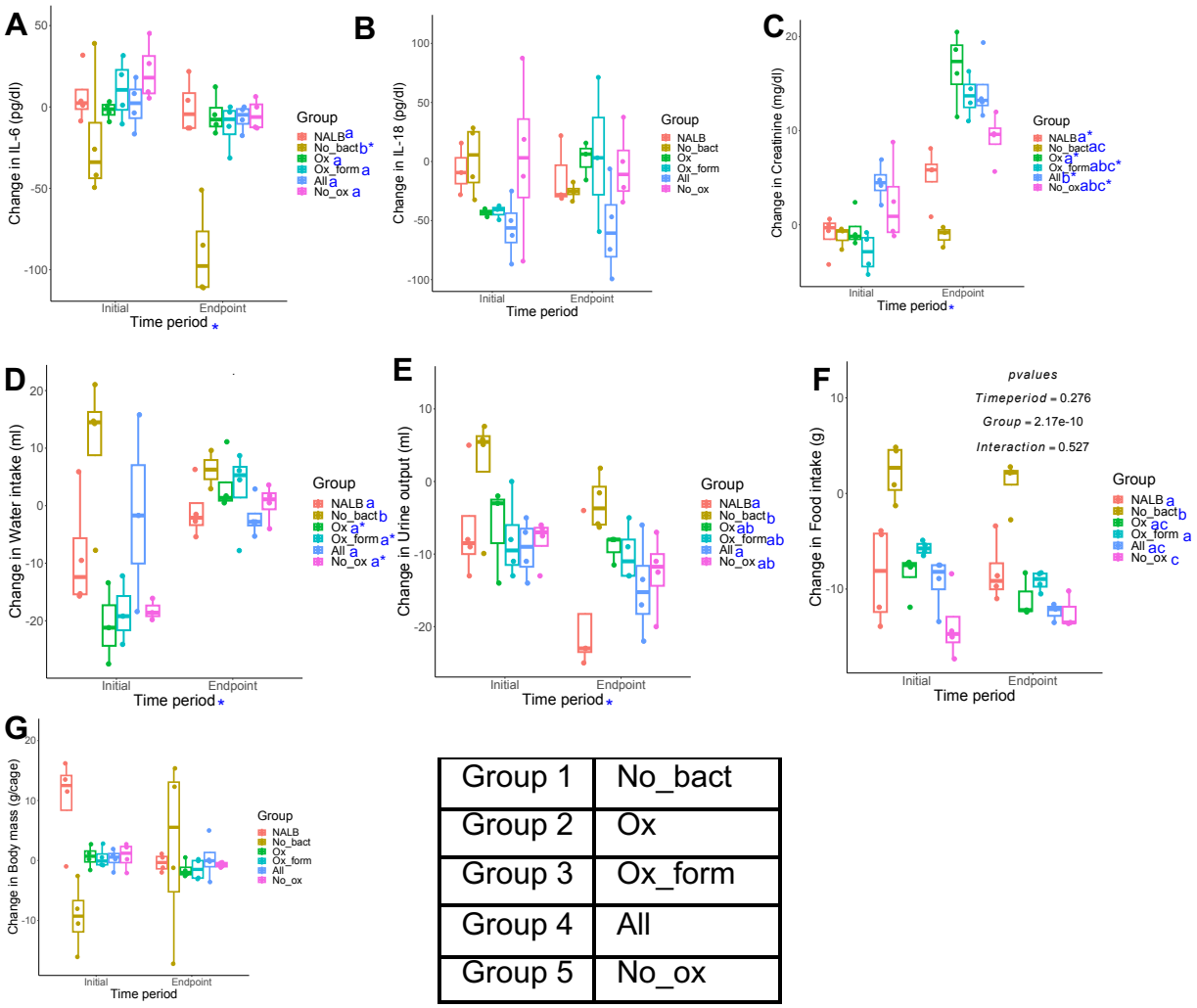

Group 1	No_bact
Group 2	Ox
Group 3	Ox_form
Group 4	All
Group 5	No_ox

Metabolic cohort

Fig. S10

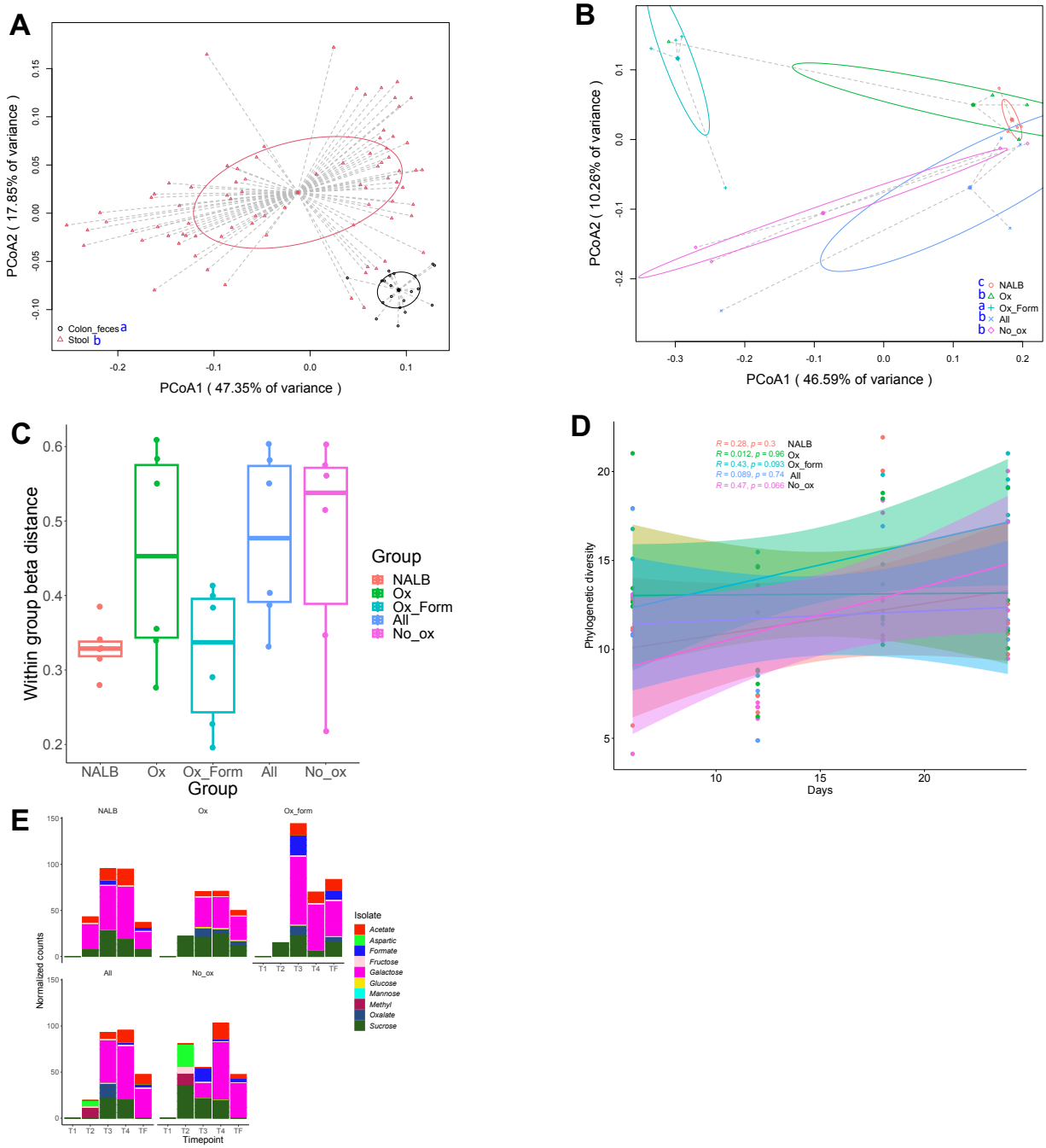

1795
1796

1797

Fig. S11

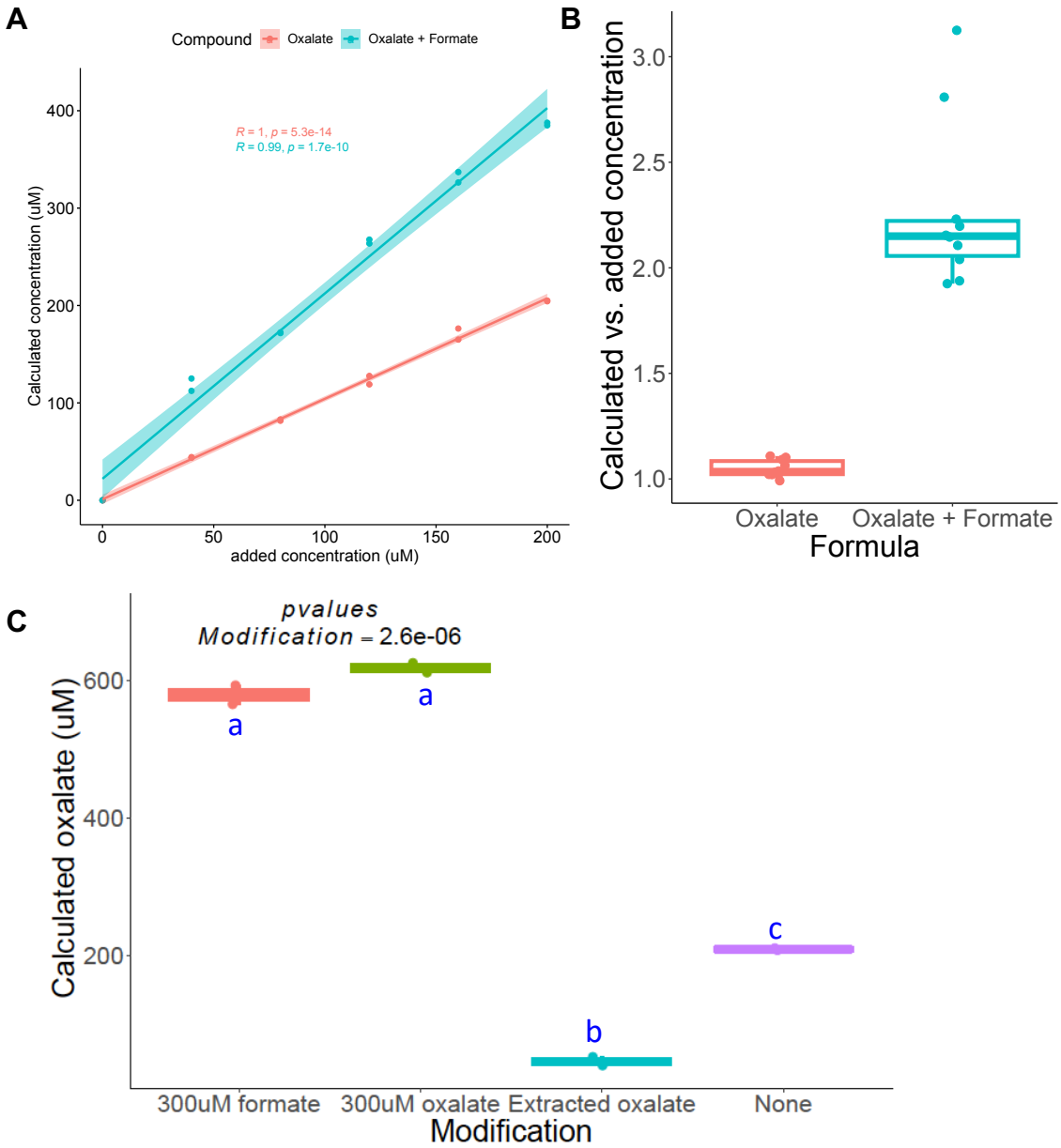

1798
1799
1800
1801
1802
1803
1804
1805
1806
1807
1808

1809
1810 **Supplementary Tables**

Table S1.

Ingredients	0% oxalate (g/Kg)	1.5% oxalate (g/Kg)	3% oxalate (g/Kg)
Casein	200	200	200
L-Cysteine	3	3	3
Corn Starch	285.5	NA	NA
Maltodextrin	120	120	120
Sucrose	100	185.4	185.4
Anhydrous Milkfat	NA	200	200
Soybean Oil	70	70	70
Cellulose	150	150	150
Mineral Mix	42	42	42
Vitamin Mix	12	12	12
Choline Bitartrate	2.5	2.5	2.5
TBHQ, antioxidant	0.014	0.054	0.054
Sodium Oxalate	0	15	30

1811
1812
1813

1814 Table S6.

Component	Amount/L	Concentration	Comments
Tryptone Peptone	2 g	0.20%	
Yeast Extract	1 g	0.10%	
Meat Extract	5 g	0.50%	
KH_2PO4	100 mL	100 mM	1M stock solution pH 7.2
$NaHCO_3$	0.4 g	4.8 mM	
$NaCl_2$	0.08 g	1.37 mM	
CaCl2	1 mL	0.80%	0.8g/100mL stock
Vitamin K (menadione)	1 mL	5.8 mM	1 mg/mL stock solution
$FeSO_4$	1 mL	1.44 mM	0.4 mg $FeSO_4$/mL stock solution
Histidine Hematin Solution	1 mL	0.10%	1.2 mg hematin/mL in 0.2M histidine
Tween 80	2 mL	0.05%	25% stock solution
Aspartic acid	0.02g		
Mannose	0.9g		
Galactose	1.8g		
Sodium acetate	6g	0.60%	
Sodium formate	4g	0.40%	
Isovaleric acid	0.1 mL	1 mM	Must be added in fume hood. Keep media, gloves, and tips in fume hood after addition for at least 5 minutes.
Propionic acid	2 mL	8 mM	Must be added in fume hood. Keep media, gloves, and tips in fume hood after addition for at least 5 minutes.
Butyric acid	2 mL	4 mM	Must be added in fume hood. Keep media, gloves, and tips in fume hood after addition for at least 5 minutes.
Resazurin	4 mL	4 mM	0.25 mg/mL stock solution
Noble Agar	12 g	1.20%	Only add agar if making plates. If broth, omit.
pH to 7			
Add DI water to 910ml			
Autoclave			
Prepare glucose, cellobiose, maltose, fructose, sucrose, and methyl-x compounds as below			
Move media to anaerobic chamber and add remaining components			
D-glucose	0.4 g	2.2 mM	Add to 10ml DI H2O and filter sterilize
Cellobiose	1 g	2.9 mM	Add to 20ml DI H2O and filter sterilize
Maltose	1 g	2.8 mM	Add to 10ml DI H2O and filter sterilize
Fructose	1 g	2.2 mM	Add to 10ml DI H2O and filter sterilize
Sucrose	1.71g		Add to 10ml DI H2O and filter sterilize
Methylvaleric acid	561ul		Combine with methyl butyric and filter sterilize
Methylbutyric acid	517ul		
sodium sulfate	2g	0.20%	Add to 10ml DI H2O and filter sterilize in anearobic chamber
L-cysteine	0.5 g	3.2 mM	Add to 10ml DI H2O and filter sterilize in anearobic chamber
$MgSO_4$-$7H_20$	1ml	0.008 mM	Stock 0.2g/100ml & autoclave
ATCC Vitamin Mix	10 mL	1%	
ATCC Trace Mineral Mix	10 mL	1%	
**Let media sit in anaerobic chamber for at least 24hrs to be fully reduced before inoculation			

1815
1816
1817

1818 Table S7.

Component	Amount/L	Concentration	
KH_2PO4	100 mL	100 mM	
$NaHCO_3$	0.4 g	4.8 mM	
$NaCl_2$	0.08 g	1.37 mM	
CaCl2	1 mL	0.80%	0.8g/100mL stock; autoclave
Vitamin K (menadione)	1 mL	5.8 mM	1 mg/mL stock solution; protect from light; autoclave
$FeSO_4$	1 mL	1.44 mM	0.4 mg $FeSO_4$/mL stock solution; filter sterilize
Histidine Hematin Solution	1 mL	0.1%	1.2 mg hematin/mL in 0.2M histidine; filter sterilize after preparation of stock; protect from light; store at 4C
NH4Cl	1 g		
Tween 80	2 mL	0.05%	
$MgSO_4$-$7H_20$***	1 mL	0.008 mM	
ATCC Vitamin Mix***	10 mL	1%	
ATCC Trace Mineral Mix***	10 mL	1%	
For sole C&E media, add one of the following to Media A			
Aspartic acid	0.02g		
Mannose	0.9g		
Galactose	1.8g		
Sodium acetate	6g	0.60%	
Sodium formate	4g	0.40%	Requires sodium sulfate
D-glucose	0.4 g	2.2 mM	Add to 10ml DI H2O and filter sterilize
Fructose	1 g	2.2 mM	Add to 10ml DI H2O and filter sterilize
Sucrose	1.71g		Add to 10ml DI H2O and filter sterilize
Methylvaleric acid	561ul		Add both methylvaeric and methylbutyric
Methylbutyric acid	517ul		
Oxalate	6.75g	50mM	
pH to 7			
Filter sterilize and bring into anaerobic chamber			
Cysteine	0.5g		Add to 10ml DI H2O and filter sterilize in anaerobic chamber
sodium sulfate	2g	0.20%	Only add if adding sodium formate

1819
1820
1821
1822
1823

1824

1825

Table S8.

Species	**Commercial source**	**Isolation source**
Oxalobacter formgienes	ATCC 35274	human
Desulfovibrio piger	DSMZ749	Sheep rumen
Methanobrevibacter smithii	DSMZ11975	animal feces
Ruminococcus gnavus	ATCC 29149	human
Coprococcus comes	ATCC 27758	human
Bacteroides thetaiotaomicron	ATCC 700349	human
Lactobacillus helveticus	ATCC 55796	Unknown
Lactobacillus plantarum	ATCC 700210	Unknown

1826